Biophysical Characterization of Amyloid Disease-Related Peptides Using Small Molecule Tools

by

Sarah Cox

A dissertation submitted in partial fulfillment
of the requirements for the degree of
Doctor of Philosophy
(Chemistry)
in the University of Michigan
2020

Doctoral Committee:

Professor Ayyalusamy Ramamoorthy, Chair
Assistant Research Professor Magdalena I. Ivanova
Professor Anna K. Mapp
Professor Brandon T. Ruotolo
Professor Peter M. Tessier

Sarah Cox

coxsj@umich.edu

ORCID iD: 0000-0001-9779-9493

Acknowledgments

First and foremost, I must thank my advisor, Prof. Ayyalusamy Ramamoorthy. Thank you for giving me the opportunity to do science with the freedom of answering questions I found interesting. Your positive mentorship over the last 5 years has been a key factor in my success as a graduate student. Thank you for preparing me the next step in my scientific career. Next, I must thank the members of my committee, Prof. Brandon T. Ruotolo, Prof. Magdalena I. Ivanova, Prof. Anna K. Mapp, and Prof. Peter M. Tessier for their support and scientific insights. A special thank you to Prof. Magdalena I. Ivanova for your collaboration and guidance. Thank you for teaching me all the ins and outs of cell culture, no matter how many times I managed to contaminate the cells. Your insightful advice in both science and in life is something I will carry with me moving forward.

Next, I must thank my fantastic lab mates past and present who make coming to work enjoyable, even when the science doesn't want to cooperate: Dr. Kyle Korshavn, Dr. Amit Pithadia, Dr. Katie Gentry, Dr. Kian Kamgar-Parsi, Dr. Vojc Kocman, Dr. Elke Prade, Dr. Mukesh Mahajan, Dr. Thirupathi Ravula, Dr. Bikash Sahoo, Dr. Joshua Damron, Dr. Tomoya Yamamoto, Dr. Krishnarjuna Bankala, Dr. Satoshi Nagao, Dr. Jia Bai, Andrea Stoddard, Christian MacDonald, Nathanial Hardin, Giacomo Di Mauro, Nirupama Sumangala, Joe Joel, Alexandra Sutter, Xiaofeng Dai, and Zhou Deng. Thank you to my wonderful army of undergraduate researchers who made all of this work possible: Fucheng Guo, Brian Lam, Ajay Prasad, Hannah Marietta, and Nick Stander. You have all made the Rams lab an enjoyable and collaborative environment to work in.

Thank you for all of your training, mentorship and support. I would not be the scientist I am today without all of you. Thank you to the Center of Chemical Genomics High Throughput Screening Core and Steve Vander Roest for all of your help in developing the screen. My undergraduate career prepared me for a successful career in graduate school. Thank you Prof. Scott Hill of Alma College, my undergraduate research advisor. Your encouragement to pursue science has landed me in with career possibilities that I didn't even realize existed. Thank you to Prof. Anne McNeil for accepting me as an undergraduate for two summers in your lab. Thank you to Dr. Kelsey King Carter, for your patience in teaching me the in's and out's of synthesis.

Thank you to my family for their unwavering love, support, and guidance. My parents, Frank and Maria Cox, thank you for always answering my calls and being on my doorstep whenever I needed help with anything. My brother Franklin Cox, thank you for always being a source of joy and a reminder to be thankful for all of life's miracles. My paternal grandparents, Frank and Janet Cox, thank you for always being proud of my accomplishments no matter how big or small. Thank you to my late maternal grandmother, Dr. Myriam E. Nieto, the first woman to receive a PhD in chemical engineering in Colombia. Your life has inspired me both inside and outside of the lab. To my extended family of friends that I have made before and throughout graduate school, thank you for always being an outlet from the lab. There are too many to list, but I appreciate you all so deeply and value our lasting friendship. Last but most certainly not least, thank you to my incredible husband, Dr. Ricardo Vazquez. Thank you for always putting your money on me and being my biggest motivator in science and in life. I can't wait to start our next adventure in Singapore with you and Jack.

Table of Contents

List of Figures

List of Tables

List of Appendices

Abstract

While amyloid fibers made up of misfolded peptides or proteins are the hallmarks of over 20 different amyloid diseases including Alzheimer's Disease and Type II Diabetes, it is the elusive and transient oligomers that are the toxic player in disease. These oligomers impact toxicity in a variety of different avenues but are highly implicated in disrupting cellular membranes causing an imbalance in cell homeostasis leading to cell death. Understanding the steps involved in amyloid oligomer formation and membrane interactions is vital to developing therapeutics for these diseases. In these studies, the use of small molecules as a chemical biology tool to trap amyloid species in the presence and absence of cellular membrane mimetics and is demonstrated through a combination of NMR spectroscopy, fluorescence kinetics, transmission electron microscopy and circular dichroism, understand the structure and related cell toxicity.

The effect of CurDAc, a water-soluble curcumin derivative, on three different amyloidogenic peptides: human-IAPP (hIAPP), amyloid-beta (Aβ) and human calcitonin (hCT) was evaluated for its inhibitory and disaggregation activity. CurDAc interaction with amyloid is structurally selective which is reflected in a strong interference with hIAPP aggregation, while showing weaker interactions with hCT and Aβ40 in comparison. Cell toxicity experiments demonstrated that CurDAc alone is non-toxic, however, remarkably both hIAPP monomers and fibers treated with CurDAc are more toxic than hIAPP monomers or fibers alone, suggesting that CurDAc stabilizes toxic species of hIAPP. Through the utilization of NMR spectroscopy, spectra of hIAPP show a limited number of solvent exposed residues of the disaggregated species, which

are in a noticeably different chemical environment than the monomer. This study shows the potential of CurDAc to be used as a chemical probe to study hIAPP and suggests the mechanism of action is sequence specific.

Amyloid-β aggregation at the cell-membrane of neuronal cells is implicated as a source of toxicity for Alzheimer's disease. Small molecules have been studied for their ability to suppress amyloid aggregation and toxicity, but often the presence of membranes negate their activity. A high throughput screen of 1,800 small molecules was performed to search for membrane active inhibitors and 21 primary hits were discovered. Through the use of fluorescence-based assays, transmission electron microscopy, and dot blot assays the initial 21 primary hits were narrowed down to 5 lead compounds. NMR spectroscopy, circular dichroism, and size exclusion chromatography allowed for further confirmation of inhibition at the membrane interface as well as insights into the secondary structure and size of Amyloid-β, respectively. Lastly, dye leakage assays allowed for understanding as to how the addition of the 5 lead compounds affected Amyloid-β's ability to permeate the lipid bilayer.

These results provide insights into small molecules that stabilize small amyloid species in the absence and presence of membranes for the development of tool compounds for deeper investigations of these transient species.

Chapter 1

Introduction to Amyloid Proteins and Their Interactions with Small Molecules and Membranes

1.1 Overview of amyloids

The term "amyloid" coming from the Latin word "amylum", meaning starch, was first coined in 1838 as a description of amylaceous constituent in plants. In 1854, it was adopted by Rudolph Virchow to describe "starchy" deposits in a post mortem brain.[1] While amyloid was named in the brain, physicians in the XVII century began to describe amyloid-like deposits in post mortem livers and bones.[2] Today, the term amyloid is used to describe proteins and peptides that can adopt highly uniform fibers which are self-templated and with beta-sheet structured unilateral characteristics. Currently, there are over 50 different known proteins or peptides in humans, bacteria, and yeast that are considered amyloids, (Table 1.1). A large portion of these amyloids are related to human disease, which can be divided into two main categories: neuropathic or non-neuropathic, depending on the area of the body where they deposit.[3] In some species, some amyloid proteins are considered to have a positive function, usually in bacteria or yeast, which impact the organism by contributing to their survival.[4] In the case of amyloids related to human illnesses, a misfolding process negatively impacts the protein by altering its native state and function.[5] It needs to be highlighted that for a portion of human diseases, the protein or peptide is intrinsically disordered and their switching mechanism to become amyloid fibers is unknown. Therefore, many scientific endeavors in a variety of disciplines have set out to understand their

structure, function, and disease-related states as well as develop treatments for diseases caused by amyloids.

Amyloid fibers, either prepared in vitro or obtained from tissue samples, are filamentous structures composed of many monomeric units of the same protein in a beta-sheet structure that oriented unilaterally to the fiber axis (Figure 1.1 B). Individual monomeric beta-sheets are held together to their neighboring units via hydrogen bonding interactions. They are generally about 10

Protein or Peptide	**Number of Residues**	**Disease**
Amyloid-β	40/42	Alzheimer's Disease
α-Synuclein	140	Parkinson's Disease
Prion Protein (PrP)	208	Creutzfeldt-Jakob Disease, Spongiform Encephalopathy, Kuru
Microtubule-associated Protein Tau (τ)	352-441	Pick Disease
Huntingtin Exon 1 (HttEx1)	103-187	Huntington Disease
Immunoglobulin Light Chains	100	Amyloidosis
Immunoglobulin Heavy Chains	190	Amyloidosis
Serum Amyloid A protein (SAA)	45-104	AA Amyloidosis
Transthyretin (TTR)	127	Senile Systemic Amyloidosis
β2-microglobulin (β2-m)	99	Dialysis-Related Amyloidosis Hereditary Visceral Amyloidosis
Apolipoprotein A/C	69-100	Apo A/C Amyloidosis
Lysozyme (LYS)	130	Lysozyme Amyloidosis
Islet Amyloid Polypeptide (IAPP)	37	Type 2 Diabetes
Calcitonin	32	Medullary Carcinoma
Insulin	51	Injection Amyloidosis
Protein or Peptide	**Number of Residues**	**Species**
Curli	variable depending on species	E.coli, Salmonella
Microcin E492	84	K. pneumoniae
Chaplins	55-225 depending on isoform	S. coelicolor
Sup35NM	253	S. cerevisiae

Table 1.1 List of commonly studied amyloid proteins. The length of the protein or peptide is variable as well the disease which it is a causative factor. Examples of non-human amyloids are also given.

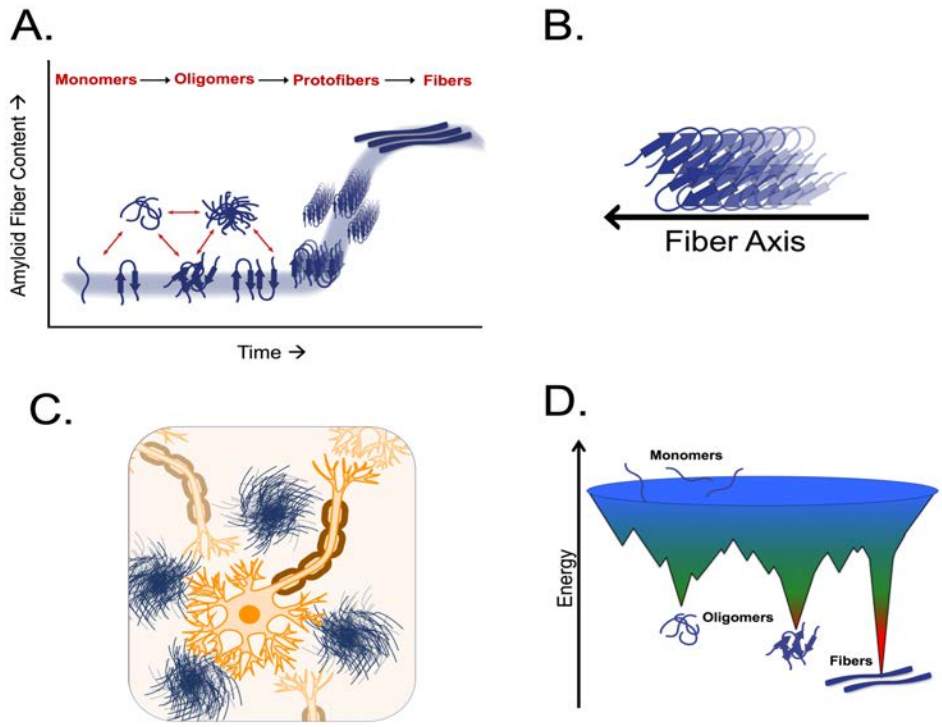

Figure 1.1. Unifying characteristics among amyloids. (A) The nucleated polymerization mechanism followed by amyloids from their disordered monomer structure to highly ordered beta sheet fibers, with a variety of structures and transitions throughout the process. (B) Final fiber structure is most commonly composted of two mirroring beta sheet fibers with individual monomers orienting perpendicularly to a unilateral fiber axis. (C) Cartoon representation of amyloid deposits occurring outside of neurons and in the extracellular space. Amyloid deposits occur outside of cells in nonneuropathic diseases as well. (D) Amyloid fibers exist at a low energy minimum making them hyper stable and highly resistant to disruption. The higher energy disordered monomer samples lower energy oligomers before making the transition to fibers.

nm in diameter but can be multiple microns in length. Typically, they are composed of two individual protofibers filaments that come together to form one final fiber held together by hydrogen bonding as well. However, there have been examples of mono-proto and tri-proto fibers too. Including their final fiber structure, there are many similarities that unify amyloidogenic proteins (Figure 1.1). These similarities include following a general aggregation mechanism going from a monomer, oligomer protofiber to fiber, binding histological dyes, depositing outside of cells, being hyper stable and resistance to breakdown or proteolysis, and containing a sequence of

hydrophobic and or aromatic residues that nucleate the self-assembly known as the amyloidogenic core.[6]

1.2 Alzheimer's disease and Amyloid-β

Alzheimer's disease (AD) is degenerative brain disease and the most common cause of dementia in the world. Unfortunately, despite many years of research, there is no known cure.[7,8] The hallmark of this disease is the formation of extracellular plaques in post-mortem brains. Currently in 2019, there are 5.8 million Americans suffering from the disease and this number is expected to triple by 2050.[9] It is believed that the "amyloid cascade hypothesis", which led to much research in many amyloid diseases, started with implicating Amyloid-β (Aβ) as the cause of AD.[10,11] Aβ is the most abundant protein found in the plaques in the extracellular space of neurons, specifically the hippocampus, amygdala, and association neocortex. It is cleaved from the larger amyloid precursor protein (APP) in the extracellular membrane of neurons.[12] The normal physiological role of both, APP and Aβ, is still unknown, however, it has been shown that they are critical for healthy brain development.[13] While there is a range of causative factors that have been implicated in AD, including metal ion dyshomeostasis, reactive oxygen species (ROS), membrane disfunction, low acetylcholine levels, and tau neurofibrillary tangles, there is still a strong case for Aβ and its aggregation to be a causative factor. These factors include a host of familial mutations in the Aβ sequence leading to a peptide with an increased aggregation rate and mutations in the secretases that cause an increased cleavage of the toxic 42 isoform.[14] An occurrence of AD is also seen in individuals with trisomy 21, also known as Down syndrome. This correlation is due to the APP gene location on chromosome 21. This leads to an increased amount of APP expressed which leads to over half of patients developing AD in their lifetimes.

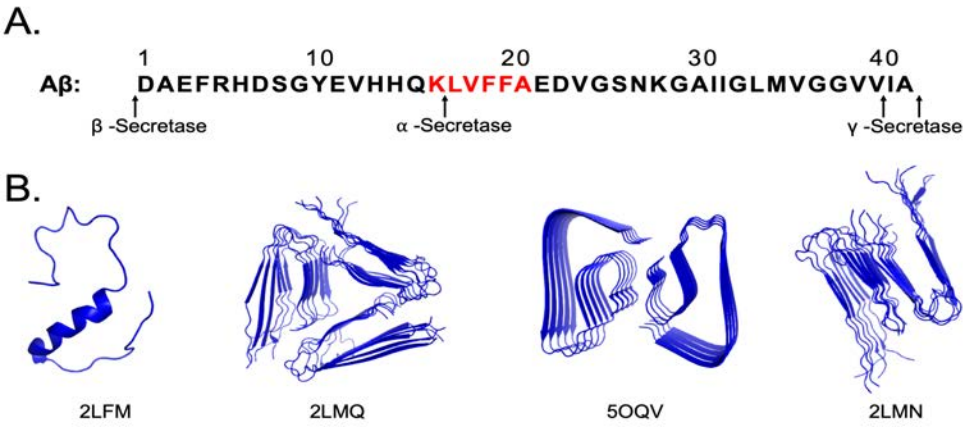

Figure 1.2 Aβ sequence and high-resolution structures. (A) Aβ sequences exist predominantly as either 40 or 42 residues through cleavage by beta and gamma secretase on the APP. Alpha secretase can occur in the amyloidogenic core highlighted in red, creating a non-amyloidogenic peptide. (B) high resolution structure of Aβ40 monomer solved by solution NMR (2LFM). Examples of 3-fold and 2-fold symmetry of Aβ40 fibers solved by solid-state NMR (2LMQ & 2LMN). Aβ42 fiber structure solved using a combination of Cryo-EM and solid-state NMR (5OQV)

This initial hypothesis and investigations into Aβ eventually led to the formation of the oligomer hypothesis. The oligomer hypothesis states that it is not the monomer or fibers that are the toxic species, instead, it is the oligomers that are created during the formation of fibers that are toxic and cause cell death.[12,15–17] There is data to support that there is no correlation between the total amount of plaques and AD symptoms and a better correlation between symptoms and levels of Aβ oligomers.[12] In addition, oligomers have also been shown to be toxic to cultured cells. This topic will be expanded on in section 1.5

The Aβ peptide is generated through sequential proteolytic cleavage of APP by beta and gamma-secretase (Figure 1.2 A). This cleavage can generate a range of peptide isoforms, with the 40-residue length peptide being the most abundant and the 42 residues length peptide being the most toxic. These peptides are cleaved inside the extracellular membrane and can subsequently, be released into the extracellular space.[14] Over 90 % of the Aβ that is cleaved from the APP results in the 40 residue peptide, with the other percentage being the 42 residue peptide isoform or in other

lengths ranging from 38-43 residues.[14] The monomeric peptide is considered and its physiological function remains unknown. At neutral pH, the peptide has an overall negative charge of -3 and is in an unstructured random coil in solution. The self-nucleating region of the peptide is residues 16-21, KLVFFA.[14] Many of the familial mutations known to cause early-onset AD are located in or near this region of the peptide. Alpha secretase, which creates a non-toxic fragment of APP, cleaves between the K and L of this region, which breaks up the amyloidogenic core. Aβ fibers have been well characterized through a variety of high-resolution methods including solid-state NMR, X-ray crystallography, and Cryo-EM. While the overall beta-sheet structure with monomer oriented perpendicular to the fiber axis is maintained, a variety of polymorphs have been observed, meaning the same overall architecture, but with finite changes in the folding as well as the fold symmetry (Figure 1.2 B) [18,19] These polymorphs can exist for a variety of reasons such as sequence, mutations, or preparation conditions. While the importance of polymorphism is not fully understood, it is thought that these differences in fiber structure may arise from the differences in oligomer formation.

1.3 Type II diabetes and hIAPP

Type II diabetes (T2D) is a widespread disease that affects over 30 million Americans, with over 80 million Americans with pre-diabetes. While the exact pathology of T2D is not clear, six factors have been identified to contribute to T2D, including insulin resistance, lipotoxicity, endoplasmic reticulum oxidative stress, tissue inflammation, amyloid deposition, and β-cell failure of islet cells in the pancreas.[3,4] While T2D can be reversed if the causes are treated early enough, permanent damage to the pancreas can happen via amyloid disruption if left untreated. The early stages of insulin resistance causes increased production of insulin. This increase in insulin leads to an increase in the co-secreted

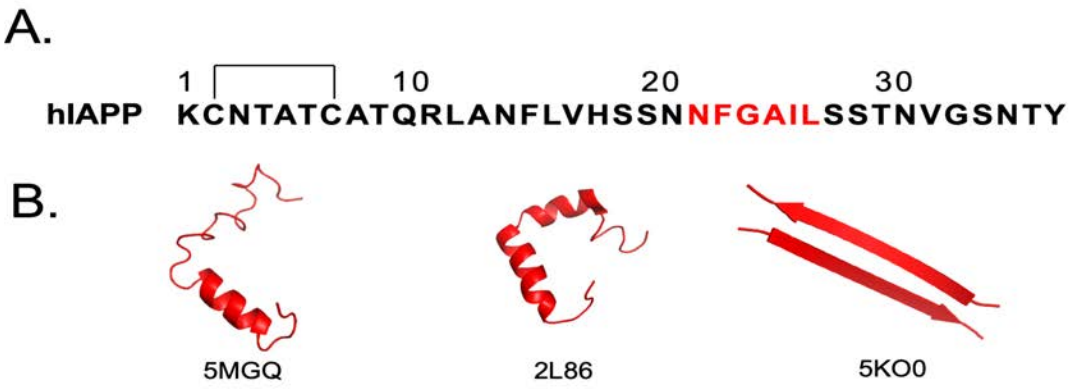

Figure 1.3 hIAPP sequence and high-resolution structures. (A) 37 residue sequence of hIAPP with the amyloidogenic core highlighted in red. A disulfide bridge exists at the N terminus between cysteines 2 and 7. The existence of this bond is important for its aggregation kinetics. (B) High resolution structures of the hIAPP monomer in solution (5MGQ) and in SDS micelles (2L86) solved using solution NMR. Fiber structure of fragment of hIAPP15-25 using MicroED (5KO0). No atomic level resolution structure of the full-length fiber exists.

peptide, human islet amyloid polypeptide (hIAPP), also known as amylin.[20] hIAPP is an amyloidogenic peptide hormone. Its normal function is to contribute to satiety after a meal. Normally, it is expressed at 90:1 insulin to hIAPP ratio and is co secreted in the insulin granules in the β-cells in the islet of Langerhans in the pancreas.[21] However, in the early stages of T2D, the increased production in insulin also increases the amount of hIAPP, increasing their propensity to aggregate.[22] The aggregation of hIAPP damages cells and amyloid fibers deposit in the extracellular space.[23] This can lead to the ultimate beta-cell failure associated with T2D, leading to patients no longer producing insulin. While hIAPP aggregation is associated with T2D, it is not the only factor contributing to the disease, but its importance in animal models has been shown.[24] In rat models of T2D expressing their native form of IAPP, which does not aggregate due to changes in residues in the amylogenic core, beta cell damage does not occur.[25] However, in the case of rat models expressing human IAPP, the beta cell damage is extensive.

hIAPP is a 37-residue peptide with a positive charge at neutral pH. It contains a disulfide bridge in the N-terminus of the peptide between cysteines 2 and 7. The presence of this bond has shown to be

important for its aggregation kinetics.[26] As with most amyloids it contains an amyloidogenic core of residues that nucleate the aggregation, in hIAPP, the residues are NFGAIL from 22-27. hIAPP follows the same self-nucleated polymerization mechanism as seen in most amyloid fibers described above. While most amyloids are thought to be toxic through the oligomer hypothesis, there is competing evidence for hIAPP that the fibers may be the toxic species in vivo models.[27]

1.4 Amyloid and membrane interactions

Lipid membranes play a crucial role in a cell's homeostasis. They are crucial in keeping cellular contents from escaping, creating ionic gradients, recruiting cofactors, cell to cell communications, bringing together transmembrane proteins by raft localization, trafficking cellular contents and cofactors both in and out of the cell. Lipid membranes are susceptible to oxidative stress and can act as a mechanism for degeneration.[28] Membranes, depending on their composition, can have a dual effect on amyloids. Specifically, they can speed up the aggregation mechanism and they are also a medium where amyloids can impart their toxic functions.[29–35] Amyloidogenic peptides, such as hIAPP and Aβ, are known to directly interact with extracellular membranes as well as take on unique confirmations once bound.[36–38] A general mechanism of toxicity has been proposed and investigated for amyloids (Figure 1.4.).[31] The first binding of the monomeric peptides' hydrophobic residues to the lipid membrane surface can cause perturbations in the membrane. These initial monomeric binders can recruit other peptides to form oligomers that can fully penetrate the membrane causing pores. These pores have been shown to allow the flux of ions such as Ca across the membrane, causing the cell to lose homeostasis and ionic potential. After the pore formation, continued aggregation of the peptides causes full membrane fragmentation via a detergent type mechanism. The membrane loses its structural integrity and large biomolecules can no longer be contained.

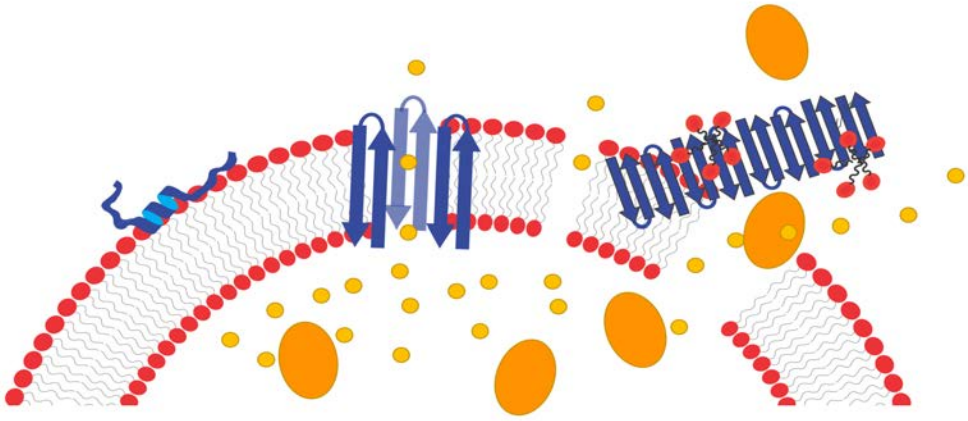

Figure 1.4. Proposed mechanism of amyloid-membrane mediated toxicity. Initial membrane surface interactions begin from a hydrophobic region of the amyloid. Aggregation at the membrane interface and oligomerization leads to the creation of small pores causing the loss of cell homeostasis via ion leakage. further aggregation on the membrane leads to full membrane disruption via lipid shedding in a detergent like mechanism allowing for the release of cellular contents.

This hypothesis has been much more investigated for Aβ. Anionic lipids, gangliosides, and cholesterol have been found to be incorporated into plaques as well as soluble oligomers from CSF.[39–42] Initial contact to anionic and zwitterionic bilayers has been shown to induce a helical conformation of the monomeric peptide portions directly interacting and the portions in solution remain relatively unstructured.[37] Shorter chain lipids, mimicking lipids that have undergone oxidative stress, have been shown to induce toxicity of Aβ and slow down aggregation. While most membrane-bound oligomers reported have a beta-sheet structure by both low-resolution experiments and simulations,[43,44] a high-resolution structure of a membrane-bound oligomer has not been solved.

This membrane toxicity hypothesis is not well investigated for hIAPP. While membrane still catalyzes the fiber formation in vitro, evidence for pore formation by oligomers is lacking. However, there is also recent evidence that fibers are the toxic species of hIAPP which does not fully support the oligomer hypothesis.[27] Furthermore, there is evidence that fibers can disrupt membranes as well as induce the formation of reactive oxygen species in cells, which is a known

cause of toxicity in many diseases including amyloids.[45,46] AFM studies have shown hIAPP to disrupt bilayer in a detergent-like mechanism after exposure to hIAPP.[23,47,48] Recently, high-resolution structural studies using NMR revealed a membrane-bound oligomer model of hIAPP of a beta-sheet dimer with a similar structure to hIAPP fiber models.[36]

1.5 Oligomer hypothesis

Oligomers are thought to be the toxic species for many amyloid diseases but are yet largely undefined.[15–17,20,49,50] These small, heterogeneous species, can vary in size and structure and are formed during the self-nucleated polymerization mechanism. When monomers interact with one another they form small oligomers of various sizes, such as dimers, trimers or higher-order species. These smaller oligomers can then interact with other oligomers forming larger species, which may then adopt the classic beta-sheet fiber architecture, becoming protofibers. Once the nucleus of protofibers have formed, very rapidly full fiber elongation takes place by multiple protofibers coming together or addition of monomers or oligomers to the protofiber template.[51–56] Once all the monomers in solution have been incorporated into fibers, the aggregation has reached the plateau phase with highly stable and non-toxic fibers as the result. Throughout these multiple transitions of structure and size, the toxic species are thought to exist.

Some oligomers are proposed to impart their toxic function, in part, by interacting directly with the cell membrane of neurons and disrupting the lipid bilayer, permeabilizing the membrane, and creating non-selective ion channels and large pores which, in turn, ablate the charge gradient necessary for neuronal function.[15,30,57–62] Lipid membranes can accelerate the aggregation of Aβ as well as facilitate the formation of unique structures of species that are specific to lipid bilayer disruption.[63] A gap in our structural understanding of many amyloid diseases occurs in oligomers. Due to their transient nature and the structural heterogeneity oligomers have been difficult to isolate and characterize

individually.[15,32,59] Low-resolution characterization of oligomeric species has been accomplished using a variety of techniques including fluorescence-based assays, circular dichroism, AFM and NMR.[64,65]Antibodies have been developed which can target both globular and fibrillar aggregates and can be used to probe for specific oligomers over time.[66] PICUP utilizes Ru metal oxidation as a way to induce radial dimerization among monomers creating covalent bonds that form oligomers which are important for learning about sizes of species but subject the peptide to harsh non-physiological condition.[67] Disulfide bond formation, which requires engineering of mutants to include non-native cysteine residues, can stabilize various dimeric forms[68] Finally, ESI-IMS-MS is able to determine molecular weight and size information of amyloid species treated by inhibitors.[69] Lipid nanodiscs have been used by varying lipid compositions that slow aggregation to study membrane-bound oligomers.[36]

Amyloid toxicity has been implicated in other mechanisms outside of membrane perturbations. Fibers are a trap for cellular factors including other proteins or metals as well as be a generation for toxic oligomers via fragmentation and nucleation.[70] This sequestering can lead to dysfunction in the proteasome and autophagy systems.[71–73] Oligomers have also been shown to interfere with RNAs transport and homeostasis.[74] Accordingly, protein aggregation interferes with nucleocytoplasmic RNA transport and RNA homeostasis. [75] Aβ specifically has been shown to bind to and interact with several extracellular receptors including NMDAR, NGF, insulin, Frizzled and PrP^c receptors.[76] Interactions with these receptors have been shown to trigger cellular apoptosis. Aβ oligomer uptake via autophagy has been shown to also cause the production of ROS inside of the cell, cause mitochondrial dysfunction, among other mechanisms of internal cellular dysfunctions, mentioned previously.[77,78]

1.6 Small molecule interactions with amyloids

There has been an extensive investigation into small molecules which may modulate the aggregation of amyloids.[14,79] However, the search for modulators aggregation has relied heavily on serendipity; oftentimes, novel classes of small molecules are accidentally discovered and improved analogs are subsequently synthesized.[80] Similarly, the prevalence of organic dyes in the literature as fiber disruption agents[81] largely follows from the early development of histological stains for amyloid deposits.[82] There are generally three different classes of small molecule amyloid modulators which may have therapeutic potential or maybe suited as chemical biology tool compounds (Figure 1.5). First, and most well-investigated are aggregation inhibitors. These small molecules can bind to monomers preventing oligomer formation, direct to off-pathway oligomers that are fiber incompetent, or bind to protofibers and prevent full fiber growth.[54-77] Second are promoters, which are compounds that can increase the rate of aggregation by increasing the transition from monomer to fiber and bypass the lifetime of oligomer species.[107–109] Last is fiber disaggregators or disrupters, these are small molecules that can break down the beat sheet structures of the fibers and resolubilize them to another smaller species.[106,110–112] The last two categories have been less investigated than inhibitors, due to the original oligomer hypothesis causing the prevention of oligomers to be highly investigated, however in recent

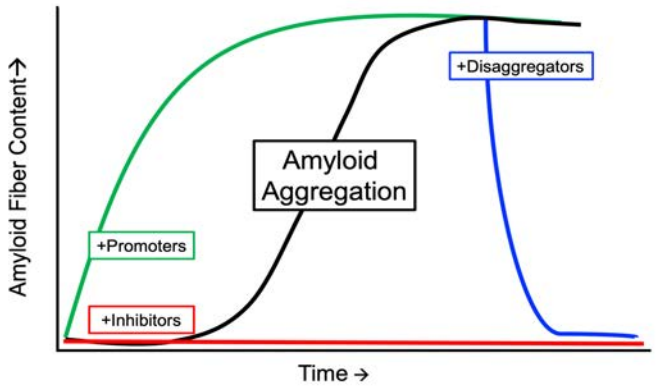

Figure 1.5 small molecule perturbations in amyloid aggregation kinetics. Small molecules are able to have multiple effects on amyloid formation (black). Inhibitors (red) added to monomers prevent aggregation to complete fiber formation. Promoters (green) added to monomers increase the rate of aggregation and push conformation to beta sheet fibers quickly by passing the oligomer state. Disaggregators (blue) disrupt the beta sheet fibers and changes the structure back to monomers or oligomers that no longer go on the aggregate to beta sheet fibers.

years, more exploration has been done into promoters or disaggregators. Recent investigations into promotors have come from the idea that fibers are generally nontoxic, and that bypassing oligomer formation may reduce the overall toxicity. The investigation into disaggregation comes from the idea that fibers may act as a seeding ground for oligomer formation and may act as a sponge for other cellular factors and that removing the total plaque load may be beneficial for some amyloid diseases.

There are a lot of structural similarities among all the compounds that act on amyloid proteins (Figure 1.6). Many of the compounds contain the potential for hydrogen bonding, are aromatic and

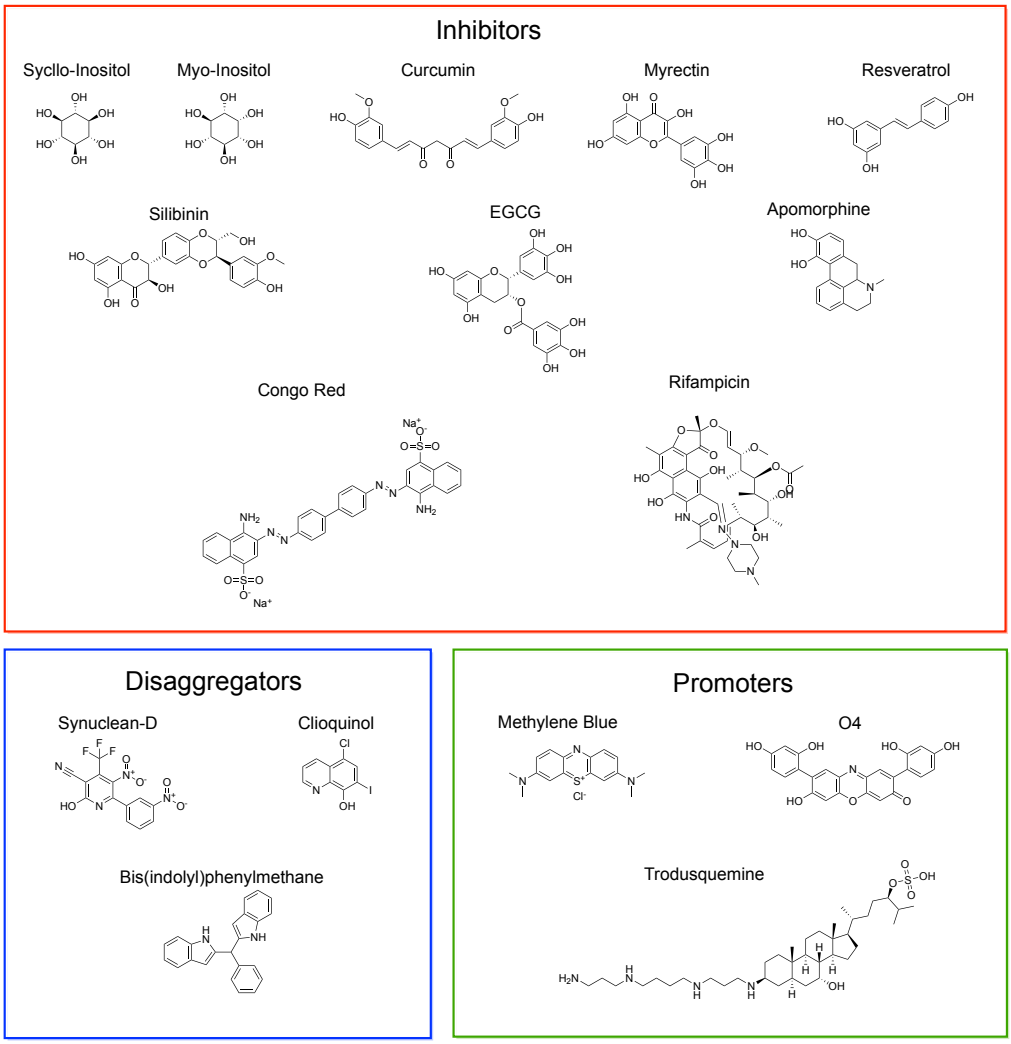

Figure 1.6 Structures of identified small molecule modulators of amyloid formation. Inhibitors, shown in the red box, is the most explored area of investigation into small molecules and amyloid formation. Promoters and disaggregators are shown in green and blue boxes respectively.

macrocyclic. [113–115] These characteristics are important for fiber disruption due to the high amount of hydrogen bonding and π-πi stacking that is needed for aggregation. Several amyloid modulating compounds function on multiple amyloids. For example, one of the most well studied small molecule inhibitors of aggregation, EGCG, was originally targeted against huntingtin aggregation in solution; it was later found to be active against α-synuclein, Aβ, and hIAPP. Additionally, O4 was found to be a promoter for Aβ as well as a disaggregator of hIAPP. Methylene blue has also found to be both a promoter and disaggregator.

1.7 Biophysical techniques to study amyloids

Many biophysical techniques are commonly employed to fully monitor the aggregation in this pathway.[116,117] Fluorescence-based assays such as thioflavin T (ThT) monitor the kinetics and solely gives signal based on fiber content. Its fluorescent intensity is increased upon binding to beta-sheet content that is highly specific to amyloid fibers. It is often used as the first line of investigation into amyloid-related questions but can be misleading depending on ligands added and is often difficult to reproduce. Circular Dichroism (CD) monitors protein folding and is used for monitoring the random coil to beta-sheet transitions at the beginning and ending of amyloid aggregation. Sometimes, an alpha-helical intermediate can be detected but more often the heterogeneity of oligomers can get lost and small differences can go undetected and signal resolution is poor. Mass spectrometry has been instrumental in providing oligomer sizes as well as ligand binding interactions.[118] the first model of a membrane oligomer is based on mass spec data. Western blotting and dot blotting have been useful in determining fiber epitopes, monomer, and oligomers with antibodies such as A11 and OC.[119,120] Size exclusion chromatography can separate proteins and peptides of a range of sizes and give an estimated oligomer size based on the elution volume. Atomic Force Microscopy (AFM) can provide a macroscopic view of aggregation

over a range of sizes including large oligomers up to fibers in real-time. It has been useful in determining aggregation rates as well as membrane interactions. Transmission Electron Microscopy (TEM) and Cryo-EM are quite useful in observing different fibers and their morphologies as well as the existence of large oligomers. Recently, high-resolution structures of amyloid fibers have been solved using Cryo-EM.[121] X-ray crystallography has also been useful in the amyloid field for solving fiber and fragment fiber structures. [122]

Nuclear magnetic resonance (NMR) is a very powerful tool for studying many facets of amyloid aggregation in both solution and solid states.[123–128] Solution NMR is typically used for characterizing the beginning stages of amyloid formation while solid-state NMR (ssNMR) is well suited for characterizing the end stages of amyloid fiber formation (Figure 1).[123] Solution based experiments can be used for looking at monomers and low order oligomers. Monomer-monomer as well as monomer ligand interactions are commonly studied using simple two-dimensional

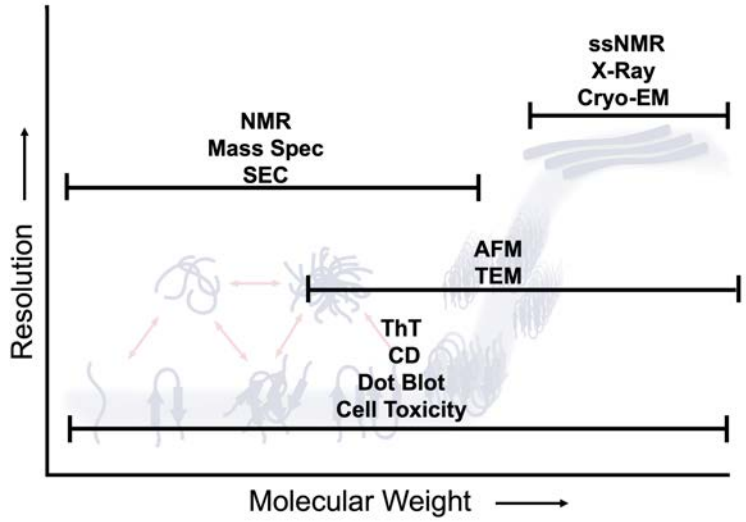

Figure 1.7 Biophysical techniques used to study amyloids ordered according to level of resolution and limitations based on molecular weight. Low resolution techniques that can be applied to the entire aggregation pathway include ThT, CD, dot blot assays, and cell toxicity experiments. With increased resolution relative to the previous techniques are AFM and TEM but they can only be used for very large oligomers or fibers. Moving to highest resolution for monomers and small oligomers is solution NMR, Mass Spec and SEC. Lastly, ssNMR X-Ray crystallography and Cryo-EM provides the highest atomic resolution for fibers.

experiments such as HSQC or HMQC in which chemical shift perturbation or line broadening observations can reveal about specific individual residues' chemical environments.[129] NOE based 2D and 3D experiments can be used to produce three-dimensional structures of aggregates and monomers in early stages of aggregation.[36] While solution NMR provides a strong tool, it also has its limitations. Restrictions in using NMR in the solution-state are mainly due to the aggregating nature of the peptide causing them to become too large over the course of some experiments and become NMR invisible due to its decreased tumbling rate. On the other hand, ssNMR experiments have been widely used in studying high-resolution structures of fully mature amyloid fibers as well as very large oligomers/protofibers that are quite stable or stabilized by freezing.[127,130]

1.8 Dissertation objectives

While amyloids and their aggregation have been heavily examined in a multitude of facets, treatment of diseases caused by them are still absent. A gap in our understanding still exists in the interactions of small molecule disaggregation and how small molecules can change the interplay between amyloids and membranes. The objectives of this dissertation are to explore these questions for hIAPP (chapter 2) and Aβ (chapter 3) respectively. First, I explore how a curcumin derivate (CurDAc) can selectively disaggregate and inhibit hIAPP over two other amyloid peptides, Aβ, and hCT (Chapter 2). Second, I set out to find new small molecules that can cease aggregation Aβ at the membrane interface (Chapter 3). Since most small molecules that are known to be inhibitors of Aβ lack activity in the presence of the membrane, I performed a high throughput screen and identified new membrane-active inhibitors.

1.9 References

1. Kyle, R. A. Amyloidosis: a convoluted story. *Br. J. Haematol.* **114**, 529–538 (2001).

2. Sipe, J. D. & Cohen, A. S. Review: History of the Amyloid Fibril. *J. Struct. Biol.* **130**, 88–98 (2000).

3. Chiti, F. & Dobson, C. M. Protein Misfolding, Functional Amyloid, and Human Disease. *Annu. Rev. Biochem.* **75**, 333–366 (2006).

4. Harrison, R. S., Sharpe, P. C., Singh, Y. & Fairlie, D. P. Amyloid peptides and proteins in review. *Rev. Physiol. Biochem. Pharmacol.* **159**, 1–77 (2007).

5. Chiti, F. & Dobson, C. M. Protein Misfolding, Amyloid Formation, and Human Disease: A Summary of Progress Over the Last Decade. *Annu. Rev. Biochem.* **86**, 27–68 (2017).

6. Nelson, R. & Eisenberg, D. Structural Models of Amyloid-Like Fibrils. in *Advances in Protein Chemistry* **79**, 235–282 (2006).

7. Ankarcrona, M. *et al.* Current and future treatment of amyloid diseases. *J. Intern. Med.* **14**, 1437–51 (2016).

8. Soejitno, A., Tjan, A. & Purwata, T. E. Alzheimer's Disease: Lessons Learned from Amyloidocentric Clinical Trials. *CNS Drugs* **29**, 487–502 (2015).

9. Association, A. 2015 Alzheimer's disease facts and figures. *Alzheimer's Dement.* **11**, 332–384 (2015).

10. Hardy, J. The Amyloid Hypothesis of Alzheimer's Disease: Progress and Problems on the Road to Therapeutics. *Science (80-.).* **297**, 353–356 (2002).

11. Hardy, J. A. & Higgins, G. A. Alzheimer's Disease: The Amyloid Cascade Hypothesis. **256**, 184–185 (1992).

12. Cavallucci, V., D'Amelio, M. & Cecconi, F. Aβ Toxicity in Alzheimer's Disease. *Mol. Neurobiol.* **45**, 366–378 (2012).

13. Müller, U. C., Deller, T. & Korte, M. Not just amyloid: Physiological functions of the amyloid precursor protein family. *Nat. Rev. Neurosci.* **18**, 281–298 (2017).

14. Hamley, I. W. The Amyloid Beta Peptide: A Chemist's Perspective. Role in Alzheimer's and Fibrillization. *Chem. Rev.* **112**, 5147–5192 (2012).

15. Benilova, I., Karran, E. & De Strooper, B. The toxic Aβ oligomer and Alzheimer's disease: an emperor in need of clothes. *Nat. Neurosci.* **15**, 349–357 (2012).

16. Nagel-Steger, L., Owen, M. C. & Strodel, B. An Account of Amyloid Oligomers: Facts and Figures Obtained from Experiments and Simulations. *ChemBioChem* **17**, 657–676 (2016).

17. Zhao, L. N., Long, H., Mu, Y. & Chew, L. Y. The toxicity of amyloid β oligomers. *Int. J. Mol. Sci.* **13**, 7303–7327 (2012).

18. Tycko, R. Amyloid Polymorphism: Structural Basis and Neurobiological Relevance.

Neuron **86**, 632–645 (2015).

19. Qiang, W., Yau, W.-M., Lu, J.-X., Collinge, J. & Tycko, R. Structural variation in amyloid-β fibrils from Alzheimer's disease clinical subtypes. *Nature* **541**, 217–221 (2017).

20. Ke, P. C. *et al.* Implications of peptide assemblies in amyloid diseases. *Chem. Soc. Rev.* **46**, 6492–6531 (2017).

21. Westermark, P., Li, Z. C., Westermark, G. T., Leckström, A. & Steiner, D. F. Effects of beta cell granule components on human islet amyloid polypeptide fibril formation. *FEBS Lett.* **379**, 203–6 (1996).

22. Gebre-Medhin, S., Olofsson, C. & Mulder, H. Islet amyloid polypeptide in the islets of Langerhans: friend or foe?

23. Jayasinghe, S. A. & Langen, R. Membrane interaction of islet amyloid polypeptide. *Biochim. Biophys. Acta - Biomembr.* **1768**, 2002–2009 (2007).

24. Wu, C. & Shea, J.-E. Structural similarities and differences between amyloidogenic and non-amyloidogenic islet amyloid polypeptide (IAPP) sequences and implications for the dual physiological and pathological activities of these peptides. *PLoS Comput. Biol.* **9**, e1003211 (2013).

25. Raleigh, D., Zhang, X., Hastoy, B. & Clark, A. The β-cell assassin: IAPP cytotoxicity. *J. Mol. Endocrinol.* **59**, R121–R140 (2017).

26. Rodriguez Camargo, D. C. *et al.* The redox environment triggers conformational changes and aggregation of hIAPP in Type II Diabetes. *Sci. Rep.* **7**, 44041 (2017).

27. Krotee, P. *et al.* Atomic structures of fibrillar segments of hIAPP suggest tightly mated β-sheets are important for cytotoxicity. *Elife* **6**, 1–26 (2017).

28. Yu, Q. & Zhong, C. Membrane Aging as the Real Culprit of Alzheimer's Disease: Modification of a Hypothesis. *Neurosci. Bull.* **34**, 369–381 (2018).

29. Tan, J., Zhang, J., Luo, Y. & Ye, S. Misfolding of a Human Islet Amyloid Polypeptide at the Lipid Membrane Populates through β-Sheet Conformers without Involving α-Helical Intermediates. doi:10.1021/jacs.8b08537

30. Butterfield, S. M. & Lashuel, H. A. Amyloidogenic protein-membrane interactions: Mechanistic insight from model systems. *Angew. Chemie - Int. Ed.* **49**, 5628–5654 (2010).

31. Sciacca, M. F. M. *et al.* Two-Step Mechanism of Membrane Disruption by Aβ through Membrane Fragmentation and Pore Formation. *Biophysj* **103**, 702–710 (2012).

32. Kotler, S. A., Walsh, P., Brender, J. R. & Ramamoorthy, A. Differences between amyloid-β aggregation in solution and on the membrane: insights into elucidation of the mechanistic details of Alzheimer's disease. *Chem. Soc. Rev.* **43**, 6692–6700 (2014).

33. Martel, A. *et al.* Membrane Permeation versus Amyloidogenicity: A Multitechnique Study of Islet Amyloid Polypeptide Interaction with Model Membranes. *J. Am. Chem. Soc.* **139**, 137–148 (2017).

34. Brender, J. R. *et al.* Membrane disordering is not sufficient for membrane permeabilization by islet amyloid polypeptide: studies of IAPP(20–29) fragments. *Phys. Chem. Chem. Phys.* **15**, 8908 (2013).

35. Johnson, R. D., Steel, D. G. & Gafni, A. Structural evolution and membrane interactions of Alzheimer's amyloid-beta peptide oligomers: new knowledge from single-molecule fluorescence studies. *Protein Sci.* **23**, 869–83 (2014).

36. Rodriguez Camargo, D. C. *et al.* Stabilization and structural analysis of a membrane-associated hIAPP aggregation intermediate. *Elife* **6**, e31226 (2017).

37. Korshavn, K. J., Bhunia, A., Lim, M. H. & Ramamoorthy, A. Amyloid-β adopts a conserved, partially folded structure upon binding to zwitterionic lipid bilayers prior to amyloid formation. *Chem. Commun.* **52**, 882–885 (2016).

38. Korshavn, K. J. *et al.* Reduced Lipid Bilayer Thickness Regulates the Aggregation and Cytotoxicity of Amyloid-β. *J. Biol. Chem.* **292**, 4638–4650 (2017).

39. Amaro, M. *et al.* GM 1 Ganglioside Inhibits β-Amyloid Oligomerization Induced by Sphingomyelin. *Angew. Chemie Int. Ed.* **55**, 9411–9415 (2016).

40. Qiang, W., Akinlolu, R. D., Nam, M. & Shu, N. Structural evolution and membrane interaction of the 40-residue β amyloid peptides: differences in the initial proximity between peptides and the membrane bilayer studied by solid-state nuclear magnetic resonance spectroscopy. *Biochemistry* **53**, 7503–14 (2014).

41. Arispe, N., Pollard, H. B. & Rojas, E. Giant multilevel cation channels formed by Alzheimer disease amyloid beta-protein [A beta P-(1-40)] in bilayer membranes. *Proc. Natl. Acad. Sci.* **90**, 10573–10577 (1993).

42. Delgado, D. A. *et al.* Distinct Membrane Disruption Pathways Are Induced by 40-Residue β-Amyloid Peptides. *J. Biol. Chem.* **291**, 12233–12244 (2016).

43. Serra-Batiste, M. *et al.* Aβ42 assembles into specific β-barrel pore-forming oligomers in membrane-mimicking environments. *Proc. Natl. Acad. Sci.* **113**, 10866–10871 (2016).

44. Jang, H., Zheng, J., Lal, R. & Nussinov, R. New structures help the modeling of toxic amyloidß ion channels. *Trends Biochem. Sci.* **33**, 91–100 (2008).

45. Pilkington, E. H. *et al.* Pancreatic β-Cell Membrane Fluidity and Toxicity Induced by Human Islet Amyloid Polypeptide Species. *Sci. Rep.* **6**, 21274 (2016).

46. Xue, W. F. *et al.* Fibril fragmentation enhances amyloid cytotoxicity. *J. Biol. Chem.* **284**, 34272–34282 (2009).

47. Sciacca, M. F. M. *et al.* Cations as Switches of Amyloid-Mediated Membrane Disruption Mechanisms: Calcium and IAPP. *Biophys. J.* **104**, 173–184 (2013).

48. Sciacca, M. F. M., Brender, J. R., Lee, D.-K. & Ramamoorthy, A. Phosphatidylethanolamine Enhances Amyloid Fiber-Dependent Membrane Fragmentation. *Biochemistry* **51**, 7676–7684 (2012).

49. Lee, S. J. C., Nam, E., Lee, H. J., Savelieff, M. G. & Lim, M. H. Towards an understanding of amyloid-β oligomers: Characterization, toxicity mechanisms, and inhibitors. *Chemical Society Reviews* **46**, 310–323 (2017).

50. Sengupta, U., Nilson, A. N. & Kayed, R. The Role of Amyloid-β Oligomers in Toxicity, Propagation, and Immunotherapy. *EBioMedicine* **6**, 42–49 (2016).

51. Silva, A. *et al.* Distribution of amyloid-like and oligomeric species from protein aggregation kinetics. *Angew. Chemie Int. Ed.* (2017). doi:10.1002/anie.201707345

52. Nag, S. *et al.* Nature of the Amyloid-ℕ Monomer and the Monomer-Oligomer Equilibrium. (2011). doi:10.1074/jbc.M110.199885

53. Crespo, R. *et al.* What Can the Kinetics of Amyloid Fibril Formation Tell about Off-pathway Aggregation? *J. Biol. Chem.* **291**, 2018–2032 (2016).

54. Iljina, M. *et al.* Kinetic model of the aggregation of alpha-synuclein provides insights into prion-like spreading. doi:10.1073/pnas.1524128113

55. Cohen, S. I. A., Vendruscolo, M., Dobson, C. M. & Knowles, T. P. J. The Kinetics and Mechanisms of Amyloid Formation Classical Theory of Nucleated Polymerization. doi:10.2

56. Stewart, K. L. & Radford, S. E. Amyloid plaques beyond Aβ: a survey of the diverse modulators of amyloid aggregation Introduction: what's in a plaque? doi:10.1007/s12551-017-0271-9

57. Quist, A. *et al.* Amyloid ion channels: a common structural link for protein-misfolding disease. *Proc. Natl. Acad. Sci. U. S. A.* **102**, 10427–32 (2005).

58. Demuro, A., Smith, M. & Parker, I. Single-channel Ca 2+ imaging implicates Aβ1–42 amyloid pores in Alzheimer's disease pathology. *J. Cell Biol.* **195**, 515–524 (2011).

59. Ahmed, M. *et al.* Structural conversion of neurotoxic amyloid-beta(1-42) oligomers to fibrils. *Nat. Struct. Mol. Biol.* **17**, 561–7 (2010).

60. Teplow, D. B. On the subject of rigor in the study of amyloid β-protein assembly. *Alzheimers. Res. Ther.* **5**, 39 (2013).

61. Chimon, S. *et al.* Evidence of fibril-like β-sheet structures in a neurotoxic amyloid intermediate of Alzheimer's β-amyloid. *Nat. Struct. Mol. Biol.* **14**, 1157–1164 (2007).

62. Sciacca, M. F. M. *et al.* Two-Step Mechanism of Membrane Disruption by Aβ through Membrane Fragmentation and Pore Formation. *Biophys. J.* **103**, 702–710 (2012).

63. Qiang, W., Akinlolu, R. D., Nam, M. & Shu, N. Structural evolution and membrane interaction of the 40-residue β amyloid peptides: Differences in the initial proximity between peptides and the membrane bilayer studied by solid-state nuclear magnetic resonance spectroscopy. *Biochemistry* **53**, 7503–7514 (2014).

64. Ruotolo, B. T., Benesch, J. L. P., Sandercock, A. M., Hyung, S.-J. & Robinson, C. V. Ion mobility-mass spectrometry analysis of large protein complexes. *Nat. Protoc.* **3**, 1139–52 (2008).

65. Pryor, N. E., Moss, M. A. & Hestekin, C. N. Unraveling the Early Events of Amyloid-β Protein (Aβ) Aggregation: Techniques for the Determination of Aβ Aggregate Size. *Int. J. Mol. Sci. Int. J. Mol. Sci* **13**, 3038–3072 (2012).

66. Breydo, L. *et al.* Structural differences between amyloid beta oligomers. *Biochem. Biophys. Res. Commun.* **477**, 700–705 (2016).

67. Rahimi, F., Maiti, P. & Bitan, G. Photo-Induced Cross-Linking of Unmodified Proteins (PICUP) Applied to Amyloidogenic Peptides. *J. Vis. Exp.* **23**, (2009).

68. Sandberg, A. *et al.* Stabilization of neurotoxic Alzheimer amyloid- oligomers by protein engineering. *Proc. Natl. Acad. Sci.* **107**, 15595–15600 (2010).

69. Young, L. M. *et al.* ESI-IMS–MS: A method for rapid analysis of protein aggregation and its inhibition by small molecules. *Methods* **95**, 62–69 (2016).

70. Olzscha, H. *et al.* Amyloid-like Aggregates Sequester Numerous Metastable Proteins with Essential Cellular Functions. *Cell* **144**, 67–78 (2011).

71. Choe, Y.-J. *et al.* Failure of RQC machinery causes protein aggregation and proteotoxic stress. *Nature* **531**, 191–195 (2016).

72. Park, S.-H. *et al.* PolyQ Proteins Interfere with Nuclear Degradation of Cytosolic Proteins by Sequestering the Sis1p Chaperone. *Cell* **154**, 134–145 (2013).

73. Hipp, M. S., Park, S.-H. & Hartl, F. U. Proteostasis impairment in protein-misfolding and -aggregation diseases. *Trends Cell Biol.* **24**, 506–514 (2014).

74. Hartl, F. U. Protein Misfolding Diseases. *Annu. Rev. Biochem.* **86**, 21–26 (2017).

75. Woerner, A. C. *et al.* Cytoplasmic protein aggregates interfere with nucleocytoplasmic transport of protein and RNA. *Science (80-.).* **351**, 173–176 (2016).

76. Kayed, R. & Lasagna-Reeves, C. A. Molecular Mechanisms of Amyloid Oligomers Toxicity. *J. Alzheimer's Dis.* **33**, 67–78 (2013).

77. Manczak, M. *et al.* Mitochondria are a direct site of Aβ accumulation in Alzheimer's disease neurons: implications for free radical generation and oxidative damage in disease progression. *Hum. Mol. Genet.* **15**, 1437–1449 (2006).

78. LaFerla, F. M., Green, K. N. & Oddo, S. Intracellular amyloid-beta in Alzheimer's disease. *Nat. Rev. Neurosci.* **8**, 499–509 (2007).

79. Härd, T. & Lendel, C. Inhibition of Amyloid Formation. *J. Mol. Biol.* **421**, 441–465 (2012).

80. Török, B. *et al.* Structure-Activity Relationships of Organofluorine Inhibitors of β-Amyloid Self-Assembly. *ChemMedChem* **7**, 910–919 (2012).

81. Hawkes, C. A., Ng, V. & McLaurin, J. Small molecule inhibitors of Aβ-aggregation and neurotoxicity. *Drug Dev. Res.* **70**, 111–124 (2009).

82. Howie, A. J. & Brewer, D. B. Optical properties of amyloid stained by Congo red: History and mechanisms. *Micron* **40**, 285–301 (2008).

83. Meng, F., Abedini, A., Plesner, A., Verchere, C. B. & Raleigh, D. P. The Flavanol (-)-epigallocatechin 3-gallate inhibits amyloid formation by islet amyloid polypeptide, disaggregates amyloid fibrils, and protects cultured cells against IAPP-induced toxicity. *Biochemistry* **49**, 8127–8133 (2010).

84. Young, L. M., Cao, P., Raleigh, D. P., Ashcroft, A. E. & Radford, S. E. Ion mobility spectrometry-mass spectrometry defines the oligomeric intermediates in amylin amyloid formation and the mode of action of inhibitors. *J. Am. Chem. Soc.* **136**, 660–70 (2014).

85. Lolicato, F., Raudino, A., Milardi, D. & La Rosa, C. Resveratrol interferes with the aggregation of membrane-bound human-IAPP: A molecular dynamics study. *Eur. J. Med. Chem.* **92C**, 876–881 (2015).

86. Andrade, S., Loureiro, J. A., Coelho, M. A. N. & Pereira, C. Interaction studies of amyloid beta-peptide with the natural compound resveratrol. 26–28 (2015).

87. Pithadia, A., Brender, J. R., Fierke, C. A. & Ramamoorthy, A. Inhibition of IAPP Aggregation and Toxicity by Natural Products and Derivatives. *J. Diabetes Res.* **2016**, (2016).

88. Hawkes, C. A., Deng, L.-H., Shaw, J. E., Nitz, M. & McLaurin, J. Small molecule β -amyloid inhibitors that stabilize protofibrillar structures in vitro improve cognition and pathology in a mouse model of Alzheimer's disease. *Eur. J. Neurosci.* **31**, 203–213 (2010).

89. Sciacca, M. F. M. *et al.* Inhibition of Aβ Amyloid Growth and Toxicity by Silybins: The Crucial Role of Stereochemistry. *ACS Chem. Neurosci.* **8**, 1767–1778 (2017).

90. Frid, P., Anisimov, S. V. & Popovic, N. Congo red and protein aggregation in neurodegenerative diseases. *Brain Res. Rev.* **53**, 135–160 (2007).

91. Fiori, J., Naldi, M., Bartolini, M. & Andrisano, V. Disclosure of a fundamental clue for the elucidation of the myricetin mechanism of action as amyloid aggregation inhibitor by mass spectrometry. *Electrophoresis* **33**, 3380–3386 (2012).

92. Zelus, C. Myricetin Inhibits Islet Amyloid Polypeptide (IAPP) Aggregation and Rescues Living Mammalian Cells from IAPP Toxicity. *Open Biochem. J.* **6**, 66–70 (2012).

93. Ono, K. *et al.* Phenolic Compounds Prevent Amyloid β-Protein Oligomerization and Synaptic Dysfunction by Site-specific Binding. *J. Biol. Chem.* **287**, 14631–14643 (2012).

94. DeToma, A. S., Choi, J.-S., Braymer, J. J. & Lim, M. H. Myricetin: A Naturally Occurring Regulator of Metal-Induced Amyloid-β Aggregation and Neurotoxicity. *ChemBioChem* **12**, 1198–1201 (2011).

95. Ehrnhoefer, D. E. *et al.* EGCG redirects amyloidogenic polypeptides into unstructured, off-pathway oligomers. *Nat. Struct. Mol. Biol.* **15**, 558–66 (2008).

96. Tomiyama, T. *et al.* Inhibition of Amyloid Protein Aggregation and Neurotoxicity by Rifampicin. *J. Biol. Chem.* **271**, 6839–6844 (1996).

97. Tomiyama, T., Kaneko, H., Kataoka, K., Asano, S. & Endo, N. Rifampicin inhibits the toxicity of pre-aggregated amyloid peptides by binding to peptide fibrils and preventing amyloid-cell interaction. *Biochem. J.* **322**, 859–865 (1997).

98. Malishev, R. *et al.* Toxicity Inhibitors Protect Lipid Membranes from Disruption by Aβ42. *ACS Chem. Neurosci.* **6**, 1860–1869 (2015).

99. Acharya, S. *et al.* Molecular Basis for Preventing α-Synuclein Aggregation by a Molecular Tweezer. *J. Biol. Chem.* **289**, 10727–10737 (2014).

100. Bieschke, J. *et al.* EGCG remodels mature α-synuclein and amyloid-β fibrils and reduces cellular toxicity. *Proc. Natl. Acad. Sci.* **107**, 7710–7715 (2010).

101. Thapa, A. *et al.* Membrane-Mediated Neuroprotection by Curcumin from Amyloid-β-Peptide-Induced Toxicity. *Langmuir* **29**, 11713–11723 (2013).

102. Thapa, A., Jett, S. D. & Chi, E. Y. Curcumin Attenuates Amyloid-β Aggregate Toxicity and Modulates Amyloid-β Aggregation Pathway. *ACS Chem. Neurosci.* **7**, 56–68 (2016).

103. Ahmad, B., Borana, M. S. & Chaudhary, A. P. Understanding curcumin-induced modulation of protein aggregation. *Int. J. Biol. Macromol.* **100**, 89–96 (2017).

104. Sparks, S., Liu, G., Robbins, K. J. & Lazo, N. D. Curcumin modulates the self-assembly of the islet amyloid polypeptide by disassembling α-helix. *Biochem. Biophys. Res. Commun.* **422**, 551–555 (2012).

105. Tu, L.-H. *et al.* Mutational Analysis of the Ability of Resveratrol To Inhibit Amyloid Formation by Islet Amyloid Polypeptide: Critical Evaluation of the Importance of

Aromatic–Inhibitor and Histidine–Inhibitor Interactions. *Biochemistry* **54**, 666–676 (2015).

106. Ladiwala, A. R. A. *et al.* Resveratrol Selectively Remodels Soluble Oligomers and Fibrils of Amyloid Aβ into Off-pathway Conformers. *J. Biol. Chem.* **285**, 24228–24237 (2010).

107. Limbocker, R. *et al.* Trodusquemine enhances Aβ42 aggregation but suppresses its toxicity by displacing oligomers from cell membranes. *Nat. Commun.* **10**, 225 (2019).

108. Bieschke, J. *et al.* Small-molecule conversion of toxic oligomers to nontoxic β-sheet–rich amyloid fibrils. *Nat. Chem. Biol.* **8**, 93–101 (2011).

109. Necula, M. *et al.* Methylene Blue Inhibits Amyloid Aβ Oligomerization by Promoting Fibrillization †. *Biochemistry* **46**, 8850–8860 (2007).

110. Pujols, J. *et al.* Small molecule inhibits α-synuclein aggregation, disrupts amyloid fibrils, and prevents degeneration of dopaminergic neurons. *Proc. Natl. Acad. Sci.* **115**, 10481–10486 (2018).

111. Ramshini, H. *et al.* Bis(indolyl)phenylmethane derivatives are effective small molecules for inhibition of amyloid fibril formation by hen lysozyme. *Eur. J. Med. Chem.* **124**, 361–371 (2016).

112. Mancino, A. M., Hindo, S. S., Kochi, A. & Lim, M. H. Effects of Clioquinol on Metal-Triggered Amyloid-β Aggregation Revisited. *Inorg. Chem.* **48**, 9596–9598 (2009).

113. Brahmachari, S., Paul, A., Segal, D. & Gazit, E. Inhibition of amyloid oligomerization into different supramolecular architectures by small molecules: mechanistic insights and design rules. *Future Med. Chem.* **9**, 797–810 (2017).

114. Ladiwala, A. R. A., Dordick, J. S. & Tessier, P. M. Aromatic Small Molecules Remodel Toxic Soluble Oligomers of Amyloid through Three Independent Pathways. *J. Biol. Chem.* **286**, 3209–3218 (2011).

115. Porat, Y., Abramowitz, A. & Gazit, E. Inhibition of Amyloid Fibril Formation by Polyphenols: Structural Similarity and Aromatic Interactions as a Common Inhibition Mechanism. *Chem. Biol. Drug Des.* **67**, 27–37 (2006).

116. Nilsson, B. L. & Doran Editors, T. M. *Peptide Self-Assembly*. **1777**, (Springer New York, 2018).

117. Iadanza, M. G., Jackson, M. P., Hewitt, E. W., Ranson, N. A. & Radford, S. E. A new era for understanding amyloid structures and disease. *Nat. Rev. Mol. Cell Biol.* **19**, 755–773 (2018).

118. Abdolvahabi, A. *et al.* How Do Gyrating Beads Accelerate Amyloid Fibrillization? *Biophys. J.* **112**, 250–264 (2017).

119. Kayed, R. Common Structure of Soluble Amyloid Oligomers Implies Common Mechanism

of Pathogenesis. *Science (80-.).* **300**, 486–489 (2003).

120. Kayed, R. *et al.* Fibril specific, conformation dependent antibodies recognize a generic epitope common to amyloid fibrils and fibrillar oligomers that is absent in prefibrillar oligomers. *Mol. Neurodegener.* **2**, 18 (2007).

121. Gremer, L. *et al.* Fibril structure of amyloid-β(1–42) by cryo–electron microscopy. *Science (80-.).* **358**, 116–119 (2017).

122. Riek, R. & Eisenberg, D. S. The activities of amyloids from a structural perspective. *Nature* **539**, 227–235 (2016).

123. Karamanos, T. K., Kalverda, A. P., Thompson, G. S. & Radford, S. E. Mechanisms of amyloid formation revealed by solution NMR. *Prog. Nucl. Magn. Reson. Spectrosc.* **88**–**89**, 86–104 (2015).

124. Ahmed, R. & Melacini, G. A solution NMR toolset to probe the molecular mechanisms of amyloid inhibitors. *Chem. Commun.* **54**, 4644–4652 (2018).

125. Michael Kovermann, Per Rogne & Magnus Wolf-Watz. Protein dynamics and function from solution state NMR spectroscopy. *Q. Rev. Biophys.* **49**, e6 (2016).

126. Mishra, R., Geyer, M. & Winter, R. NMR spectroscopic investigation of early events in IAPP amyloid fibril formation. *ChemBioChem* **10**, 1769–1772 (2009).

127. Meier, B. H., Riek, R. & Böckmann, A. Emerging Structural Understanding of Amyloid Fibrils by Solid-State NMR. *Trends Biochem. Sci.* **42**, 777–787 (2017).

128. Fawzi, N. L., Ying, J., Ghirlando, R., Torchia, D. A. & Clore, G. M. Atomic-resolution dynamics on the surface of amyloid-β protofibrils probed by solution NMR. *Nature* **480**, 268–272 (2011).

129. Schleucher, J. *et al.* A general enhancement scheme in heteronuclear multidimensional NMR employing pulsed field gradients. *Journal of Biomolecular NMR* **4**, (1994).

130. Tycko, R. Solid-State NMR Studies of Amyloid Fibril Structure. *Annu. Rev. Phys. Chem.* **62**, 279–299 (2011).

Chapter 2

Small Molecule Induced Toxic Human-IAPP Species Characterized by NMR

The content for this chapter will be included in the following reference:

Cox, S.J., Rodriguez Camargo, D.C.**,** Lee, Y.H., Padmini, V., Reif, B., Ivanova, M.I., Ramamoorthy, A. Small Molecule Induced Toxic Human-IAPP Species Characterized by NMR. Submitted

2.1 introduction

Transitions from monomer to fiber have been well studied since the beginning of the amyloid hypothesis.[1] While the monomers and fibers have been well characterized, the transient and difficult to isolate oligomers are thought to be the most toxic species in 30 different amyloid diseases.[2,3] Characterization of oligomers has been a difficult task but strides have been made[4]. In contrast to oligomers, fibers are considered non-toxic, but they have been hypothesized to serve as nucleating sites for toxic species formation.[5] Therefore, it may be advantageous to remove them to reduce the number of nucleation sites.

Small molecules have been sought out to interact with many different points in the aggregation process and can function as inhibitors, promoters, or disaggregators.[6–11] These tool compounds are advantageous to target many types of biological molecules including amyloids. They are highly tunable to the function needed, can bind tightly to the target protein, and can pass through cell membranes with little difficulty.[12–16] CurDAc, a curcumin derivative, has increased

water-solubility and stability compared to its parent molecule (Figure A.1). It has- been shown to inhibit hIAPP both in the presence and absence of lipid bilayers and negate hIAPP's aggregation-induced lipid membrane disruption. [17]

In this study, the effects of CurDAc on three different amyloid peptides, amyloid-β ($A\beta_{40}$), human islet amyloid polypeptide (hIAPP), and human calcitonin (hCT), were examined. While these three peptides have similar polypeptide length ranging from 32-42 amino acids, they differ in their isoelectric point, hydrophobicity, and aggregation kinetics (Figure A.2). These similarities and differences make them ideal for understanding the structural specificity of small molecules. NMR spectroscopy is ideal for studying these types of systems because of the residue-specific structural information that can be gained from the experiments. When NMR is coupled with other biophysical techniques, the kinetics, protein structure/fold, and protein interactions of the isolated species can be understood. Integrating these experiments with cell-based assays, further information can be gained on how these species can act towards disease-relevant cells. Here, we show the use of CurDAc to generate a toxic oligomer of hIAPP which arises from both monomer interactions and fiber disruptions, and we compare how this small molecule acts against two other amyloids.

2.2 Results and Discussion

Fiber growth was monitored by utilizing Thioflavin-T (ThT), which is a widely used fluorescence reporter for amyloid fiber formation that gives kinetic and mechanistic information about amyloid aggregation (Figure 2.1A-F). [18,19] Using ThT fluorescence assays, both inhibition and disaggregation profiles were obtained for all three peptides, hIAPP (Fig.1 A&D), $A\beta_{40}$ (Fig. 1 B&E), and hCT (Fig. 1 C&F). While CurDAc was able to modulate the aggregation of the three

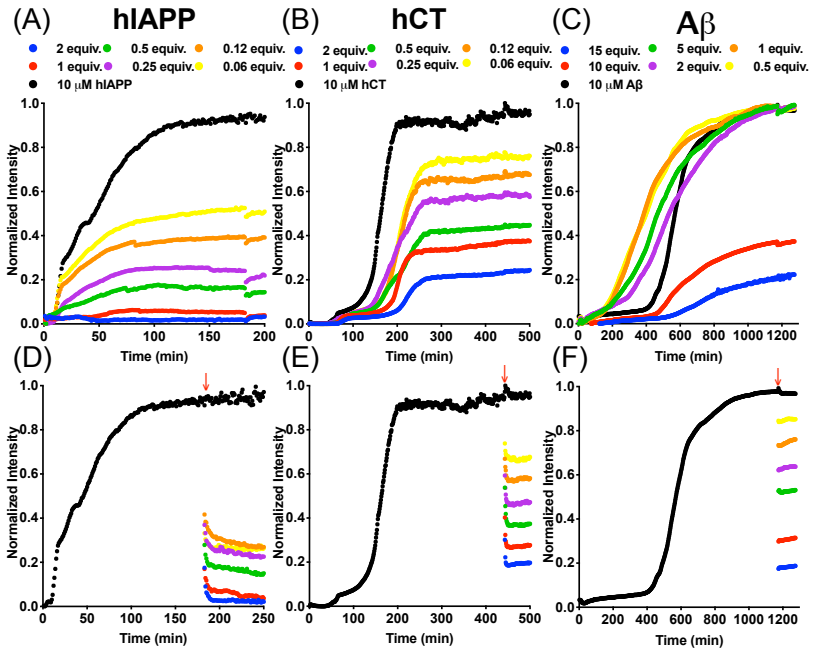

Figure 2.1 Inhibition and disaggregation of amyloid peptides by CurDAc. ThT fluorescence inhibition curves of hIAPP, hCT and $A\beta_{40}$ (A-C respectively) in the presence of varying molar equivalents of CurDAc. Disaggregation curves of hIAPP, hCT and $A\beta_{40}$ (D-F respectively) using the same molar equivalents as the inhibition experiments. Red arrow indicates when CurDAc was added. All experiments were done in pH 7.4 phosphate buffer with slow orbital shaking at 25°C for hIAPP/hCT and 37°C for $A\beta_{40}$.

amyloid peptides, it displayed a distinct difference in potency. For hIAPP, as the concentration of CurDAc was increased from 0.06 to 2 molar equivalents, the overall final ThT signal intensity with respect to the control decreased indicating a decrease of fiber formation (Figure 2.1A). Not only is the overall intensity lower, but also the slope of the elongation phase is extended, indicating a possible change in the secondary nucleation step.[18] CurDAc acted as a fibrillation inhibitor for hCT as well; however, it was not as effective with hIAPP. For $A\beta_{40}$, the concentration range that was tested on hIAPP and hCT did not affect the inhibition of fibril formation (Figure 2.1C). Superstoichometric ratios (10-15 molar equivalents) were needed to see a depression of fibril formation in $A\beta_{40}$ (Figure 2.1C). Interestingly, the lag time at lower equivalencies of CurDAc was decreased by about 200 minutes, an effect that was not observed with the other two peptides. We

believe that the change in kinetics based on the concentration of CurDAc is due to a colloidal inhibition effect and charge-charge repulsion of CurDAc with $A\beta_{40}$.[20,21]

Amyloid disaggregation as a method of removing plaque loads could be an avenue to reduced toxicity since plaques have been hypothesized to serve as nucleating sites for toxic oligomers.[22] Despite their innate hyperstability, amyloid fibrils have been shown to be disaggregated by harsh methods including heat, pH, and organic solvents as well as small molecules, peptides, antibodies, and proteins.[9,23–26,26–30] In terms of small molecules, most fibers require molar excess of the disaggregating compound for disassembly. In Figure 2.1D, ThT curves show the disaggregation of hIAPP fibers upon the addition of CurDAc (red arrows) in the same stoichiometric ratios of CurDAc as in the inhibition experiments A similar trend is seen for hCT in that there is an immediate drop in ThT intensity followed by a decline and plateau, however the steepness of decline is much stronger and the curve plateaus much quicker compared to that observed for hIAPP (Figure 2.2E). For Aβ, we unexpectedly saw drops in intensity for all of the equivalents examined, however, these curves have no increase or decrease in intensity after the initial drop (Figure 2.2F). The initial steep decline in ThT intensity is followed by an eventual plateau. To rule out the possibility of ThT displacement we repeated these same experiments with higher excess of ThT and the same trend was observed (Fig. S3), leading us to believe that another mechanism is at work. Using Isothermal Titration Calorimetry (ITC), the binding of CurDAc to $A\beta_{40}$ or hIAPP was studied to further investigate the nature of the interaction (Figure A.4 and Table A.1). In the ITC experiments for hIAPP, no interaction was observed between hIAPP monomers and CurDAc. CurDAc interaction with hIAPP fibers was found to have a dissociation constant (K_d) value of ~7 μM. For $A\beta_{40}$ fibers, no binding could be detected for 10 molar equivalent

concentrations of CurDAc (Figure A.10). This data further supports that the disaggregation effect is not a result of ThT displacement given the very similar binding constants of CurDAc to hIAPP fibers (~7μM) and ThT to amyloid fibers (~10 μM). [31]

Building on the ThT data of selectivity and potent disaggregation of hIAPP, we looked to NMR to provide us with a deeper understanding of this interaction. By looking at the total proton NMR signal intensity of hIAPP in solution we analyzed the aggregation kinetics of hIAPP monomers in the presence of CurDAc (Figure A.5). Since large aggregates (typically >100-kDa) do not contribute to the narrow spectral lines observed in solution NMR experiments, the measured ^{1}H NMR intensity should be inversely proportional to the amount of aggregated hIAPP peptide present in the sample. For example, it has previously been shown that sigmoidal intensity decay plots indicating monomer depletion due to the self-assembly process to form amyloid fibers can be used to determine the kinetics and mechanisms.[32–34] Interestingly, hIAPP in the presence of CurDAc at neutral pH loses signal intensity faster than in the absence of CurDAc. Most of the peaks in the NMR spectrum disappeared within 10 hours for the peptide alone. In the presence of CurDAc, the peaks in the NMR spectrum disappeared in less than one hour, indicating the formation of NMR invisible species, such as a large off-pathway oligomer. [35] hIAPP is an unstable peptide under in vitro conditions, which is in accordance with quick self-assembly of the peptide to form aggregates under neutral conditions. [36] It is also known that the formation of the N-terminus disulfide bridge is important for its aggregation kinetics, and in this NMR study, the oxidized form of hIAPP is used throughout. Due to the accelerated aggregation and signal loss at neutral pH, we lowered the sample pH to 5.3, which is the physiological pH of hIAPP when stored in insulin granules at high concentrations in the pancreatic beta cells. [37] This strategy allowed us

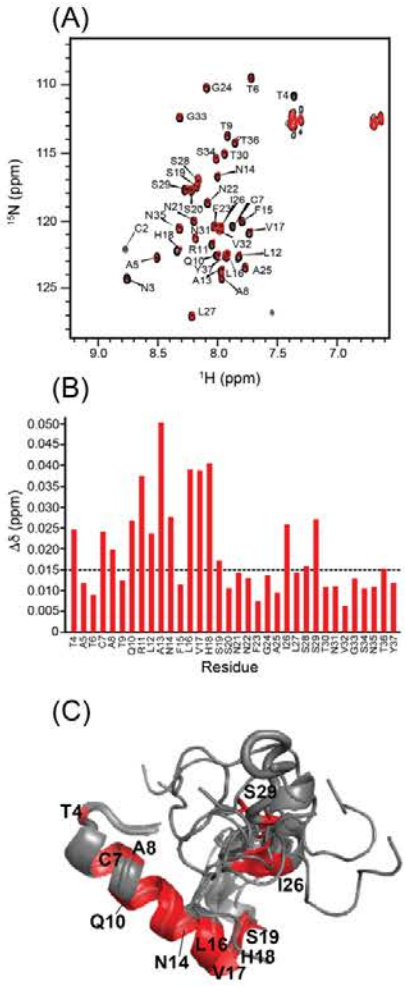

Figure 2.2 hIAPP monomer and CurDAc interactions characterized by NMR. (A) 2D ^{1}H/^{15}N SOFAST-HMQC spectra exhibiting the interaction between 100 μM hIAPP(black) with 100 μM CurDAc (red) at pH 5.3 acetate buffer. (B) Chemical shift perturbations for the backbone amide ^{15}N and proton resonances as a function of the amino acid sequence position. The dashed line indicates the mean for the observed CSPs with the stronger shift changes above 0.015. (C) Monomer structure of hIAPP (PDB:5MGQ) solved by NMR experiments at pH 5.3 is used in this study to identify the residues interacting with CurDAc (highlighted in red).

to perform longer NMR experiments on hIAPP and enabled us to do additional analyses of the interaction with CurDAc due to the increased lifetime of the monomeric sample. The net-charge of hIAPP becomes slightly more positive at pH 5.3, due to a greater portion of H18 residues becoming protonated. At this pH, hIAPP stayed relatively soluble for 30 hours with only 20% signal loss (Figure A.5 and A.6). At a 1:1 molar ratio with CurDAc, the hIAPP signal decreases

more rapidly with 70% of the signal lost after 20 hours with complete signal loss at 40 hours (Figure A.5). This observation suggests that CurDAc can quickly initiate hIAPP aggregation and inhibits the fibrillar structure morphology of the aggregate species in the same way as other flavanols and confirms our initial observations using other biophysical methods.[11]

Using two-dimensional NMR techniques, such as SOFAST-HMQC, it is possible to obtain residue-specific information of the CurDAc-hIAPP complex interaction (Figure 2.2A). Chemical shift perturbations (CSPs) are a valuable tool for characterizing protein-ligand interactions, even if the chemical shift changes are very small.[38] In comparison to the reference $^{1}H/^{15}N$ HMQC spectrum of hIAPP alone, small CSPs were observed, in CurDAc containing samples, for residues in the N terminal and central regions as indicated by the peaks above the (horizontal) dashed line indicating the mean (Figure 2.2 B). Most strongly affected residues include T4, C7, A8, Q10-N14, L16-S19, I26, and S29 and are highlighted on the monomeric structure (Figure 2.2C).[39] One of the highly affected residues, H18, is known to be important for its aggregation and toxicity.[40,41] Most of these residues are neither aromatic nor carry a charge, indicating that the mechanism of action is most likely not due to electrostatic or pi-pi interactions. Interestingly, we were able to identify that the CurDAc causes an effect not only at the N terminus but also in the central region, specifically near the GAIL sequence (residues I26 and S29) which is the nucleating region for amyloid aggregation.[42] Using three different kinds of software to predict secondary structure, the Random-Coil Index, Secondary Structural Propensities database, and the Delta-Delta of the C□ chemical shift, the C□, CO, HN chemical shifts were analyzed and are shown in Figure A.7.[43,44] All three approaches predict that the N-terminus of hIAPP has an alpha-helical conformation, with a slight beta-sheet tendency near the amyloidogenic core (residues 24-27) and the remainder of the peptide present is in a random-coil, which is similar to the structure of the hIAPP monomer. This

could explain why CurDAc inhibits fibril formation, due to the possible lack of a beta-strand for self-recognition and steric zipper formation by this essential sequence.

Fibers represent a large insoluble form that is invisible for the traditional solution NMR experiments due to the anisotropic interactions, such as dipolar couplings and chemical shift anisotropy not being fully averaged out which induces line broadening.[45,46] In the event that portions of the peptides that form the fibers start to become soluble and can tumble sufficiently fast in the solution, the peptide signal will become sharp and the newly soluble peptide species can be identified and quantified. The starting NMR spectrum of the hIAPP fibers can be seen in Figure 2.3A in black, in which very few peaks were observed. 72 hours after the addition of CurDAc, strong peaks appeared in the spectrum as shown in the amide region (red) of the NMR spectrum. As shown in Figure 2.3C, after the addition of CurDAc to fibers, the signal intensity for the peaks observed in the proton NMR spectrum raised steadily over 72 hours.

By using 2D SOFAST-HMQC NMR experiments, we were able to identify some of the peaks which appeared after 72h of adding CurDAc to hIAPP fibers. These resonances are attributed to mobile regions of the peptide and the disrupted aggregates of hIAPP fibers in solution (Figure 2.3B). 3D HNCA and 3D HNCOCA experiments were performed to identify some of these residues that appeared in the spectra of CurDAc-induced disaggregated hIAPP species (Figure A.8). The 2D and 3D NMR spectra were not straightforward in their characterization due to the low concentration of disaggregated species which contributes to the observed NMR signal. However, these experiments do allow us to determine some of the residues and regions of hIAPP that have become visible as a result of disaggregation. From our partial assignment, we have identified the affected residues to be A8, L12, V17, H18, S19, S20, N21, and I26. All of these

residues were also identified as residues affected by CurDAc interactions with hIAPP monomers by CSPs (Figure 2.2B).

Figure 2.3D shows the model of the amino acid sequence with the highlighted residues in red being the ones identified by the disaggregation of fibers. Out of the identified residues, V17-N21 are sequentially grouped, while A8, L12, and I26 are distributed randomly. While we were able to assign most of the visible residues signals, a few signals remained unassigned. It is possible that these unassigned peaks may belong to other residues that are near the three randomly distributed residues (A8, L12, I26).

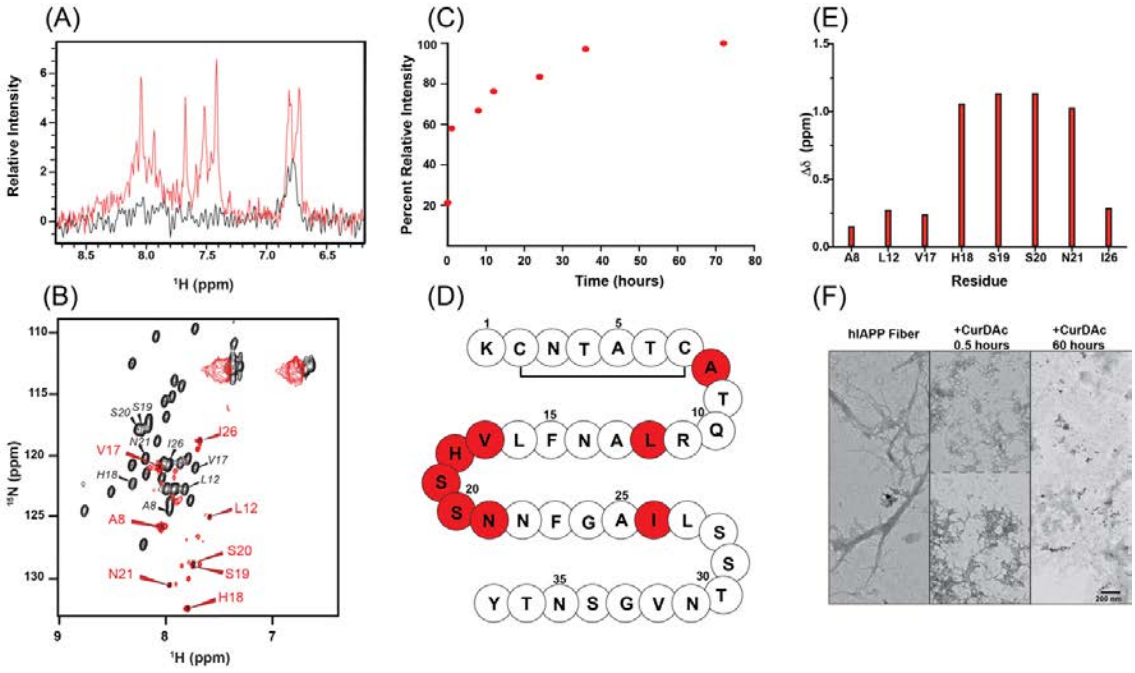

Figure 2.3 NMR monitors disaggregation of hIAPP fibers. (A) Proton NMR spectra of 90 μM hIAPP fibers (black) and 90 μM hIAPP with 90 μM CurDAc after 72-hour incubation with CurDAc (red) at pH 7.4 in phosphate buffer. (B) 2D ^{1}H/^{15}N SOFAST-HMQC NMR spectra of hIAPP monomers (black) and the disaggregated species (red) at a 1:1 peptide:CurDAc molar ratio. Peak assignments of the monomer are also shown for reference. (C) Normalized overall proton peak intensity of hIAPP fibers as a function of disaggregation by CurDAc over 72 hours. (D) Amino acid sequence model of hIAPP with highlighted residues identified after CurDAc disaggregation in red. (E) Chemical shift perturbations for the backbone amide ^{15}N and proton resonances of the identified residues in reference to that of monomers. (F) TEM images of hIAPP fibers (left) and hIAPP species after 0.5 hours (middle) and 60 hours (right) disaggregation.

The residue H18 was identified in both the monomer interaction with CurDAc and as a mobile residue after disaggregation of fibers by CurDAc, and it is known to be a key residue in contributing to the toxicity of hIAPP.[40] The residues located in the N terminus are shown to interact with CurDAc and they are important for the initial contacts in self-assembly. [47,48] When comparing the visible residues to known hIAPP monomer and fiber structures, residues V17-I26 can all be found in a loop region of the peptide. [39,49,50] Due to this we believe there are two possibilities for the absence of other residue signals. One possibility is the residues are in a highly flexible/mobile loop region of an oligomeric structure, while unseen residues are buried within the oligomer causing NMR signal loss.[45] The second possibility is that while a smaller species is becoming disaggregated, they are exchanging between bound and unbound states from the larger fiber structure. This could cause a broadening of the residues that were not identified in the spectrum, making only these highly mobile loop residues visible which are not in exchange.[51] Figure 2.3E shows the chemical shift perturbations of the identified residues. 6 out of the 8 residues have a significant upfield shift in the proton dimension and a downfield shift in the nitrogen dimension indicating a drastically different chemical environment as compared to the monomer. These chemical shift values do not fall in the typical range of known secondary structural chemical shifts for these residues.[52] The CurDAc induced disaggregation of hIAPP fibers was corroborated using TEM (Figure 2.3F). TEM shows the difference between hIAPP fiber morphology before and after the addition of CurDAc. The disruption of aggregates increases over time as seen with the decreasing amount and size of hIAPP fibers indicating the fiber disaggregation.

Thus, our NMR experiments demonstrate the ability of CurDAc to disaggregate fully matured amyloid fibers of hIAPP, which is in excellent agreement with ThT based fluorescence and TEM. Most importantly, the NMR results reveal which amino acid regions are the most mobile

resulting from the interaction of CurDAc with hIAPP fibers. However, the poor S/N and the absence of a complete set of resonances in the NMR spectra dampened our efforts in determining the high-resolution 3D structure of CurDAc induced disaggregated hIAPP species. Therefore, the development and application of approaches to enhance the S/N for NMR studies on such samples could be worthwhile as they can be useful to study a variety of amyloid proteins and their interaction with small-molecule compounds. Nevertheless, the NMR results reported in this study provide rare insights into the formation of an off-pathway hIAPP species and reveal the key amino acid residues that are solvent-exposed and may be a part of a larger complex.

Given this exciting NMR data, we turned to other biophysical techniques to support our findings. By recording CD spectra of hIAPP overtime after the addition of CurDAc, the secondary structural changes associated with the disaggregation of fibers could be monitored. Before the addition of CurDAc, a strong peak was observed at 218 nm indicating a beta-sheet conformation (Figure A.9). There was also a shoulder at 200 nm, which could indicate a portion of the peptide remaining in random-coil. Using CD fitting software, BeStSel, we analyzed the data to understand the possible distribution of conformations in the samples (Table A.2).[53] While a majority of the structural content was determined to be a beta-sheet, after the addition of CurDAc a small helical conformation was observed between 30 minutes and 40 hours of the ongoing fiber dissociation. For $A\beta_{40}$ and hCT, CD experiments indicated the formation of a stable beta-sheet secondary structure in the same time span as the ThT curves which was maintained after the addition of CurDAc (Figures S10).

The CD samples were examined using TEM and fibers were observed for all three different peptides before the addition of CurDAc. Since CurDAc's effect on hIAPP is most pronounced, we

monitored TEM over an extended time in accordance with the NMR and CD experiments (Figure A.9) in which the remodeling observed in the former techniques can be visualized. For hCT after the addition of CurDAc, more amorphous type aggregates can be seen after remodeling with two molar equivalents (Figure A.11). For $A\beta_{40}$, the fibers maintained their architecture at 10 molar equivalents of CurDAc but appeared to be overall shorter in length than before addition (Figure A.11).

There is considerable interest in understanding cellular toxicity of amyloid species in order to evaluate the potency of small-molecule amyloid inhibitors and potentially to develop

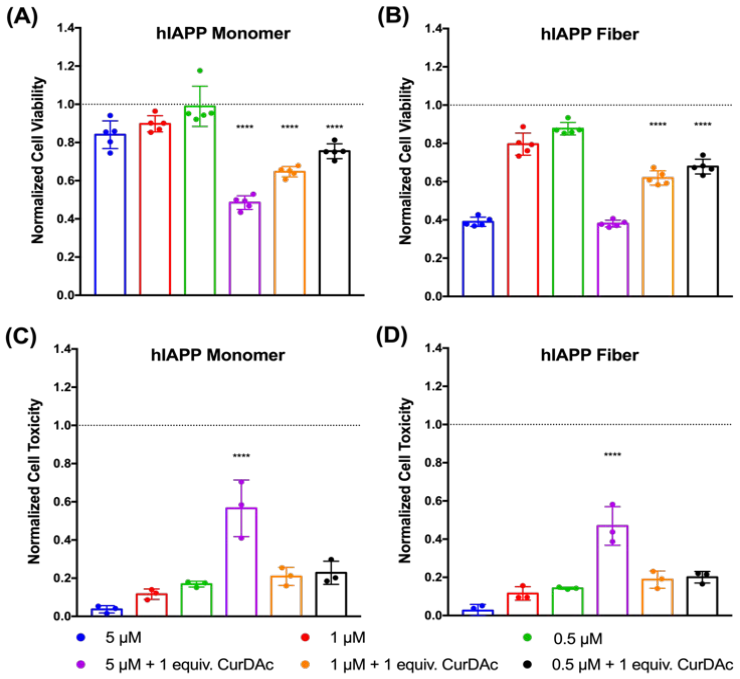

Figure 2.4 Cell toxicity measurements of hIAPP monomer and fibers in the presence and absence of CurDAc. RIN-5F cell viability measured by MTT reduction in the presence of hIAPP monomers and fibers without CurDAc and after 24-hour incubation with CurDAc (A-B). Cell toxicity final intensity after 13 hours of monitoring by CellTox Green fluorescence (C-D). 5, 1 and 0.5 μM peptide were used for all experiments in the presence or absence of 1 molar equivalent of CurDAc. Ordinary one-way ANOVA tests with Tukey's multiple comparisons were performed in respect to cells treated with hIAPP in the presence or absence of CurDAc, ****$p<0.0001$, indicate levels of significant differences. Data is shown as mean +/- SD with N=5 or 3 independent measurements. Additional statistically significant data can be found in Table A.3.

compounds to treat the related amyloid disease. While fibers are thought to be relatively inert, cytotoxic species are pointed at pre-fibrillar oligomers in the case of many different amyloid-related diseases. In this study, the 3-(4,5-dimethylthiazol-2-yl)-2,5-diphenyltetrazolium bromide (MTT) dye reduction assay was utilized, which requires the conversion of MTT to formazan via mitochondrial enzymes indicating metabolic health (Figure 2.4). Freshly prepared monomers, or fibers grown for 24 hours, were added to the rat pancreatic islet cell line, RIN-5F, at varying concentrations and were allowed to incubate with adherent cells for 24 hours before measuring toxicity. It was found that the fibers exhibited greater toxicity than the monomers by decreasing the cell viability by greater than 40 percent at the highest concentrations used. When monomers and fibers were treated with CurDAc after 24 hours, the toxicities of both were increased in comparison to the non-treated samples. The toxicity of fibers increased by about 15 percent when disaggregated and the monomers increased upwards of 20 percent for all the concentrations. It is interesting to note that the toxicities of both monomers and fibers treated with CurDAc, exhibited very similar levels of toxicity indicating a level of similarity between the two. The toxicity of CurDAc to its parent compound curcumin was also compared, and it was found that both were nontoxic by the MTT assay (Figure A.12). To corroborate our findings using the MTT assay, the CellTox Green assay was utilized (Figure 2.4 and A.13). This assay was in agreement with MTT results, in which we observed increased toxicity for the peptide that had been treated with CurDAc after 13 hours of incubation. These results indicate co-incubation of hIAPP monomers or fibers with CurDAc promotes the formation of toxic species. Statistical significance calculations were performed using ordinary one-way ANOVA tests with Tukey's multiple comparisons. All values of the comparisons are shown in Table A.3.

2.3 Conclusion

While amyloid aggregation has been extensively studied, the use of small molecules as a chemical biology tool provides advantages to traditional methods of stabilization. This study has shown the potential of CurDAc to act as a peptide-specific chemical probe to study hIAPP and to disrupt fully mature fibers and prevent monomers from forming fibers. This is the first example in the literature of using NMR to follow fiber disruption at atomic resolution which allowed us to identify solvent-exposed residues in the species formed after disaggregation. Most of these residues, which are in the loop regions of known monomer and fiber structures, have distinct chemical shifts. This suggests that these residues are in a new chemical environment and/or structurally distinct and may be part of a larger oligomeric species that is not visible for solution NMR studies. TEM served as a visual confirmation in which the fibers can be seen being broken down upon incubation with equimolar amounts of CurDAc. Notably, these disaggregated species were more toxic than the fibers or monomers to cultured cells. We believe that the results reported in this study can be used to provide a starting point to develop other small molecules for the purpose of amyloid modulation or oligomer characterization. Using tool compounds like CurDAc could provide new avenues to probe and isolate the pathways of oligomer formation, which may lead to further understanding of the toxic oligomer hypothesis.

2.4 Experimental Section

2.4.1 Materials and Reagents

All reagents were purchased from commercial suppliers and used as received unless noted otherwise. $A\beta_{40}$ was purchased from BioBasic (Markham, ON, Canada) at >95% purity and used without further purification. hIAPP was purchased from AnaSpec (Fermont, CA, USA) at >95%

purity and used without further purification unless otherwise noted. Human calcitonin peptide was synthesized via FMOC chemistry as described previously. To ensure consistent monomeric starting conditions, peptides were dissolved in hexafluoroisopropanol (HFIP) at a concentration of 1 mg/ml and then lyophilized for 48 hours. Powders were kept at -80 C until needed for experiments. CurDAc was synthesized in the same method as previously described.[17] All other reagents were purchased from Sigma-Aldrich (St. Louis, MO, U.S.A).

2.4.2 Thioflavin-T Assay.

hIAPP monomer sample was prepared by dissolving the lyophilized peptide either dilute HCl at pH 4 (hIAPP) or buffer (hCT and $A\beta_{40}$) to a stock concentration between 150 – 200 μM, kept at 0 ^{O}C (ice), vortexed for 15 s. and bath sonicated (at 0 ^{O}C) for 1 min. Fresh monomer samples were diluted into Phosphate buffer (pH 7.4) containing 50 mM NaCl for each subsequent experiment. The kinetics of amyloid formation were monitored by the fluorescent, amyloid-specific dye ThT. All samples were prepared by diluting the stock solution to a final concentration of 10 μM in the presence of 20 μM ThT. Samples were plated in triplicate on Corning 96- well plates, maintained at 25 C (hCT and hIAPP) or 37 C ($A\beta_{40}$), and subject to continuous, slow orbital shaking. Fluorescence readings were taken on a Biotek Synergy 2 microplate reader and were read from the bottom with an excitation wavelength of 440 nm (30 nm bandwidth) and an emission wavelength of 485 nm (20 nm bandwidth) at three-minute intervals. For studies exploring fibril remodeling, fibrils were initially formed in the 96-well plate for 24 h. After mature fibrils were formed CurDAc was added directly to wells at varying concentrations, diluting the volume by less than 1% to maintain signal intensity. The experiment was then restarted under identical conditions to those

used to monitor fibril formation. After data acquisition, raw fluorescence values were background subtracted and then normalized.

2.4.3 Circular Dichroism

Single point CD measurements were carried out at a concentration of 40 μM peptide in the absence or presence of varying concentrations of CurDAc. CD measurements were performed on a JASCO J- 1500 CD Spectrometer using a 0.1 cm path length cell. Spectra were acquired at 25 °C using a bandwidth of 2nm, a scan rate of 200 nm/min, and averaging spectra over 5 scans with a smoothing factor of 11. Measurements were taken immediately after mixing the sample (t = 0 h) and after various time points at 25 °C (hIAPP and hCT) or 37 °C ($A\beta_{40}$) under slow orbital shaking (conditions mimicking those used in ThT kinetic assays). hIAPP time course disaggregation experiment was analyzed using BeStSel using the multiple spectra analysis tool with a scaling factor of 10.

2.4.4 Transmission Electron Microscopy

Samples used in TEM analysis were taken directly from the time course CD experiments after 24h incubation (both for the modulation of fiber formation and the remodeling of preformed fibrils). Glow discharged grids (Formar/carbon 200 mesh, Electron Microscopy Sciences, Hatfield, PA, U.S.A.) were treated with samples (7 μL) for 2 min at room temperature. Excess buffer was removed via blotting and then washed three times with dd H2O. Each grid was then incubated with uranyl acetate staining solution (1% w/v in ddH2O, 7 μL) for 1 min, and excess stain was blotted away. Images from each sample were taken on a JEOL 1400-plus TEM (80 kV) at 12,000x magnification.

2.4.5 Cell Toxicity Experiments

RIN-5F(ATCC# CRL-2058 batch number 61465080) cells were grown in RPMI-1640 media with 2 mM L-glutamine supplemented with 10% fetal bovine serum in a humidified incubator at 37 °C with environment of 5% CO2. Cells were kept between passage numbers below 25. 10-cm cell culture dishes were used for culturing, and 96 flat bottom well trays for the MTT assays. Cells were plated at 50,000 cells per well in 90 μL and were allowed to adhere for 24 hours.

To prepare hIAPP fibrils to be used in cell toxicity experiments, lyophilized hIAPP monomer was solubilized in Milli-Q water brought to pH 4 using HCl and diluted to appropriate concentration using 20 mM Phosphate buffer (pH 7.4) containing 50 mM NaCl. Peptide was then treated with 1 equivalent of CurDAc. Peptide was incubated for 24 hours at room temperature with shaking at 750 rpm to form fibrils. Monomer was freshly dissolved in the same manner and then diluted in buffer. 10-fold stocks of peptide were added to each well at 10 μL for a final volume of 100 μL. After 24-h incubation of cells with aggregates, the MTT cell proliferation assay (Promega, G4000) was used to determine the toxicity of samples following the manufacturer protocol. 10 μL of the MTT dye solution was added to each well and set to incubate at 37 °C for 3-3.5 hours. 100 μL of stop solution was added and set to incubate for 12 hours. The absorbance of each well as then measured at both 570 nm and 700 nm (700 nm for background correction). All cellular viability values were normalized to cells treated with buffer. Values reported are the average of five independent trials and the error is reported as the standard deviation of these averages.

CellTox Green Cytotoxicity experiments were performed as per the manufacturer's suggestions (Promega G8741). Cells were plated at 50,000 cells per well in a 96 well plate. Peptide and compounds were prepared and added in the same manner as the MTT assay above. Immediately

after the addition, the plate was put in a FLUOstar omega plate reader equipped with an atmospheric control unit kept at 37 °C with 5% CO_2 and 20%O_2. The plate was read every 10 minuets at 485ex/520em. All cellular toxicity values were normalized to cells treated with buffer. Values reported are the average of three independent trials and the error is reported as the standard deviation of these averages. Ordinary one-way ANOVA tests with Tukey's multiple comparisons were performed.

2.4.6 NMR Experiments

All NMR experiments were performed at 25 °C, employing Bruker Avance 500 and 850 MHz spectrometers, equipped with cryogenic probes. Referencing of the proton chemical shifts to the water resonance frequency, the ^{15}N and ^{13}C shifts were referenced indirectly. Almost complete backbone assignments were obtained using triple resonance assignment experiments helped from Non Uniform Sampling approach.[54,55] NMR spectra were processed using the software TopSpin (Bruker). Spectra were analyzed using ccpNMR analysis.[56] CSPs were calculated in respect to each nuclei. [57] The signal intensity of disaggregation experiments were found by taking the intensity of the final FID and normalizing it as maximal amount dissolved over a course of the experiments.

NMR Sample preparation Lyophilized powder of the recombinant human IAPP(1-37) produced as mentioned in our previous protocol was dissolved into NMR buffer (30 mM deuterated acetic acid buffer, pH 5.3) to yield a final peptide concentration of maximal 100 μM.[58] For the case of phosphate buffer or the powder was dissolved in 100 μL of the acetate buffer and diluted until 500 μL with the buffer selected. Phosphate buffer contain 50 mM sodium phosphate with pH 7.4 and 50mM sodium chloride was added when this was necessary. The solution was supplemented with

10 % D_2O. The samples were measured and stored at 25 °C. For the NMR sample of the fibrils, the peptide was initially dissolved in 30 mM deuterated acetic acid, pH 5.3. To prepare the peptide, the solution was mixed with phosphate buffer contain NaCl at pH 7.4 and the sample was incubated for approximately 12 h at room temperature. The CurDAc Solution was prepared into water to a high concentration of 10 mM and mixed with the IAPP as required. The sample was transferred in a NMR tube for solution-state NMR measurements.

2.4.7 Isothermal Titration Calorimetry

Isothermal titration calorimetric experiments were performed with a VP-ITC instrument (Marvern Instrument, UK). The concentrations of CurDAc in the ITC syringe was 1mM for fiber experiments or 500 μM for monomer experiments. The concentration hIAPP was 30 μM and $A\beta_{40}$ was 100 μM in the ITC cell. 10 mM phosphate buffer (pH 7.4) with 100 mM NaCl was used. Titration experiments consisted of 19 injections spaced at 300/600 s intervals for fibers and 100s interval for monomer. Injection volume and injection duration was 0.2 μl for 0.4s and 2 μl for 4 sec. fibers were stirred at 1000 rpm and monomer at 750 rpm with reference power of 5 μcal/sec

2.5 Acknowledgements

This study was supported by the funds from the National Institutes of Health (AG048934 to A.R.). We thank Professor Akira Naito for providing us the synthetic calcitonin peptide. We thank Dr. Katherine Gentry and Dr. Vojč Kocman for their careful edits of this manuscript. The content is solely the responsibility of the authors and does not necessarily represent the official views of the National Institutes of Health.

2.6 References

1. Hardy, J. The Amyloid Hypothesis of Alzheimer's Disease: Progress and Problems on the

Road to Therapeutics. Science (80-.). **297**, 353–356 (2002).

2. Benilova, I., Karran, E. & De Strooper, B. The toxic Aβ oligomer and Alzheimer's disease: an emperor in need of clothes. Nat. Neurosci. **15**, 349–357 (2012).

3. Chiti, F. & Dobson, C. M. Protein Misfolding, Functional Amyloid, and Human Disease. Annu. Rev. Biochem. **75**, 333–366 (2006).

4. Nagel-Steger, L., Owen, M. C. & Strodel, B. An Account of Amyloid Oligomers: Facts and Figures Obtained from Experiments and Simulations. ChemBioChem **17**, 657–676 (2016).

5. Tipping, K. W., van Oosten-Hawle, P., Hewitt, E. W. & Radford, S. E. Amyloid Fibres: Inert End-Stage Aggregates or Key Players in Disease? Trends Biochem. Sci. **40**, 719–727 (2015).

6. Hamley, I. W. The amyloid beta peptide: a chemist's perspective. Role in Alzheimer's and fibrillization. Chem. Rev. **112**, 5147–92 (2012).

7. Härd, T. & Lendel, C. Inhibition of Amyloid Formation. J. Mol. Biol. **421**, 441–465 (2012).

8. LeVine, H. & Walker, L. C. What amyloid ligands can tell us about molecular polymorphism and disease. Neurobiol. Aging **42**, 205–212 (2016).

9. Ladiwala, A. R. A., Dordick, J. S. & Tessier, P. M. Aromatic Small Molecules Remodel Toxic Soluble Oligomers of Amyloid through Three Independent Pathways. J. Biol. Chem. **286**, 3209–3218 (2011).

10. Reinke, A. A. & Gestwicki, J. E. Insight into Amyloid Structure Using Chemical Probes. Chem. Biol. Drug Des. **77**, 399–411 (2011).

11. Cao, P. & Raleigh, D. P. Analysis of the Inhibition and Remodeling of Islet Amyloid Polypeptide Amyloid Fibers by Flavanols. Biochemistry **51**, 2670–2683 (2012).

12. Schürmann, M., Janning, P., Ziegler, S. & Waldmann, H. Small-Molecule Target Engagement in Cells. Cell Chem. Biol. **23**, 435–441 (2016).

13. Khera, N. & Rajput, S. Therapeutic Potential of Small Molecule Inhibitors. J. Cell. Biochem. **118**, 959–961 (2017).

14. Copeland, R. A. & Boriack-Sjodin, P. A. The Elements of Translational Chemical Biology. Cell Chem. Biol. **25**, 128–134 (2018).

15. Young, L. M., Ashcroft, A. E. & Radford, S. E. Small molecule probes of protein aggregation. Curr. Opin. Chem. Biol. **39**, 90–99 (2017).

16. Retooling chemical probes. Nat. Chem. Biol. **6**, 157–157 (2010).

17. Pithadia, A. S. et al. Influence of a curcumin derivative on hIAPP aggregation in the absence and presence of lipid membranes. Chem. Commun. **52**, 942–945 (2016).

18. Meisl, G. et al. Molecular mechanisms of protein aggregation from global fitting of kinetic models. Nat. Protoc. **11**, 252–272 (2016).

19. Crespo, R. et al. What Can the Kinetics of Amyloid Fibril Formation Tell about Off-pathway Aggregation? J. Biol. Chem. **291**, 2018–2032 (2016).

20. Prade, E. et al. Sulindac Sulfide Induces the Formation of Large Oligomeric Aggregates of the Alzheimer's Disease Amyloid-β Peptide Which Exhibit Reduced Neurotoxicity. Biochemistry **55**, 1839–1849 (2016).

21. Young, L. M. et al. Screening and classifying small-molecule inhibitors of amyloid formation using ion mobility spectrometry–mass spectrometry. Nat. Chem. **7**, 73–81 (2015).

22. Citron, M. Alzheimer's disease: strategies for disease modification. Nat. Rev. Drug Discov. **9**, 387–398 (2010).

23. Solomon, B., Koppel, R., Frankel, D. & Hanan-Aharon, E. Disaggregation of Alzheimer beta-amyloid by site-directed mAb. Proc. Natl. Acad. Sci. U. S. A. **94**, 4109–12 (1997).

24. Baker, J. D. et al. Human cyclophilin 40 unravels neurotoxic amyloids. PLOS Biol. **15**, e2001336 (2017).

25. Song, Y., Moore, E. G., Guo, Y. & Moore, J. S. Polymer-Peptide Conjugates Disassemble Amyloid β Fibrils in a Molecular-Weight Dependent Manner. J. Am. Chem. Soc. **139**, 4298–4301 (2017).

26. Zhu, D., Gong, G., Wang, W. & Du, W. Disaggregation of human islet amyloid polypeptide fibril formation by ruthenium polypyridyl complexes. J. Inorg. Biochem. **170**, 109–116 (2017).

27. Qu, A. et al. The synergistic effect between KLVFF and self-assembly chaperones on both disaggregation of beta-amyloid fibrils and reducing consequent toxicity. Chem. Commun. **53**, 1289–1292 (2017).

28. Takahashi-Ito, K., Makino, M., Okado, K. & Tomita, T. Memantine inhibits β-amyloid aggregation and disassembles preformed β-amyloid aggregates. Biochem. Biophys. Res. Commun. **493**, 158–163 (2017).

29. Wang, Q., Ning, L., Niu, Y., Liu, H. & Yao, X. Molecular Mechanism of the Inhibition and Remodeling of Human Islet Amyloid Polypeptide (hIAPP 1–37) Oligomer by Resveratrol from Molecular Dynamics Simulation. J. Phys. Chem. B **119**, 15–24 (2015).

30. Wang, Q. et al. Tanshinones Inhibit Amyloid Aggregation by Amyloid-β Peptide, Disaggregate Amyloid Fibrils, and Protect Cultured Cells. ACS Chem. Neurosci. **4**, 1004–1015 (2013).

31. Groenning, M. Binding mode of Thioflavin T and other molecular probes in the context of amyloid fibrils—current status. J. Chem. Biol. **3**, 1–18 (2010).

32. Brender, J. R. et al. Membrane disordering is not sufficient for membrane permeabilization by islet amyloid polypeptide: studies of IAPP(20–29) fragments. Phys. Chem. Chem. Phys. **15**, 8908 (2013).

33. Suzuki, Y. J. et al. Structural and dynamic membrane properties of .alpha.-tocopherol and .alpha.-tocotrienol: Implication to the molecular mechanism of their antioxidant potency. Biochemistry **32**, 10692–10699 (1993).

34. Bellomo, G. et al. Aggregation kinetics of the Aβ1–40 peptide monitored by NMR. Chem. Commun. **54**, 7601–7604 (2018).

35. Soong, R., Brender, J. R., Macdonald, P. M. & Ramamoorthy, A. Association of Highly Compact Type II Diabetes Related Islet Amyloid Polypeptide Intermediate Species at Physiological Temperature Revealed by Diffusion NMR Spectroscopy. J. Am. Chem. Soc. **131**, 7079–7085 (2009).

36. Brender, J. R. et al. Probing the Sources of the Apparent Irreproducibility of Amyloid Formation: Drastic Changes in Kinetics and a Switch in Mechanism Due to Micellelike Oligomer Formation at Critical Concentrations of IAPP. J. Phys. Chem. B **119**, 2886–2896 (2015).

37. Jha, S. et al. PH dependence of amylin fibrillization. Biochemistry **53**, 300–310 (2014).

38. Schieborr, U. et al. How much NMR data is required to determine a protein-ligand complex structure? ChemBioChem **6**, 1891–1898 (2005).

39. Rodriguez Camargo, D. C. et al. The redox environment triggers conformational changes and aggregation of hIAPP in Type II Diabetes. Sci. Rep. **7**, 44041 (2017).

40. Brender, J. R., Hartman, K., Reid, K. R., Kennedy, R. T. & Ramamoorthy, A. A Single Mutation in the Nonamyloidogenic Region of Islet Amyloid Polypeptide Greatly Reduces Toxicity †. Biochemistry **47**, 12680–12688 (2008).

41. Brender, J. R. et al. Zinc stabilization of prefibrillar oligomers of human islet amyloid polypeptide. Chem. Commun. **49**, 3339 (2013).

42. Wiltzius, J. J. W. et al. Atomic structure of the cross-beta spine of islet amyloid polypeptide (amylin). Protein Sci. **17**, 1467–74 (2008).

43. Berjanskii, M. V & Wishart, D. S. A Simple Method To Predict Protein Flexibility Using Secondary Chemical Shifts. J. Am. Chem. Soc. **127**, 14970–14971 (2005).

44. Marsh, J. A., Singh, V. K., Jia, Z. & Forman-Kay, J. D. Sensitivity of secondary structure propensities to sequence differences between α- and γ-synuclein: Implications for fibrillation. Protein Sci. **15**, 2795–2804 (2006).

45. Kotler, S. A. et al. High-resolution NMR characterization of low abundance oligomers of amyloid-β without purification. Sci. Rep. **5**, 11811 (2015).

46. Wang, J. et al. Real-time monitoring of the aggregation of Alzheimer's amyloid-β via 1 H magic angle spinning NMR spectroscopy. Chem. Commun. **54**, 2000–2003 (2018).

47. Mishra, R., Geyer, M. & Winter, R. NMR spectroscopic investigation of early events in IAPP amyloid fibril formation. ChemBioChem **10**, 1769–1772 (2009).

48. Brender, J. R. et al. Probing the Sources of the Apparent Irreproducibility of Amyloid Formation: Drastic Changes in Kinetics and a Switch in Mechanism Due to Micellelike Oligomer Formation at Critical Concentrations of IAPP. J. Phys. Chem. B **119**, 2886–2896 (2015).

49. Rodriguez Camargo, D. C. et al. Stabilization and structural analysis of a membrane-associated hIAPP aggregation intermediate. Elife **6**, e31226 (2017).

50. Luca, S., Yau, W.-M., Leapman, R. & Tycko, R. Peptide Conformation and Supramolecular Organization in Amylin Fibrils: Constraints from Solid-State NMR †. Biochemistry **46**, 13505–13522 (2007).

51. Fawzi, N. L., Ying, J., Ghirlando, R., Torchia, D. A. & Clore, G. M. Atomic-resolution dynamics on the surface of amyloid-β protofibrils probed by solution NMR. Nature **480**, 268–272 (2011).

52. Mielke, S. P. & Krishnan, V. V. Characterization of protein secondary structure from NMR chemical shifts. Prog. Nucl. Magn. Reson. Spectrosc. **54**, 141–165 (2009).

53. Micsonai, A. et al. Accurate secondary structure prediction and fold recognition for circular dichroism spectroscopy. Proc. Natl. Acad. Sci. **112**, E3095–E3103 (2015).

54. Sattler, M. Heteronuclear multidimensional NMR experiments for the structure determination of proteins in solution employing pulsed field gradients. Prog. Nucl. Magn. Reson. Spectrosc. **34**, 93–158 (1999).

55. Billeter, M. Non-uniform sampling in biomolecular NMR. J. Biomol. NMR **68**, 65–66 (2017).

56. Vranken, W. F. et al. The CCPN data model for NMR spectroscopy: Development of a software pipeline. Proteins Struct. Funct. Genet. **59**, 687–696 (2005).

57. Williamson, M. P. Using chemical shift perturbation to characterise ligand binding. Prog. Nucl. Magn. Reson. Spectrosc. **73**, 1–16 (2013).

58. Rodriguez Camargo, D. C. et al. Cloning, expression and purification of the human Islet Amyloid Polypeptide (hIAPP) from Escherichia coli. Protein Expr. Purif. **106**, 49–56 (2015).

Chapter 3

High Throughput Screening at the Membrane Interface Reveals New Inhibitors of Amyloid-β

The content for this chapter will be included in the following reference:

> Cox, S.J., Lam, B., Prasad, A., Marietta, H.A., Stander, N.V., Joel, J.G., Sahoo, B.R., Guo, F., Stoddard, A.K., Ivanova, M.I., Ramamoorthy, A. High Throughput Screening at the Membrane Interface Reveals New Inhibitors of Amyloid-β. Submitted

3.1 Introduction

Alzheimer's disease (AD) is a deadly and debilitating ailment that currently affects 50 million people worldwide.[1] Early research into AD focused on the presence of indicative protein amyloid-beta (Aβ) fibrils due to their prominence in postmortem examination of patients' brains. However, it is now hypothesized that small, toxic, intermediate species, known as oligomers, are the predominant toxic amyloid-beta ($A\beta_{40}$) species in AD.[2] Aβ peptides are produced from the cleavage of amyloid precursor protein (APP) in the extracellular membrane by β and γ-secretases. Cellular membranes have been implicated to be a site of potential toxicity and can act as a catalyst for amyloid aggregation.[3] Some oligomers are proposed to impart their toxic function by interacting directly with the cell membrane of neurons then disrupting and permeabilizing the membrane. As a result, non-selective ion channels and large pores are created which, in turn, ablate the charge gradient necessary for neuronal function.[4] Many studies suggest that lipid membranes are able to accelerate the aggregation of Aβ as well as facilitate the formation of unique structures of Aβ species that are specific to lipid bilayer disruption.[5]

There has been extensive investigation into small molecules with the ability to modulate the aggregation of Aβ in solution.[6] However, the search for modulators of Aβ aggregation has relied heavily on serendipity; often times, a novel class of inhibitors is accidentally discovered, and improved analogues are subsequently synthesized.[7] Relying on accidental discoveries is unlikely to generate a diverse enough chemical portfolio to successfully generate a drug candidate that can demonstrate clinical efficacy. Thus, it is essential to identify new and novel chemical species which may be specifically capable of modulating membrane-assisted $A\beta_{40}$ aggregation for use as toxic Aβ oligomer probes.[2] Here, through the usage of a small molecule library, 5 compounds have been identified that modulate the formation of $A\beta_{40}$ aggregates in the presence of lipid membrane. These small molecules represent an avenue for the development and further investigation of $A\beta_{40}$ and membrane interactions.

3.2 Results and Discussion

Using a library of over 1,800 compounds, selected for their chemical diversity and biological activity, the screening was performed by the addition of $A\beta_{40}$ in the presence of large unilamellar vesicles (LUVs) composed of a mixture of 7:3 molar ratio of DOPC:DOPG, which represents the charge distribution of eukaryotic membranes (Figure 3.1A). To probe the interactions between the lipid bilayer, small molecules, and $A\beta_{40}$, we used a fluorescence readout assay regularly employed in amyloid studies using Thioflavin-T (ThT) dye. ThT assays provide insights into the kinetics of amyloid formation, which facilitates the identification of compounds that are able to inhibit the formation of β-sheet rich amyloid aggregates. Signal intensity can be proportional to the fibers present and decreases in intensity can be indicative of a decrease in overall fiber content (Figure B.1). We optimized screening conditions, achieving a Z-score of 0.46 (Figure 3.1C). 40 reproducible hits were selected after ruling out initially fluorescent compounds

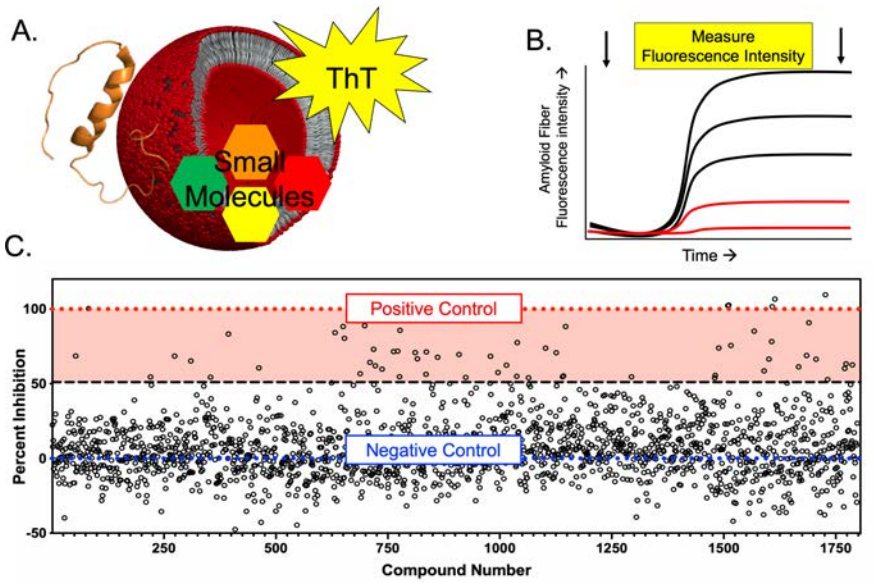

Figure 3.1. (A) An illustration of the components of the screen: $A\beta_{40}$ monomer (2LFM), LUVs, small molecules and ThT. (B) schematic of reading the assay plates before aggregation and then heating and shaking the plates before reading the final fluorescence intensity after 24 hours of incubation. (C) Percent Inhibition as calculated from final fluorescent intensity of every compounded screened for inhibition. Value of twin plates are averaged and normalized in respect to the positive (red line) and negative controls (blue line).

and compounds which did not give a matching read-out in twin sets of plates. These 40 compounds were then used for a concentration response curve (CRC) titration screen to determine the activity of the compounds in a range of concentrations (Figures B.2 and B.3). Results from the CRC screen helped us to narrow down the 40 initial hits to 21 primary hits based on the calculated IC50 values and the exclusion of known compounds with PAINS properties (Figure 3.2, Tables B.1 and B.2).[7] Structural similarities exist among the 21 hit compounds. Many are heterocyclic, planar and contain functional groups capable of hydrogen bonding, properties which have been identified to be important in amyloid modulation. The compounds were given abbreviations based on similarities and functional groups: Anthroquinone/naphthoquinone (AQ), benzendiols (BD), benzofuran (BF) Tetrahydroquinoline (THQ), thiourea (TU), and dihydroquinazolin (DHQ). While some of these compounds have been previously reported as inhibitors of other amyloid peptides, none have been identified to inhibit membrane associated aggregation.

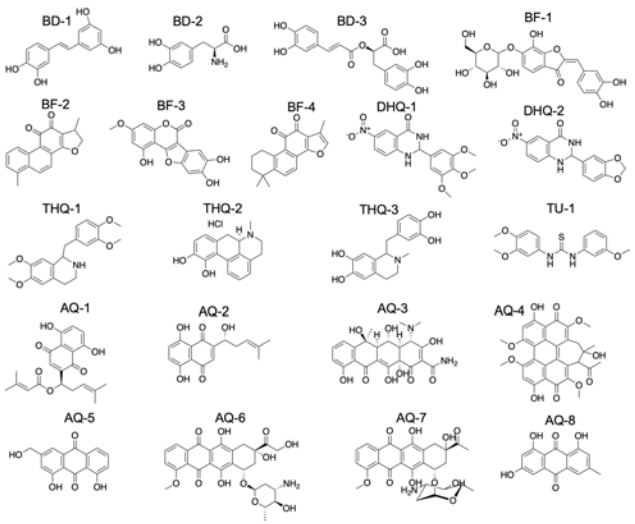

Figure 3.2. 21 primary small molecule hits chosen after initial screen and CRC testing. Compound abbreviations were given based on similarities between functional groups and can be found in Table B.1.

The selected 21 compounds were first subjected to full ThT kinetic profiles with measurements taken every 5 minutes (Figure 3.3). Each compound was tested at 10, 5 and 2 molar equivalents in respect to the concentration of $A\beta_{40}$ while in the presence of 500 μM LUVs. Initially by the ThT assay, many appear to be promising and robust inhibitors, with many compounds negating the aggregation fully at all the concentrations tested. Some interesting kinetic traces were also observed from compounds that didn't inhibit fully i.e. THQ-1, THQ-3, TU-1, DHQ-2 and BF-4. THq-3 and BF-4 extended the lag time at higher concentrations, indicating changes in the primary nucleation steps. TU-1 and DHQ-2 showed a decrease in the final fluorescence intensity but the lag time remained the same, pointing to a change in secondary nucleation. THQ-1 demonstrated interesting kinetics with an increase and decrease in intensity. These unusual kinetics could indicate that THQ-1 has preferential interactions with amyloid fibers, acting like a disaggregator, or that the structure of the aggregates is ThT active but then evolves into something that is no longer able to bind to ThT.

However, as critical as the ThT assay is to studying amyloid aggregation, it is also subject to fluorescent quenching, overlap, or displacement by other compounds. Because of this, secondary confirmation not relying on fluorescence was performed to further narrow down the hit compounds. To do this we used the dot blot assay utilizing the OC anti-amyloid fiber antibody, which is known to bind to the general amyloid fiber β-sheet epitope (Figures 3.4 and B.4).[9] While many of the compounds looked to be complete inhibitors by the ThT assay, the strong antibody reactivity observed for $A\beta_{40}$ in the presence of 7 out of the 21 compounds indicated that they do

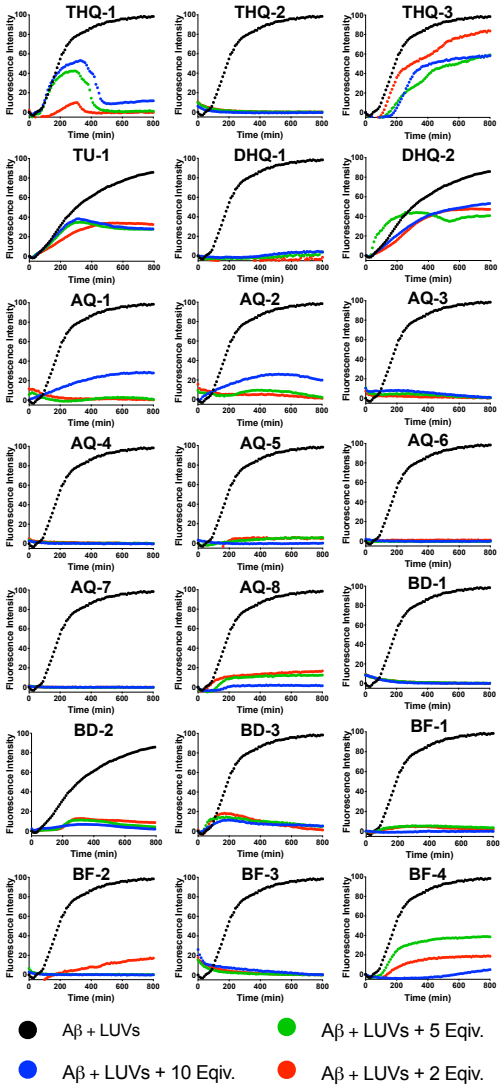

Figure 3.3. ThT fluorescence kinetics for the 21 selected compounds from CRC testing. 10 μM $A\beta_{40}$ was mixed with varying concentrations of small molecule (10, 5, & 2 equivalents) and 500 μM LUVs in 20 mM phosphate 50 mM NaCl buffer at 37 °C with slow shaking.

not inhibit fiber formation. After identifying compounds that interfere with ThT, we then examined the compounds that gave 50% or less reactivity by the dot blot assay by examining them via Transmission Electron Microscopy (TEM) (Figure 3.4). We also selected a single compound, BD-3, to validate that the OC antibody did not give a false positive response, and saw fibers on the grid. Out of the 15 compounds investigated, 5 of them inhibited $A\beta_{40}$ fibers, thus AQ-4, THQ-1, BF-3, DHQ-1 and DHQ-2, were selected for a deeper investigation. THQ-1, DHQ-1 and BF-3 were more uniform in the appearance of the aggregates while DHQ-2 and AQ-4 looked amorphous. Of the other 9 compounds that had fiber formation identified at this stage, many of

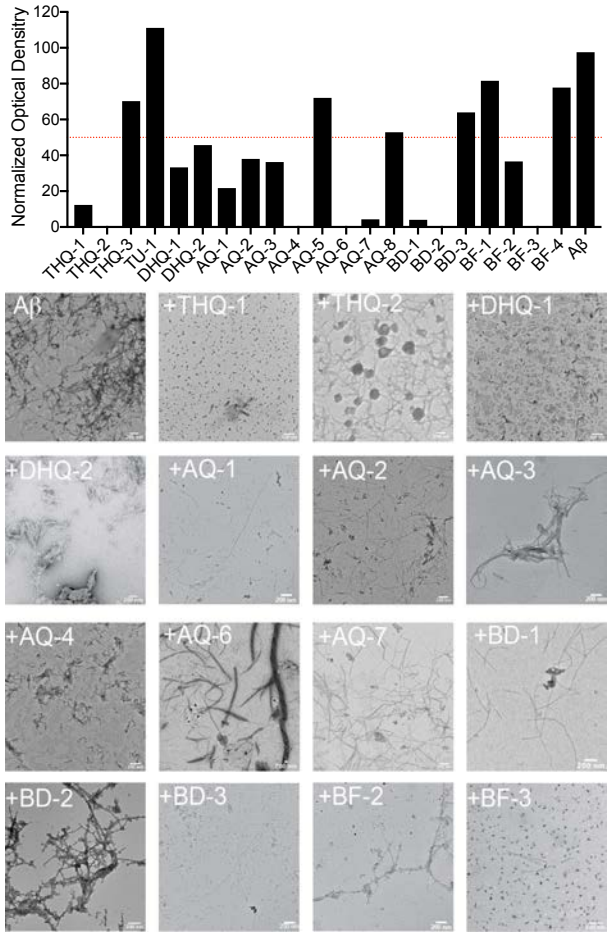

Figure 3.4. (Top) Signal intensities from the dot blot assay using the OC antibody. Samples were measured after ThT experiments with 5 equivalents of a compound in respect to $A\beta_{40}$. Red line indicates 50% signal. (Bottom) TEM images of compounds that gave less than 50% antibody reactivity from the dot blot assay. Samples were measured after ThT experiments with 5 equivalents of a compound in respect to $A\beta_{40}$. Scale bar is 200 nm.

them exhibited very interesting and distinct fiber morphologies, which could be of interest for further investigation, as some of them have been reported to be amyloid inhibitors in the absence of membrane. Some of them appeared to produce fibers that were unbranched and highly uniform (AQ-1, AQ-2, AQ-7, and BD-1) Other showed less ordered morphologies, with attributes such as branching or amorphous aggregates attached to the outside of the fibers (THQ-1, AQ-3, BD-2, and BF-2). Investigations into these structures may prove fruitful in understanding both the binding selectivity's of ThT and the OC antibody, since these 9 compounds have generated fiber structures that are invisible to both of these techniques.

Understanding the secondary structure transitions is important for amyloid investigation, as there is a known shift from a random-coil monomer to β-sheet fiber. To study the compounds' effects on Aβ secondary structure, the 5 non-water-soluble compounds were incorporated in the lipid bilayer, which was confirmed by UV-Vis (Figure B.5). Upon incorporation of the compounds in the LUVs at a 10:1 lipid to compound molar ratio, we monitored the Aβ structural transitions by circular dichroism (CD) experiments as well as by ThT kinetics (Figures 3.5 and B.6). After 22 hours, AQ-4 and BF-3 still exhibited a random-coil structure. DHQ-2 and THQ-1 showed a minor

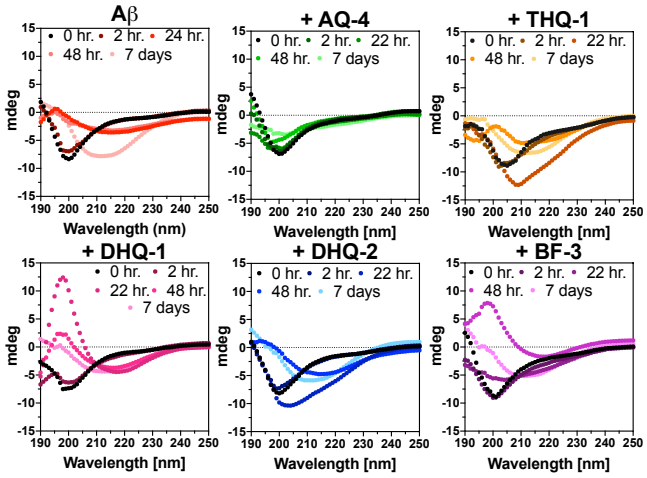

Figure 3.5. CD spectra of 25 μM $A\beta_{40}$ in the presence of 500 μM of compound loaded LUVs from 0 hours – 7 days.

helical conformation, while DHQ-1 showed a strong β-sheet conformation for Aβ. Up to 7 days, AQ-4 maintained random-coil conformation, whereas BF-3, DHQ-1, and DHQ-2 showed β-sheet conformation. THQ-1, however, showed poor signal and showed some slight β-sheet characteristics for Aβ was not fully interpretable at 48 hours, but appeared more clearly β-sheet after 7 days.

Using NMR, we investigated the interaction of $A\beta_{40}$ with the 5 compounds both with and without the presence of loaded LUVs using SOFAST-HMQC experiments (Figures 3.6 and B.7). This experiment is useful in determining the level of peptide aggregation (or monomer depletion) in solution. Because large aggregates such as amyloid fibers tumble slowly on the NMR timescale, they do not contribute to the observed signal and any signal is conferred to be fast tumbling oligomers or monomers. The signal to noise ratios, volume and line width of each peak as were analyzed (Figures 3.6 and B.7). In the presence of LUVs, $A\beta_{40}$ showed 21 well-resolved peaks at time zero. After 24 hours, many of the peaks remained visible, but with decreased signal to noise intensities, indicating a depletion of monomers in solution via aggregation or binding to LUVs. Many of the peaks also broadened at 24 hours, another sign of aggregation. At 96 hours, almost all peaks had become invisible on the spectra and with very poor signal to noise ratio. For all 5 compound samples, NMR spectra showed the same $A\beta_{40}$ peaks as the control, however THQ-1 exhibited poor S/N. After 24 hours a decrease in the S/N ratio can be seen for all 5 samples, but notably THQ-1 had no detectable signals remaining. After 96 hours, DHQ-1 DHQ-2 and AQ-4 still maintained good signal to noise ratio in comparison to the 0 hour and 24-hour time point. The BF-3 S/N continued to decrease at 96 hours indicating the $A\beta_{40}$ in this sample either aggregated the most in comparison or had the greatest amount that bound to the LUVs and no longer was

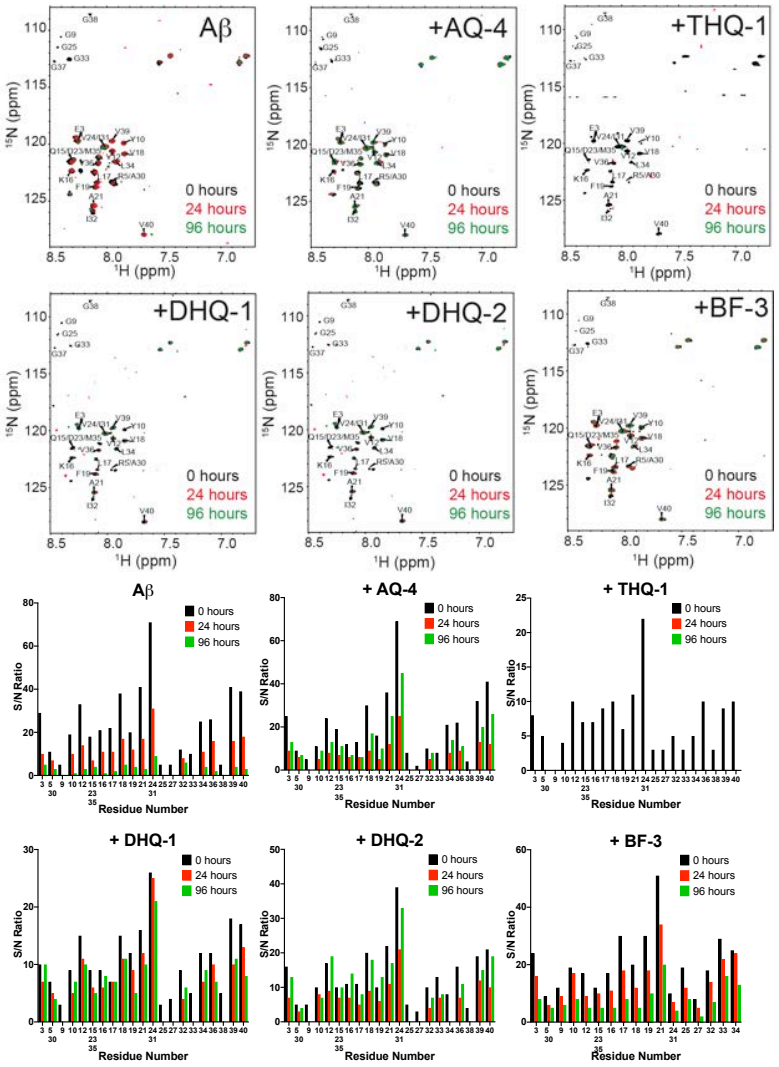

Figure 3.6. (Top) SOFAST-HMQC NMR spectra of 25 μM ^{15}N- Aβ$_{40}$ in the presence of 500 μM of compound loaded LUVs at 0 (black), 24 (red) and 96 hours (green). **(**Bottom**)** Signal to noise ratios taken from spectra at 0, 24 and 96 hours.

tumbling freely. AQ-4 showed a significant increase in linewidth after at 24 and 96 hours in comparison to the control. BF-3 also showed an increase in linewidth at 24 hours, but then decreased below the control after 96 hours. DHQ-1 and DH-2 showed minor changes in linewidth but overall maintained the same linewidths at all timepoints. It is also probable that some of the signal loss and changed in linewidth could be due to the binding of Aβ$_{40}$ to the 100 nm LUVs. This binding could cause the loss in signal intensity due to the decreased tumbling rate of the very large

LUV. Investigations utilizing smaller membrane mimetics such as nanodiscs and implementing paramagnetic quenching could be an enlightening next step to understand these systems.

Experiments in the absence of LUVs were also performed in order to investigate the compound interactions on $A\beta_{40}$ itself (Figures B.8-B.10). After 96 hours the control sample of $A\beta_{40}$ alone the S/N ratio was very poor, and only residue V39 was visible via linewidth and peak volume. The sample with THQ-1, well resolved peaks of $A\beta_{40}$ were seen at all time points, opposite of what was seen with lipids. This indicates that THQ-1 interacts and inhibits $A\beta_{40}$ aggregation but does not interact well in the presence of lipids, at least when loaded with lipids, since it appeared to be a strong inhibitor in the assays prior to loading the compounds in LUVs. Samples of $A\beta_{40}$ with AQ-4, DHQ-1 and DHQ-2 all showed decreased S/N ratio and peak volume after 96 hours in comparison to the samples with LUVs. The $A\beta_{40}$ sample with BF-3 remained comparable to the sample with LUVs in S/N ratio and peak volume. All 5 sample with compounds showed increases in linewidths for all 5 samples after 96 hours, indicative of slower to tumbling of these residues due to binding via protein-protein interactions or the protein ligand interactions.

After the NMR measurements, the samples in presence of lipids were analyzed using Size Exclusion Chromatography (SEC) (Figures 3.7 and B.11). Three distinct peak areas were seen and the area under each curve was quantified to determine the distribution of aggregates within the

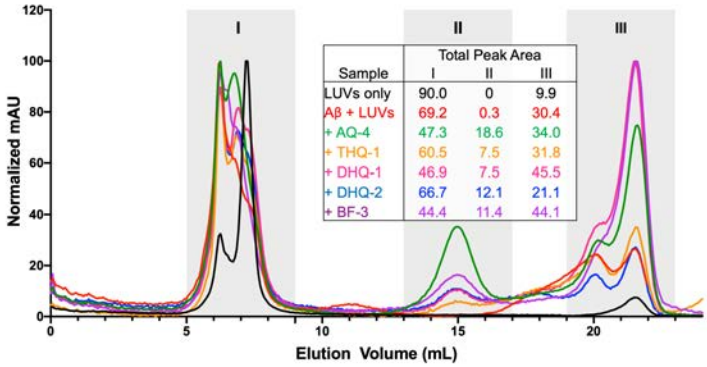

Figure 3.7. (Top) Size exclusion chromatography of $A\beta_{40}$ NMR samples in the presence of compound loaded LUVs. Normalized area under the curve of each peak area was measured for all samples.

sample. Peak area 1 (between 5 and 8 mL) consisted of multiple peaks most likely made up of LUVs and $A\beta_{40}$ amyloid fibers. Peak area 2 (15 mL) most possibly corresponds to an oligomer of 4 monomers (~17 kDa) or an oligomer of 3 monomers with each bound to 2 compounds (~16 kDa). Lastly, Peak area 3 could correspond to monomer and dimer of $A\beta_{40}$, eluting at 21.5 and 20 mL respectively. Since, these samples contain lipids, it is possible that a portion of the intensity of the peaks is also lipids that have been fragmented from the LUVs. For AQ-4, DHQ-1 and BF-3, over 50% of the eluted sample was either in peak area 2 or 3, indicating the presence of a small amount of fibers. While the control, THQ-1, and DHQ-2 samples had 60% or more of the total signal in peak area 1. The control samples showed no signal inside of peak area 2. Additionally, there was a very small peak seen at 11 mL which could indicate a very large oligomer or protofibers. Inside peak area 1, three distinct peaks were observed: one for LUVs at 7.5 mL, one for fibers at 6.5 mL, and in between them; there is also a less resolved peak that may be $A\beta_{40}$ bound to LUVs, which is also not well resolved with the control sample of $A\beta_{40}$ in LUVs. For the control LUVs sample, a small percentage of the total sample eluted in peak area 3, which could correspond to small lipid micelles. This could indicate that some of the signal in the other samples may also

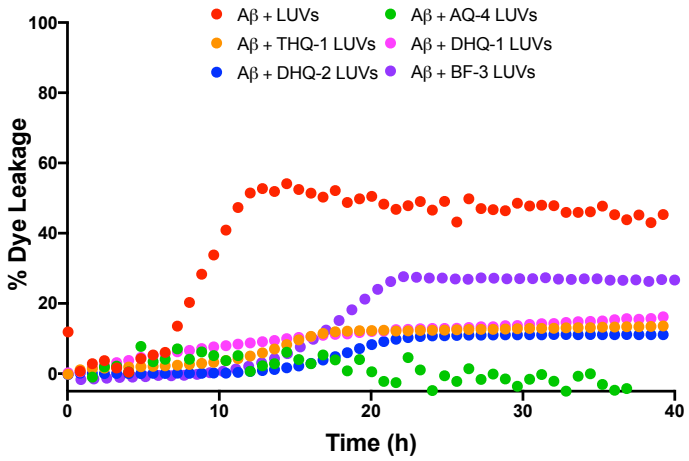

Figure 3.8 Dye leakage experiments using compound loaded LUVs filled with 6-carboxyfluorscin. Dye leakage was measured in 20 mM phosphate 50 mM NaCl buffer at 37 °C with slow shaking over 40 hours. Percentage of dye released was determined after LUV lysis with triton-X.

contain micelles or lipids that have been fragmented from the bilayer as the result of the peptide aggregation on the membrane.

Since A β_{40} has been shown to cause pore formation and fragmentation of the lipid bilayer it is useful to know if the compounds change this proposed mechanism of toxicity. To investigate how the incorporation of the compounds changes the interactions with the lipid bilayer, we performed a dye leakage assay using lipid vesicles loaded with the 5 compounds filled with 6-carboxyfluroescien (Figure 3.8). As previously seen, $A\beta_{40}$ caused significant dye leakage (50%) of vesicles composed of 7:3 DOPC:DOPG lipids, indicating that the peptide is disrupting the lipid bilayer during its aggregation. It is interesting to note that the lag time of the dye leakage is longer than that of the ThT assays of the loaded vesicles (Figure B.6). This extended lag time may indicate and importance of the fiber mediated fragmentation of the vesicles. Loaded vesicles with the 5 compounds all caused less dye leakage than the control. DHQ-1, DHQ-2 and THQ-1 all showed final dye leakage intensities around 15%, indicating a partial blockage of membrane disruption by $A\beta_{40}$. AQ-4 showed very little dye leakage, while BF-3 showed the most. BF-3 loaded vesicles final dye leakage intensity was almost 30% double the dye leakage of the other inhibitors. The lag time of the dye leakage is also extended in comparison to the control in which the control is ~5 hours and the BF-3 vesicles are ~15 hours. These finding are quite fascinating when in conjunction with all the other biophysical data.

3.3 Conclusion

A high-throughput screen has led to the identification of 5 membrane active $A\beta_{40}$ amyloid inhibitors, with a brief summary in Table 1. Among them, DHQ-1, DHQ-2 and THQ-1 were found to be the least robust as shown by NMR, SEC and CD results, whereas BF-3 and AQ-4 exhibited the most evidence that they are able to stop the aggregation (or trap the aggregates) at the

membrane interface. AQ-4 showed the highest ratio of oligomers by SEC, a constant random-coil signal from CD as well as maintaining good signal intensity in samples with and without membrane. This could indicate that even though AQ-4 interacts with the membrane, it is also able to directly interact with $A\beta_{40}$.. AQ-4 also showed the least amount of dye leakage. Perhaps this is due to the fact that it seems to maintain its random coil structure and it could be possible that while it is interacting with the membrane surface, it is superficially interacting and not able to penetrate the bilayer because of its secondary structure. BF-3 also had interesting results. It showed no aggregation by ThT, appeared beta-sheet by CD, and maintained NMR signal but saw an overall loss in intensity in every residue and showed smaller species by SEC. These observations could indicate that while BF-3 does not allow $A\beta_{40}$ to aggregate, some $A\beta_{40}$ population is still binding to the membrane surface. BF-3 particularly showed the most amount of dye leakage and taking this into consideration with the loss of signal intensity via NMR experiments would indicate that it is binding to the membrane and casing pore formation. While DHQ-1 DHQ-2 and THQ-1 are less membrane active, they are still novel scaffolds for the inhibition of $A\beta_{40}$. Although DHQ-1 and DHQ-2 showed some differences in activity, they may be a good starting point for developing derivatives. Given their similar architecture and sites for potential for synthesis, they could be used in an interesting study for structure activity relationship (SAR) analysis. The initial investigation and subsequent rule out of THQ-1 demonstrates the need for deep characterization for amyloid and small molecule interactions.

Given AQ-4 and BF-3 parallels in membrane activity, it is possible that this may be due to their planar structure and lack of free rotation among the aromatic groups. However, many compounds initially investigated as part of the 21 primary hits also had this feature but produced

Compound	Biophysical Technique						
	ThT	CD	NMR	Dot Blot	TEM	SEC	Dye Leakage
AQ-4 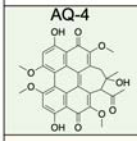	Complete inhibition	Random coil	Peaks remain visible, high S/N ratio at 96 h.	No binding	Amorphous, no fibers	>50% in peaks II/III	>10%
THQ-1 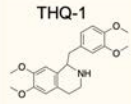	Abnormal curve	Weak beta sheet /mixture	No visible peaks	15% binding	Small particles, few fibers	>60% in peak I	15%
DHQ-1 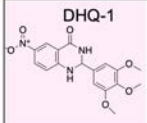	Complete inhibition	Beta sheet	Peaks remain visible, high S/N ratio at 96 h.	30% binding	Small particles, few fibers	>50% in peaks II/III	15%
DHQ-2 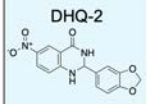	Partial inhibition	Beta sheet	Peaks remain visible, high S/N ratio at 96 h.	40% binding	Amorphous, few fibers	>60% in peak I	15%
BF-3 	Complete inhibition	Beta sheet	Peaks remain visible, S/N ratio decreased at 96 h.	No binding	Small particles, few fibers	>50% in peaks II/III	30%

Table 3.1. Summary of findings using biophysical techniques used to characterize the 5 compounds.

prominent fibers, so clearly there must be unique properties possessed by these two compounds and their interplay between $A\beta_{40}$ and the membrane which render their inhibitory activity. With the presented data as a starting point, NMR would be a robust tool to investigate the structure of the $A\beta_{40}$ in the presence of compounds as well as in conjunction with the membrane.

3.5 Materials and Methods

3.5.1 Screening Protocol

A library of 1,800 compounds were selected from Pilot Prestwick, Navigator Pathways and Maybridge libraries from the Center of Chemical Genomics (CCG) from the University of Michigan High Throughput Screening core facility. Thioflavin-T was selected as the primary read out for the screen and was used at 20 μM final concentration. All reagents were kept on ice until

dispensing onto the plate. The screening was performed using $A\beta_{40}$ expressed in *E.coli* and purified as described elsewhere[23] and was used at a final concentration of 10 μM. Large unilamellar vesicles (LUVs) of a 7:3 mixture of 1,2-dioleoyl-sn-glycero-3-phosphocholine (DOPC) and 1,2-dioleoyl-sn-glycero-3-phospho-(1'-rac-glycerol) (DOPG) were prepared from chloroform stocks and made into lipid films by evaporating chloroform under nitrogen gas and then by lyophilization. Films were then rehydrated into buffer and then extruded to a size of 100 nm and were used at a final concentration of 500 μM. lipids and extruder were purchased from Avanti polar lipids. A buffer of 20 mM Phosphate 50 mM NaCl at pH 7.4 was used in all experiments. The assay was performed in 384 polystyrene plates from corning (product number 3640) with a non-binding surface. Each well was equipped with a single 0.5 mm sterile glass bead that will be added using a custom made bead dispenser from LabTIE, in order to act as a miniature stir rod to overcome the surface tension to ensure sufficient mixing during shaking.[24] Buffer was initially loaded into plates at a volume of 15 μL before adding the compounds dissolved in DMSO at a final concentration of 100 μM using a Biomek FX liquid handling automatic workstation. The remaining buffer, ThT, LUVs and $A\beta_{40}$ were added using Plates Thermo Fischer Mutli Drop Combi to a final volume of 30 μL and then sealed. Initial fluoresce readings were done from each plate at 440ex/480em using a Perkin Elmer 2014 Envision Multilabel plate reader on bottom read setting. After the initial reading, plates were moved to a mutilplate shaker kept inside an incubator set at 37 °C and were shaken for 24 hours at 750 rpm. After 24 hours of heating and shaking the plates fluorescence intensity was measured again. Each compound was added to duplicate plates in order to rule out false positives and to overcome the reproducibility issues among wells often seen with amyloid aggregation assays. After initial hits were identified, the top 40 hits were validated via the same protocol as described; however the compounds were titrated at 8 concentrations between 2-100 μM using TTP Labtech's

Mosquito nanolitre hit picking system. From the concentration response curves (CRC) 21 compounds were selected based on the generated IC50 values and as well as removing compounds known to be PAINS. After the 21 compounds were selected, fresh compounds were bought from manufactures as shown in TableB.1 and dissolved in DMSO. Full kinetic ThT profiles were obtained for each compound at 100, 50 and 20 μM concentrations. Reagents were prepared in the same manner as done in the screen but with using multichannel pipettes in place of robotic handling. Samples were plated in quadruplicates on 384 well plates, maintained at 37 °C and subject to continuous, slow orbital shaking. Fluorescence readings were taken on a Biotek Synergy 2 microplate reader and were read from the bottom with an excitation wavelength of 440 nm (30 nm bandwidth) and an emission wavelength of 485 nm (20 nm bandwidth) at three-minute intervals.

3.5.2 Dot Blot Assay

2 μL from the 50 μM compound containing ThT assay wells were spotted onto the nitrocellulose membrane in duplicate. Wells containing only compound and the LUVs were also spotted for control. Non-specific binding sites were blocked by soaking in 5% BSA in TBS-T for 30 min at RT. The primary Anti-Amyloid Fibrils OC Antibody at a 1:2000 dilution in 5% BSA in TBS-T for 30 min at RT. The membrane was washed with TBS-T (3 x 5 min). Rabbit secondary antibody at a 1:1000 dilution was incubated for 30 min at RT. The membrane was washed with TBS-T (1 x 15 min and 2 x 5 min), and then incubated with ECL reagent for 1 min and sealed. Immediately after ECL reagent incubation, membranes were exposed using X-ray film in a dark room for 30 seconds. Images and intensities of spots were processed using ImageJ software.

3.5.3 Transmission Electron Microscopy

Samples used in TEM analysis were taken directly from ThT experiments on the wells of 5 equivalents of compound after 24h incubation. Glow discharged grids (Formar/carbon 200 mesh, Electron Microscopy Sciences, Hatfield, PA, U.S.A.) were treated with samples (7 μL) for 2 min at room temperature. Excess buffer was removed via blotting and then washed three times with ddH_2O. Each grid was then incubated with uranyl acetate staining solution (1% w/v in ddH_2O, 7 μL) for 1 min, and excess stain was blotted away. Images from each sample were taken on a JEOL 1400-plus TEM (80 kV) at varying magnifications.

3.5.4 Small molecule incorporation into lipids

The 5 compounds were dissolved into chloroform stocks and then added to lipid mixtures in chloroform at a 10:1 lipid to compound molar ratio. The lipid films were made as described above for final concentrations of 50 μM compound within 500 μM lipids. Compounds containing LUVs were extruded and then checked for incorporation using UV-Vis measurements. Extruded solutions appeared clear and maintained clarity for up to 7 days on the bench top.

3.5.5 Circular Dichroism

Single point CD measurements were carried out at 25 μM $A\beta_{40}$ concentration in the presence of 500 μM lipids loaded with 50 μM of compound. CD measurements were performed on a JASCO J- 1500 CD Spectrometer using a 0.1 cm path-length cell. Spectra were acquired at 25 °C using a bandwidth of 2 nm, a scan rate of 200 nm/min, and averaging spectra over 10 scans with a smoothing factor of 13. Measurements were taken immediately after mixing the sample (t = 0 h) and after various time points.

3.5.6 NMR experiments

2D $^{1}H/^{15}N$ SOFAST-HMQC NMR spectra were recorded on a Bruker 800 MHz NMR spectrometer equipped with a 5mm triple resonance inverse detection TCI

cryoprobe. NMR samples were prepared in 20 mM phosphate, 50 mM NaCl buffer (pH 7.4) containing 10% D_2O at 298.2 K. Freshly dissolved ^{15}N-labeled $A\beta_{40}$ was mixed with liposomes containing 500 μM of lipids and 50 μM of incorporated compound, as well as in the absence of lipids with the compounds dissolved in deuterated DMSO at 50 μM. All NMR samples were stored at 37 °C during the time-lapse measurements. Each NMR spectrum was obtained using 256 t_1 increments, 16 scans, 16 dummy scans and a recycle delay of 0.2 s. NMR data were processed using TopSpin 3.5 (Bruker) and analyzed using Sparky 3.114.

3.5.7 Size exclusion chromatography

NMR samples were used for SEC characterization. 200 μL of each sample was loaded using Superdex 75 Increase LS Tricorn 10/300 column operated on an AKTA purifier (GE Healthcare, Freiburg, Germany) read at 214 nm with a flow rate of 1mL/min.

3.5.8 Dye Leakage assay

Lipids and the 5 small molecules in chloroform were placed in vials at the desired ratios and solvent was evaporated with N2 gas. Films were hydrated with 50 mM 6-carboxyfluorescein dye and put through no less than five freeze-thaw cycles. Following this, these samples were extruded through a 100 nm pore membrane no less than 21 times and filtered through a disposable PD-10 desalting column to separate dye filled vesicles from free 6-carboxyfluorescein in solution. The first 3.5 mL of elutant from the column were discarded and the following 1.5 mL of elutant of dye filled vesicles was collected. DLS was checked for to ensure 100 nm LUVs present in fractions. LUVs were diluted into buffer and then used for dye leakage assays on a 96 well plate in 20 mM phosphate 50 mM NaCl buffer at 37 °C with slow shaking over 40 hours in the presence of freshly prepared 10 μM $A\beta_{40}$ Percentage of dye released was determined after LUV lysis with triton-X and calculated as previously described. [5]

3.6 References

1. Hamley, I. W. The amyloid beta peptide: a chemist's perspective. Role in Alzheimer's and fibrillization. *Chem. Rev.* **112**, 5147–92 (2012).
2. Benilova, I., Karran, E. & De Strooper, B. The toxic Aβ oligomer and Alzheimer's disease: an emperor in need of clothes. *Nat. Neurosci.* **15**, 349–357 (2012).
3. Kotler, S. A., Walsh, P., Brender, J. R. & Ramamoorthy, A. Differences between amyloid-β aggregation in solution and on the membrane: insights into elucidation of the mechanistic details of Alzheimer's disease. *Chem. Soc. Rev.* **43**, 6692–6700 (2014).
4. Terakawa, M. S., Yagi, H., Adachi, M., Lee, Y.-H. & Goto, Y. Small Liposomes Accelerate the Fibrillation of Amyloid β (1–40). *J. Biol. Chem.* **290**, 815–826 (2015).
5. Sciacca, M. F. M. *et al.* Two-Step Mechanism of Membrane Disruption by Aβ through Membrane Fragmentation and Pore Formation. *Biophys. J.* **103**, 702–710 (2012).
6. Qiang, W., Akinlolu, R. D., Nam, M. & Shu, N. Structural evolution and membrane interaction of the 40-residue β amyloid peptides: Differences in the initial proximity between peptides and the membrane bilayer studied by solid-state nuclear magnetic resonance spectroscopy. *Biochemistry* **53**, 7503–7514 (2014).
7. Johnson, R. D., Steel, D. G. & Gafni, A. Structural evolution and membrane interactions of Alzheimer's amyloid-beta peptide oligomers: new knowledge from single-molecule fluorescence studies. *Protein Sci.* **23**, 869–83 (2014).
8. Quist, A. *et al.* Amyloid ion channels: a common structural link for protein-misfolding disease. *Proc. Natl. Acad. Sci. U. S. A.* **102**, 10427–32 (2005).
9. Butterfield, S. M. & Lashuel, H. A. Amyloidogenic protein-membrane interactions: Mechanistic insight from model systems. *Angew. Chemie - Int. Ed.* **49**, 5628–5654 (2010).

10. Korshavn, K. J., Bhunia, A., Lim, M. H. & Ramamoorthy, A. Amyloid-β adopts a conserved, partially folded structure upon binding to zwitterionic lipid bilayers prior to amyloid formation. *Chem. Commun.* **52**, 882–885 (2016).

11. Ladiwala, A. R. A., Dordick, J. S. & Tessier, P. M. Aromatic Small Molecules Remodel Toxic Soluble Oligomers of Amyloid through Three Independent Pathways. *J. Biol. Chem.* **286**, 3209–3218 (2011).

12. Bieschke, J. *et al.* Small-molecule conversion of toxic oligomers to nontoxic β-sheet–rich amyloid fibrils. *Nat. Chem. Biol.* **8**, 93–101 (2011).

13. Necula, M., Kayed, R., Milton, S. & Glabe, C. G. Small Molecule Inhibitors of Aggregation Indicate That Amyloid beta Oligomerization and Fibrillization Pathways Are Independent and Distinct. *J. Biol. Chem.* **282**, 10311–10324 (2007).

14. Kroth, H. *et al.* Discovery and structure activity relationship of small molecule inhibitors of toxic β-amyloid-42 fibril formation. *J. Biol. Chem.* **287**, 34786–34800 (2012).

15. Choi, J.-S., Braymer, J. J., Nanga, R. P. R., Ramamoorthy, A. & Lim, M. H. Design of small molecules that target metal-Aβ species and regulate metal-induced Aβ aggregation and neurotoxicity.

16. Patel, V. *et al.* Small molecules and Alzheimer's disease: misfolding, metabolism and imaging. *Curr. Alzheimer Res.* **12**, 445–461 (2015).

17. Lee, S. *et al.* Rational design of a structural framework with potential use to develop chemical reagents that target and modulate multiple facets of Alzheimer's disease. *J. Am. Chem. Soc.* **136**, 299–310 (2014).

18. Doig, A. J. & Derreumaux, P. Inhibition of protein aggregation and amyloid formation by small molecules. *Curr. Opin. Struct. Biol.* **30**, 50–56 (2015).

19. Young, L. M. *et al.* Screening and classifying small-molecule inhibitors of amyloid formation using ion mobility spectrometry–mass spectrometry. *Nat. Chem.* **7**, 73–81 (2015).

20. Young, L. M., Ashcroft, A. E. & Radford, S. E. Small molecule probes of protein aggregation. *Curr. Opin. Chem. Biol.* **39**, 90–99 (2017).

21. Cummings, J. L., Morstorf, T. & Zhong, K. Alzheimer's disease drug-development pipeline: few candidates, frequent failures.

22. Baell, J. & Walters, M. A. Chemistry: Chemical con artists foil drug discovery. *Nature* **513**, 481–483 (2014).

23. Sahoo, B. R. *et al.* Alzheimer's amyloid-beta intermediates generated using polymer-nanodiscs. *Chem. Commun.* **54**, 12883–12886 (2018).

24. Abdolvahabi, A. *et al.* How Do Gyrating Beads Accelerate Amyloid Fibrillization? *Biophys. J.* **112**, 250–264 (2017).

Chapter 4

Conclusions and Perspectives

4.1 General Conclusions

The complexities of amyloid diseases make them a difficult target for treatment development.[1–4] The variations in the aggregation pathway contribute to the lack of understanding which singular components are the root cause.[5–9] Many years of research, for AD in particular, has been spent investigating treatments of various types to treat these diseases, but the research has fallen short and no treatments to treat the underlying cause has been FDA approved.[10–17] While high resolution structures exist for the monomers and fibers of most amyloid diseases, it is the various states in the aggregation pathway that remain out of reach. Development of tools to isolate these species so that they can be fully characterized can lead to a deeper understanding of their nature, either toxic or not. Through a combination of biophysical techniques, we have characterized and identified tool compounds that are able to study intermediates.

Chapter 2 focuses on the selectivity of CurDAc, a water-soluble curcumin derivative on its peptide selectivity and its ability disaggregate to hIAPP as well as prevent aggregation. It was observed that CurDAc was a more potent inhibitor and disaggregator of hIAPP over hCT and Aβ40 by carrying out biophysical experiments including the ThT assay, CD, TEM and ITC experiments. Additionally, utilizing single and multidimensional NMR experiments we were able to characterize both the monomer based inhiation of hIAPP aggregation as well as the disaggregation of hIAPP fibers. For the monomer:CurDAc interactions, few chemical shifts were observed.

However, the peptide does not remain visible for NMR experiments indicating an increase in the size of the aggregate. The disaggregated species was structurally distinct from the monomer according to NMR. The peak positions of the disaggregated species identified from 2D and 3D NMR experiments have distinct chemical shifts in comparison to the monomer but do not necessarily match known chemical shift values based on secondary structure for those particular amino acids. However, most of the residues identified in the disaggregated species exist in a loop region of the monomer and fiber models, as well as a membrane bound intermediate of hIAPP. This evidence suggests that these residues are incorporated into a larger oligomeric species that is too large for solution NMR studies, while the identified residues are solvent exposed. TEM confirmed the disaggregation of fibers to smaller aggregates. Importantly, it was identified that both the CurDAc inhibited and disaggregated hIAPP were toxic to cultured cells, indicating the isolation of toxic intermediate using a small molecule tool.

Chapter 3 continued on the idea of small molecule tools to isolate amyloid intermediates. However, this work focused on the importance of membrane as a site for amyloid toxicity, which is important for AD. Generation of Aβ occurs in the plasma membrane and it has been shown to bind to and disrupt membranes as well as bind to membrane bound receptors.[18–28] Given the importance of membranes, we set out to identify small molecules that could act aggregation inhibitors and tool compounds in the presence of a membrane, since most Aβ inhibitors do not function with membranes. A high throughput screen of 1,800 small molecules revealed 5 membrane-active $A\beta_{40}$ inhibitors were found, none of which had been investigated for amyloid inhibition before. Although there were 5 inhibitors identified, they differed in their activity. Of the compounds, DHQ-1, DHQ-2, and THQ-1 were found to be the least inhibiting by NMR, SEC and CD, whereas BF-3 and AQ-4 stopped the aggregation the most. AQ-4 had the highest amount of

smaller species by SEC, maintained a random coil CD signal and visible C terminus by NMR. BF-3 also showed a large amount of smaller species and had NMR peaks visible throughout the whole sequence but appeared beta sheet by CD. Interestingly, BF-3 allowed dye leakage from membranes with in without GM1 indicating that $A\beta_{40}$ is disrupting the bilayer however AQ-4 did not.

4.2 Future Outlook

The work presented in this dissertation have created an avenue for the development of tool compounds to manipulate amyloid aggregation. Given the many complexities of amyloid diseases and lack of treatments, it is crucial that research at a variety of angles continues forward. This work has provided a starting point for possible derivatization of small molecule tools for amyloid modulation for the purposes of disaggregation, promotion and inhibition at the membrane. Similarities among identified inhibitor compounds provide a starting point for structure activity relationships to be drawn. Compounds that didn't inhibit in the presence of a membrane could also be investigated for this purpose.

While the research presented here has provided new insights into amyloid disaggregation and inhibition, atomic level resolution structures were out of reach. While preliminary structural data in chapters 2 and 3 were presented, further structural biology works are needed to achieve the highest level of atomic level resolution of the intermediates. Stabilizing and isolating amyloid intermediates would enable atomic-resolution dynamic-structural studies using a combination of solution and solid-state NMR techniques. While solution NMR can be applied to monitor the formation of small molecular weight oligomeric intermediates, large size aggregates, protofibers and fibers can be investigated using well-established solid-state NMR techniques. Isolation and purification of the intermediates would be suitable for solid state NMR experiments.[29] Current advancements in other methods such as Cryo-EM have proven to be useful for the amyloid field,

solving a number of fiber structures.[30–35] With advancements in resolution and class averaging, it is possible that large oligomer structures may be solved with Cryo-EM. [36,37] Recent successful developments of near-native membrane mimetics, such as lipid-nanodiscs, would be a next step for the evolution of the work shown in chapter 3. Recently, nanodiscs were used to trap an oligomer of hIAPP , used in biophysical characterization including high-resolution NMR experiments and molecular dynamics simulations to generate the first high-resolution structural model.[38] The use of the nanodiscs could be an avenue to pursue for the investigating the structures of the small molecules and $A\beta_{40}$ interactions at the membrane interface.

While much work continues to emerge in the amyloid field, a lack of answers has caused a reflection on the 'amyloid hypothesis'. [14,39,40] This may be because the 'toxic oligomer" still remains a structural mystery and the transient and ever evolving nature of them makes it quite difficult to apply the existing biophysical and biochemical techniques available to fully characterize them. With new methods to isolate the intermediate species presented here, hopefully amyloid research will move forward in providing answers to patients and loved ones affected with these diseases.

4.3 References

1. Knowles, T. P. J., Vendruscolo, M. & Dobson, C. M. The amyloid state and its association with protein misfolding diseases. *Nat. Rev. Mol. Cell Biol.* **15**, 384–396 (2014).
2. Iadanza, M. G., Jackson, M. P., Hewitt, E. W., Ranson, N. A. & Radford, S. E. A new era for understanding amyloid structures and disease. *Nat. Rev. Mol. Cell Biol.* **19**, 755–773 (2018).
3. Chiti, F. & Dobson, C. M. Protein Misfolding, Functional Amyloid, and Human Disease.

Annu. Rev. Biochem. **75**, 333–366 (2006).

4. Dobson, C. M. The Amyloid Phenomenon and Its Links with Human Disease. *Cold Spring Harb. Perspect. Biol.* **9**, a023648 (2017).

5. Ke, P. C. *et al.* Implications of peptide assemblies in amyloid diseases. *Chem. Soc. Rev.* **46**, 6492–6531 (2017).

6. Zhao, L. N., Long, H., Mu, Y. & Chew, L. Y. The toxicity of amyloid β oligomers. *Int. J. Mol. Sci.* **13**, 7303–7327 (2012).

7. Chiti, F. & Dobson, C. M. Protein Misfolding, Amyloid Formation, and Human Disease: A Summary of Progress Over the Last Decade. *Annu. Rev. Biochem.* **86**, 27–68 (2017).

8. Knowles, T. P. J., Vendruscolo, M. & Dobson, C. M. The amyloid state and its association with protein misfolding diseases. *Nat. Rev. Mol. Cell Biol.* **15**, 384–396 (2014).

9. Hartl, F. U. Protein Misfolding Diseases. *Annu. Rev. Biochem.* **86**, 21–26 (2017).

10. Karran, E. & De Strooper, B. The amyloid cascade hypothesis: are we poised for success or failure? *J. Neurochem.* **139**, 237–252 (2016).

11. Doig, A. J. *et al.* Why Is Research on Amyloid-β Failing to Give New Drugs for Alzheimer's Disease? *ACS Chemical Neuroscience* **8**, 1435–1437 (2017).

12. Hung, S.-Y. & Fu, W.-M. Drug candidates in clinical trials for Alzheimer's disease. *J. Biomed. Sci.* **24**, 47 (2017).

13. Soejitno, A., Tjan, A. & Purwata, T. E. Alzheimer's Disease: Lessons Learned from Amyloidocentric Clinical Trials. *CNS Drugs* **29**, 487–502 (2015).

14. Mullane, K. & Williams, M. Alzheimer's therapeutics: Continued clinical failures question the validity of the amyloid hypothesis—but what lies beyond? *Biochem. Pharmacol.* **85**, 289–305 (2013).

15. von Schaper, E. Everything but amyloid: new thinking prompts FDA revamp. *Nat. Publ. Gr.* **36**, (2018).

16. Ankarcrona, M. *et al.* Current and future treatment of amyloid diseases. *J. Intern. Med.* **14**, 1437–51 (2016).

17. Citron, M. Alzheimer's disease: strategies for disease modification. *Nat. Rev. Drug Discov.* **9**, 387–398 (2010).

18. Pilkington, A. W. *et al.* Hydrogen Peroxide Modifies Aβ–Membrane Interactions with Implications for Aβ 40 Aggregation. *Biochemistry* **58**, 2893–2905 (2019).

19. Di Scala, C. *et al.* Common molecular mechanism of amyloid pore formation by Alzheimer's β-amyloid peptide and α-synuclein. *Sci. Rep.* **6**, 28781 (2016).

20. Kotler, S. A., Walsh, P., Brender, J. R. & Ramamoorthy, A. Differences between amyloid-β aggregation in solution and on the membrane: insights into elucidation of the mechanistic details of Alzheimer's disease. *Chem. Soc. Rev.* **43**, 6692–6700 (2014).

21. Quist, A. *et al.* Amyloid ion channels: a common structural link for protein-misfolding disease. *Proc. Natl. Acad. Sci. U. S. A.* **102**, 10427–32 (2005).

22. Sciacca, M. F. M. *et al.* Two-Step Mechanism of Membrane Disruption by Aβ through Membrane Fragmentation and Pore Formation. *Biophys. J.* **103**, 702–710 (2012).

23. Terakawa, M. S., Yagi, H., Adachi, M., Lee, Y.-H. & Goto, Y. Small Liposomes Accelerate the Fibrillation of Amyloid β (1–40). *J. Biol. Chem.* **290**, 815–826 (2015).

24. Limbocker, R. *et al.* Trodusquemine enhances Aβ42 aggregation but suppresses its toxicity by displacing oligomers from cell membranes. *Nat. Commun.* **10**, 225 (2019).

25. Delgado, D. A. *et al.* Distinct Membrane Disruption Pathways Are Induced by 40-Residue β-Amyloid Peptides. *J. Biol. Chem.* **291**, 12233–12244 (2016).

26. Xue, W. F. *et al.* Fibril fragmentation enhances amyloid cytotoxicity. *J. Biol. Chem.* **284**, 34272–34282 (2009).

27. Matsuzaki, K. How Do Membranes Initiate Alzheimer's Disease? Formation of Toxic Amyloid Fibrils by the Amyloid β-Protein on Ganglioside Clusters. *Acc. Chem. Res.* **47**, 2397–2404 (2014).

28. Bode, D. C., Baker, M. D. & Viles, J. H. Ion Channel Formation by Amyloid-β 42 Oligomers but Not Amyloid-β 40 in Cellular Membranes. *J. Biol. Chem.* **292**, 1404–1413 (2017).

29. Kotler, S. A. *et al.* High-resolution NMR characterization of low abundance oligomers of amyloid-β without purification. *Sci. Rep.* **5**, 11811 (2015).

30. Schmidt, M. *et al.* Peptide dimer structure in an Aβ(1–42) fibril visualized with cryo-EM. *Proc. Natl. Acad. Sci.* **112**, 11858–11863 (2015).

31. Liberta, F. *et al.* Cryo-EM fibril structures from systemic AA amyloidosis reveal the species complementarity of pathological amyloids. *Nat. Commun.* **10**, 1104 (2019).

32. Li, B. *et al.* Cryo-EM of full-length α-synuclein reveals fibril polymorphs with a common structural kernel. *Nat. Commun.* **9**, 3609 (2018).

33. Fitzpatrick, A. W. P. *et al.* Cryo-EM structures of tau filaments from Alzheimer's disease. *Nature* **547**, 185–190 (2017).

34. Gremer, L. *et al.* Fibril structure of amyloid-β(1–42) by cryo–electron microscopy. *Science (80-.).* **358**, 116–119 (2017).

35. Tayeb-Fligelman, E. *et al.* The cytotoxic Staphylococcus aureus PSMα3 reveals a cross-α amyloid-like fibril. *Science (80-.).* **355**, (2017).

36. Mitra, A. K. Visualization of biological macromolecules at near-atomic resolution: Cryo-

electron microscopy comes of age. *Acta Crystallographica Section F: Structural Biology Communications* **75**, 3–11 (2019).

37. Bai, X., McMullan, G. & Scheres, S. H. W. How cryo-EM is revolutionizing structural biology. *Trends Biochem. Sci.* **40**, 49–57 (2015).

38. Rodriguez Camargo, D. C. *et al.* Stabilization and structural analysis of a membrane-associated hIAPP aggregation intermediate. *Elife* **6**, e31226 (2017).

39. Makin, S. The amyloid hypothesis on trial. *Nature* **559**, S4–S7 (2018).

40. Herrup, K. The case for rejecting the amyloid cascade hypothesis. *Nat Neurosci* **18**, 794–799 (2015).

Appendix A

Supporting Information for Chapter 2

A.1 Supplementary Figures

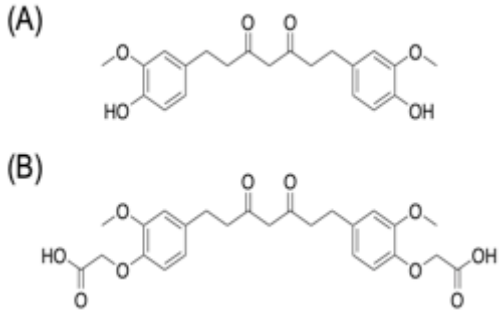

Figure A.1 Chemical structures of curcumin (A) and its water-soluble derivative, CurDAc (B).

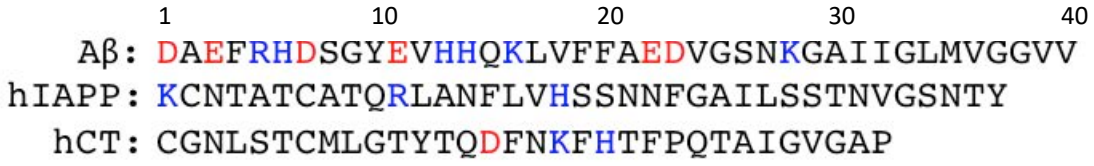

Figure A.2 Amino acid sequences of the three different amyloid peptides (amyloid-beta, human-IAPP and human-calcitonin) used in this study. Color indicates charge of residue at pH 7.4: red is acidic, blue is basic, black is uncharged.

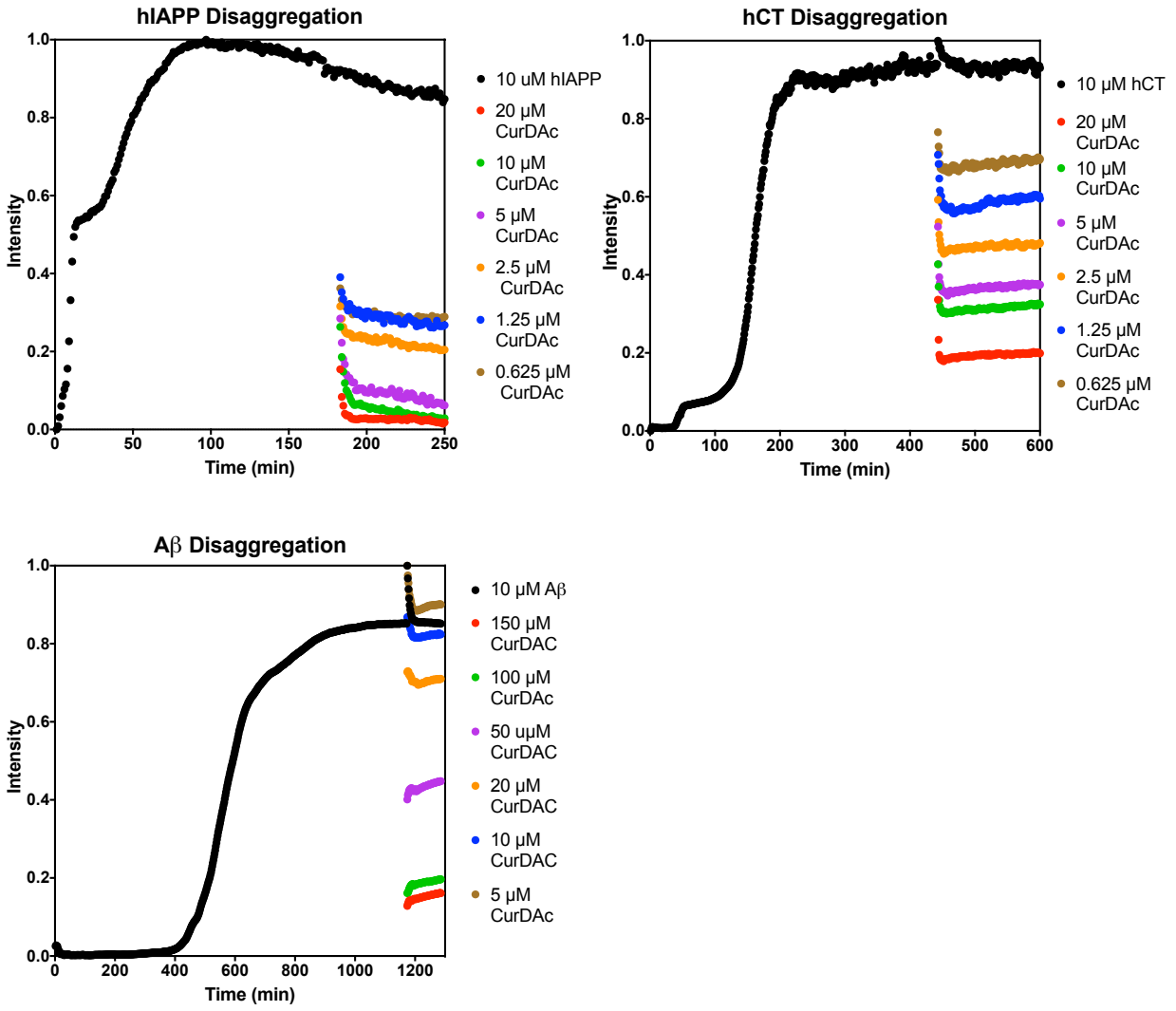

Figure A.3 Kinetic disaggregation curves using 4 equivalents of ThT. 10 μM peptides (hIAPP, hCT and Aβ) were allowed to aggregate to form amyloid fibers, as shown in the black curve in each figure, with 40 μM ThT to monitor aggregation. Wells were then treated with the same stoichiometric ratios of CurDAc as shown in the previous experiments (Figure 1).

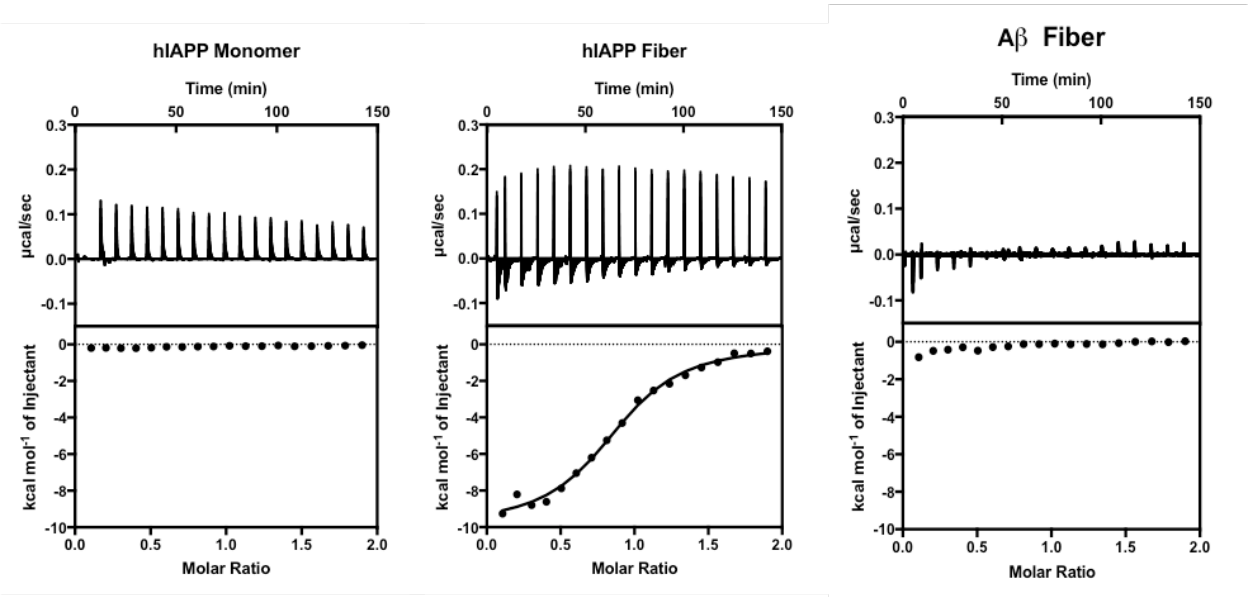

Figure A.4 Isothermal titration calorimetry (ITC) experimental traces showing the monomer and binding with CurDAc over time. hIAPP monomer and Aβ fiber show no thermodynamic binding. hIAPP fibers with CurDAc show endothermic interaction.

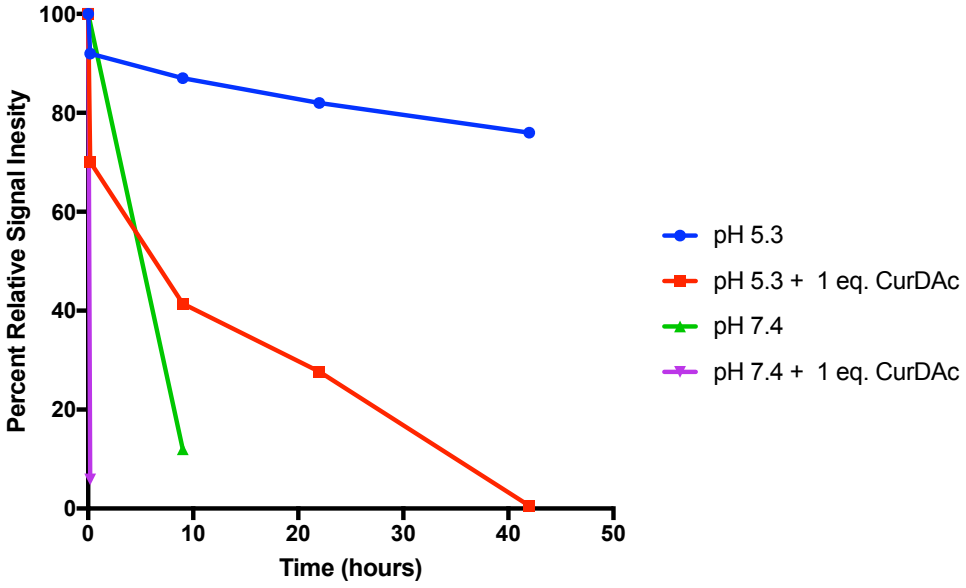

Figure A.5 NMR aggregation kinetics of hIAPP and hIAPP + CurDAc as measured by 1D ^{1}H signal intensity. 100 μM hIAPP dissolved into pH 7.4 phosphate or pH 5.3 acetate buffers with and without CurDAc were used to measure the proton NMR spectra of the soluble hIAPP peptide. Experimentally measured proton NMR signal intensities are plotted over the time. First spectra were taken immediately after addition of CurDAc to hIAPP monomer and subsequent spectra were taken at various time points.

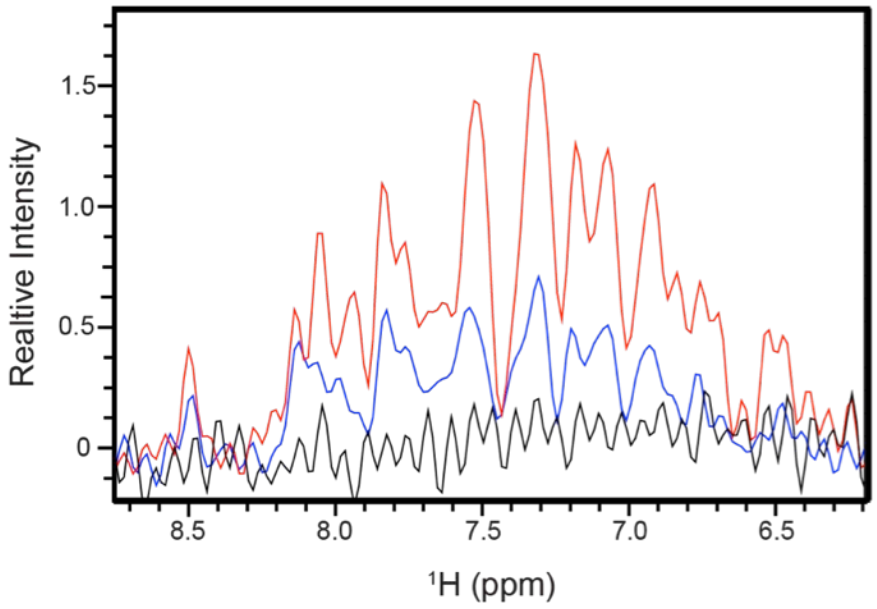

Figure A.6 ^{1}H NMR spectra of hIAPP monomer with 1 equivalent of CurDAc over time obtained from a 850 MHz NMR spectrometer at 25 °C. Red trace spectrum shows 80 μM hIAPP + CurDAc at pH 5.3 acetate buffer at 0 hours. Blue trace spectrum shows the same sample after 9 hours of incubation, and black is after 40 hours.

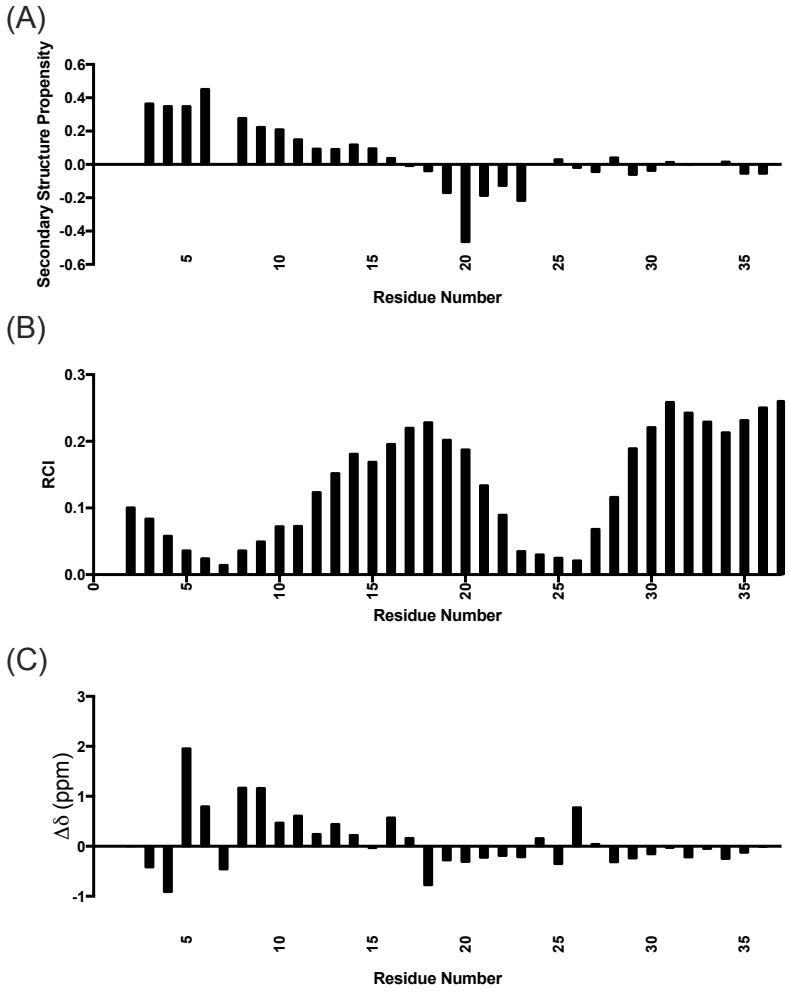

Figure A.7 Secondary structure predictions of hIAPP monomer in the presence of CurDAc using the C_α, C_β, HN and N chemical shifts. (A) Secondary structure propensities from the Forman Kay group. (B) Random Coil Index from the Wishart group and (C) the $\Delta\delta$ of the C_α chemical shifts. All three show a tendency of an alpha-helical structure at the N-terminus, a small portion of a beta-sheet confirmation near the amyloidogenic core, and then a random coil for the rest of the peptide, which is closely similar to the hIAPP monomer structure.

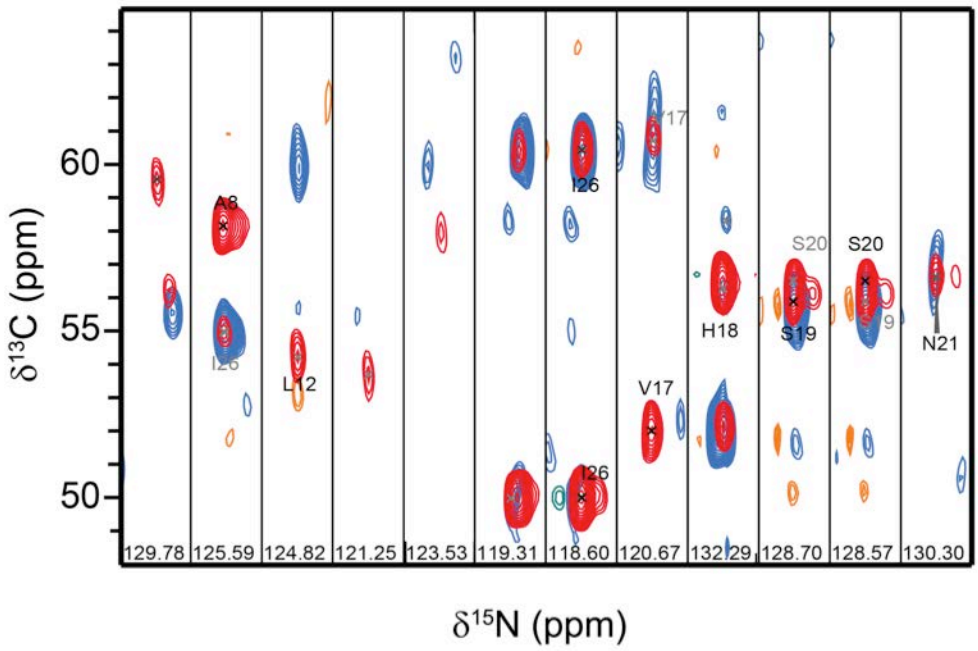

Figure A.8 3D HNCA and HNCOCA experiments performed after 72-hour incubation of hIAPP with CurDAc at a 1:1 molar ratio at pH 7.4 phosphate buffer obtained from a 850 MHz NMR spectrometer at 25 °C.

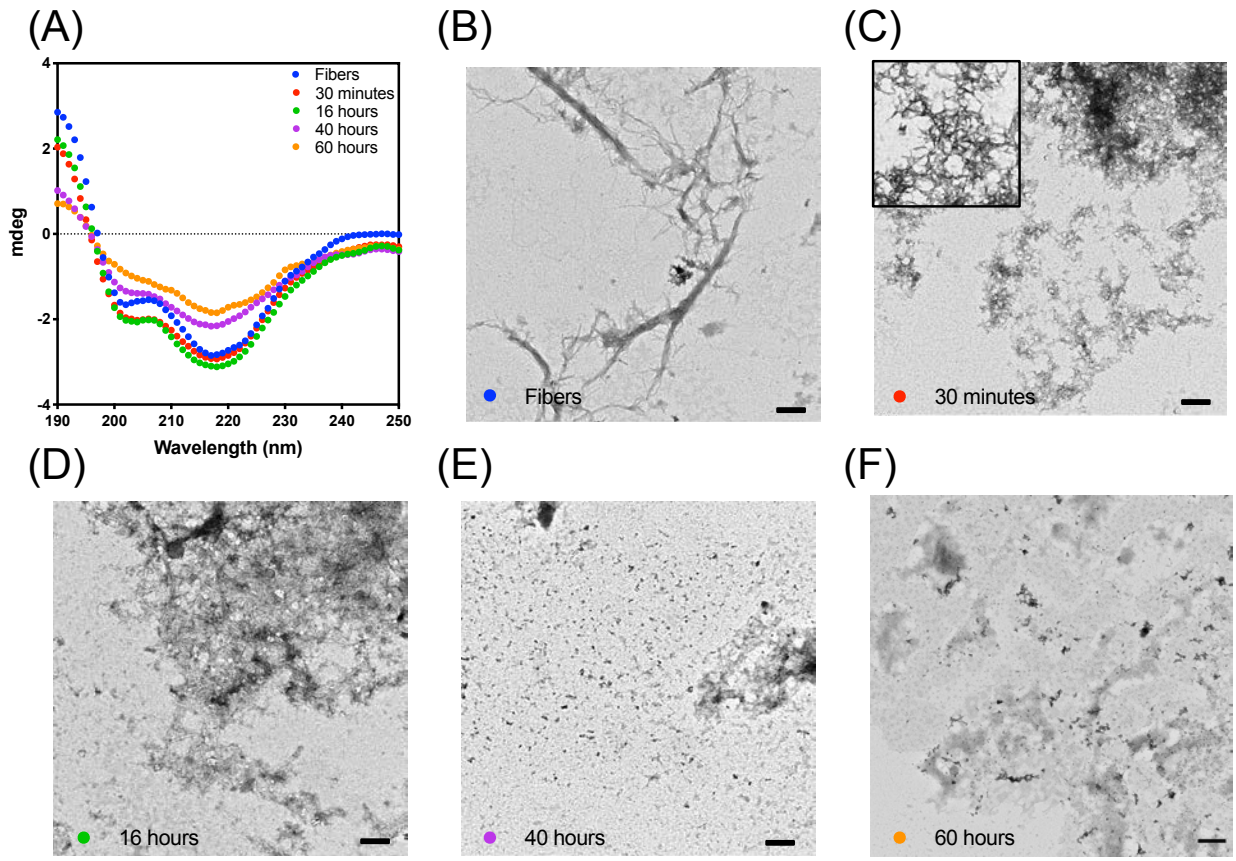

Figure A.9 Circular dichroism (CD) and TEM of hIAPP fibers before and after CurDAc treatment. (A) CD spectra of hIAPP fibers in the presence of one molar equivalent of CurDAc over a course of 60 hours in phosphate buffer at pH 7.4. TEM images of hIAPP fibers (B) followed by hIAPP samples in the presence of CurDAc at 30 minutes to 60 hours (C-F) scale bar is 200 nm. Full images are represented in this figure while panels of B, C and F are show in main text figure 3F.

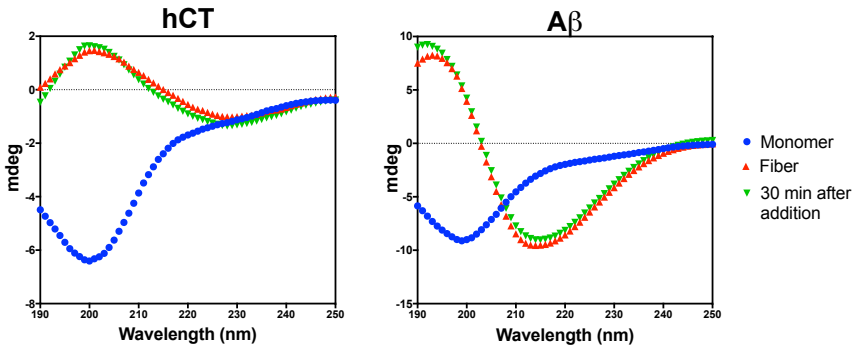

Figure A.10 CD spectra of hCT and Aβ before and after treatment with CurDAc. 40 μM peptide monomers in pH 7.4 phosphate buffer show random coil at time zero, and after 24 hours peptides show beta-sheet conformation. hCT was treated with 2 equivalents of CurDAc, and Aβ with 10 equivalents, and then measured again after 30 minutes of incubation.

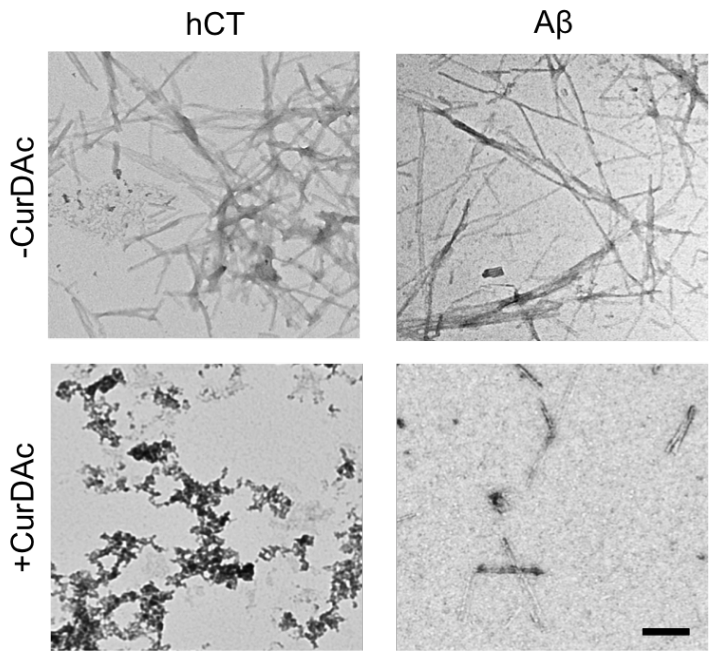

Figure A.11 hCT and Aβ TEM images before and after treatment with CurDAc. Top, 40 μM hCT (left) and Aβ (right) after 24 hours shaking at pH 7.4 phosphate buffer at 25°C and 37°C. Bottom, 30 minutes after the addition of CurDAc. 2 equivalents of CurDAc were added to hCT and 10 Equivalents were added to Aβ. Scale bar is 100 nm.

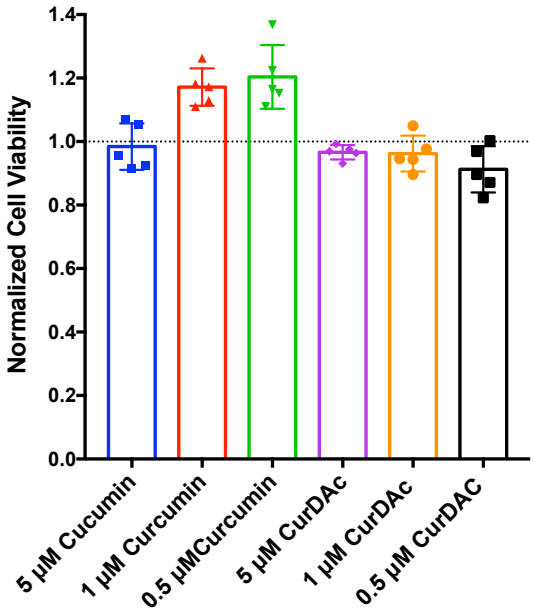

Figure A.12 MTT cell toxicity assay of curcumin and CurDAc. RIN-5F cells treated with varying amounts of curcumin or CurDAc. MTT reduction was measured after 24 hours.

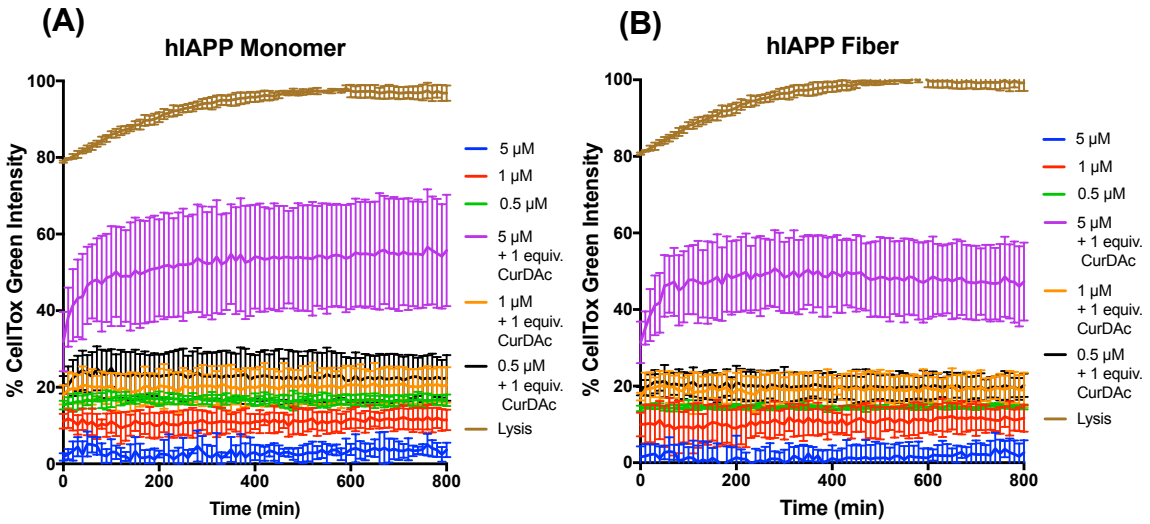

Figure A.13 RIN-5F cell death monitored every 10 minutes for 13 hours by CellTox Green fluorescence in the presence of hIAPP monomers or fibers with varying amounts of CurDAc.

A.2 Supplementary Tables

hIAPP Fibers + CurDAc	
ΔG_{bind} (kcal mol^{-1})	-7.3
ΔH_{bind} (kcal mol^{-1})	-9.9
$-T\Delta S_{bind}$ (kcal mol^{-1})	2.6
K_d (μM)	6.8
n (value)	0.88

Table A.1 hIAPP fiber and CurDAc parameters as determined from isothermal titration calorimetry (ITC) data (Figure A.4). Dissociation constant (K_d), ΔH_{bind} and n value were obtained by fitting with one site binding model. ΔG_{bind} was calculated based on the relation of $\Delta G_{bind} = -RT\ln K_a = RT\ln K_d$. $(-)T\Delta S_{bind}$ was finally obtained based on the relation of $\Delta G_{bind} = \Delta H_{bind} - T\Delta S_{bind}$.

Number	Residue	C_β ppm	C_α ppm	N ppm	HN ppm
2	CYS			122.1123	8.7772
3	ASN	39.086	52.678	124.2993	8.7713
4	THR	70.7557	61.1146	110.6628	7.3559
5	ALA	18.1791	54.5815	122.7183	8.5197
6	THR	69.2207	62.9297	109.5424	7.7255
7	CYS	40.8762	56.1385	120.4087	7.8619
8	ALA	18.5302	53.6451	124.1765	7.9618
9	THR	69.2217	63.1576	113.7145	7.9175
10	GLN	28.6872	56.2058	122.5101	7.995
11	ARG	30.3224	56.6439	107.936	8.0404
12	LEU	41.949	55.3473	122.5421	7.8186
13	ALA	18.7643	53.0598	123.6314	7.959
14	ASN	38.3345	53.3773	116.6722	7.9961
15	PHE	38.7921	58.0063	120.0362	7.793
16	LEU	41.8671	55.4569	122.3817	7.9103
17	VAL	32.3546	62.3499	120.7697	7.7196
18	HIS	28.8801	55.1115	122.0749	8.3102
19	SER	63.6187	57.9878	117.5163	8.1642
20	SER	63.5594	58.1272	117.7381	8.2202
21	ASN	38.512	53.0921	120.0117	8.1941
22	ASN	38.33	53.0878	118.6576	8.0778
23	PHE	38.6758	53.2115	120.383	8.0217
24	GLY		45.0546	110.1381	8.093
25	ALA	19.0472	52.1137	123.4318	7.7682
26	ILE	38.3073	53.4572	120.4079	7.9671
27	LEU	42.0765	55.069	127.034	8.21
28	SER	63.6187	57.9614	117.0866	8.1641
29	SER	63.589	58.1391	117.6773	8.2614
30	THR	69.4109	61.8517	115.0143	7.9413
31	ASN	38.4558	53.1274	121.2654	8.1871
32	VAL	32.3427	62.4194	120.7386	7.9667
33	GLY		45.1069	112.3688	8.3088
34	SER	63.5668	58.0292	115.4101	8.0113
35	ASN	38.4711	53.1296	120.5407	8.3178
36	THR	69.4109	62.0605	114.2089	7.8543
37	TYR	38.4335	57.7016	122.6677	7.9345

Table A.2 Chemical shifts from 3D HNCA, HNCOCA experiments of CurDAc interactions with the hIAPP monomer used to generate secondary structure prediction in table S7.

Sample	Helix 1	Helix 2	Total Helix	Anti 1	Anti 2	Anti 3	Para	Turn	Total β-Sheet	Others	NRMSD
hIAPP Fiber	0	0	0	7.1	7.46	19.93	9.32	10.23	54.04	45.97	0.0215
30 Minutes	9.14	0	9.14	0	0	19.46	20.12	8.66	48.24	42.63	0.0334
16 Hours	10.49	1.83	12.32	0	0	16.6	19.67	7.48	43.75	43.93	0.0366
40 Hours	0	2.69	2.69	0	0	14.23	23.63	13.73	51.59	45.72	0.0529
60 Hours	0	0	0	0	1.87	10.25	21.36	15.85	49.33	50.68	0.0535

Table A.3 Parameters obtained by fitting circular dichroism spectra of hIAPP time course disaggregation with CurDAc using BeStSEL. Values are shown in percentage of total content.

Samples Compared	Significant?	Summary	Adjusted P Value
hIAPP monomer MTT Experiments			
5 μM vs. 5 μM + 1 equiv. CurDAc	Yes	****	<0.0001
1 μM vs. 1 μM + 1 equiv. CurDAc	Yes	****	<0.0001
0.5 μM vs. 0.5 μM + 1 equiv. CurDAc	Yes	****	<0.0001
5 μM + 1 equiv. CurDAc vs. 1 μM + 1 equiv. CurDAc	Yes	**	0.0034
5 μM + 1 equiv. CurDAc vs. 0.5 μM + 1 equiv. CurDAc	Yes	****	<0.0001
1 μM + 1 equiv. CurDAc vs. 0.5 μM + 1 equiv. CurDAc	No	ns	0.0855
hIAPP Fiber MTT Experiments			
5 μM vs. 5 μM + 1 equiv. CurDAc	No	ns	0.9985
1 μM vs. 1 μM + 1 equiv. CurDAc	Yes	****	<0.0001
0.5 μM vs. 0.5 μM + 1 equiv. CurDAc	Yes	****	<0.0001
5 μM + 1 equiv. CurDAc vs. 1 μM + 1 equiv. CurDAc	Yes	****	<0.0001
5 μM + 1 equiv. CurDAc vs. 0.5 μM + 1 equiv. CurDAc	Yes	****	<0.0001
1 μM + 1 equiv. CurDAc vs. 0.5 μM + 1 equiv. CurDAc	No	ns	0.1464
hIAPP Monomer CellTox Green Experiments			
5 μM vs. 5 μM + 1 equiv. CurDAc	Yes	****	<0.0001
1 μM vs. 1 μM + 1 equiv. CurDAc	No	ns	0.5995
0.5 μM vs. 0.5 μM + 1 equiv. CurDAc	No	ns	0.9128
5 μM + 1 equiv. CurDAc vs. 1 μM + 1 equiv. CurDAc	Yes	***	0.0002
5 μM + 1 equiv. CurDAc vs. 0.5 μM + 1 equiv. CurDAc	Yes	***	0.0003
1 μM + 1 equiv. CurDAc vs. 0.5 μM + 1 equiv. CurDAc	No	ns	0.9998
hIAPP Fiber CellTox Green Experiments			
5 μM vs. 5 μM + 1 equiv. CurDAc	Yes	****	<0.0001
1 μM vs. 1 μM + 1 equiv. CurDAc	No	ns	0.5284
0.5 μM vs. 0.5 μM + 1 equiv. CurDAc	No	ns	0.7522
5 μM + 1 equiv. CurDAc vs. 1 μM + 1 equiv. CurDAc	Yes	****	<0.0001
5 μM + 1 equiv. CurDAc vs. 0.5 μM + 1 equiv. CurDAc	Yes	***	0.0001
1 μM + 1 equiv. CurDAc vs. 0.5 μM + 1 equiv. CurDAc	No	ns	0.9999

Table A.4 Statistical significance calculated by one-way ANOVA using Tukey's multiple comparison tests. Comparisons were done between cells treated with hIAPP with and without CurDAc.

Appendix B

Supporting Information for Chapter 3

B.1 Supplementary Figures

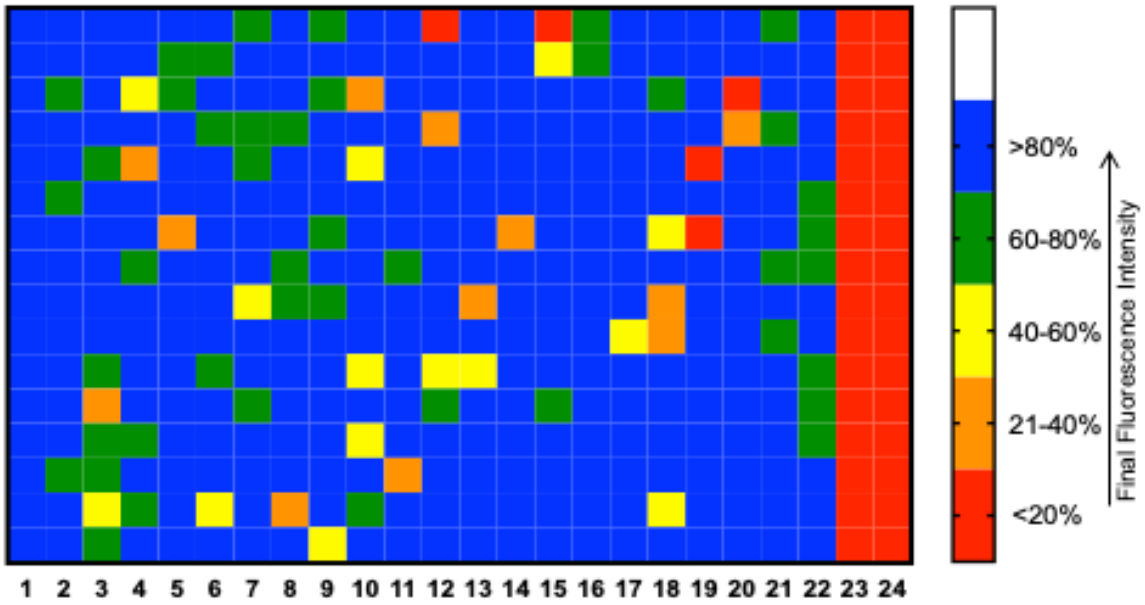

Figure B.1. Representative data of final ThT fluorescence intensity of a 384 well plate from the screen. Columns 1 and 2 were negative controls and columns 23 and 24 were positive controls. Each individual well had a unique compound outside of the controls. Wells with lowest intensity (red or orange) were further investigated in this study.

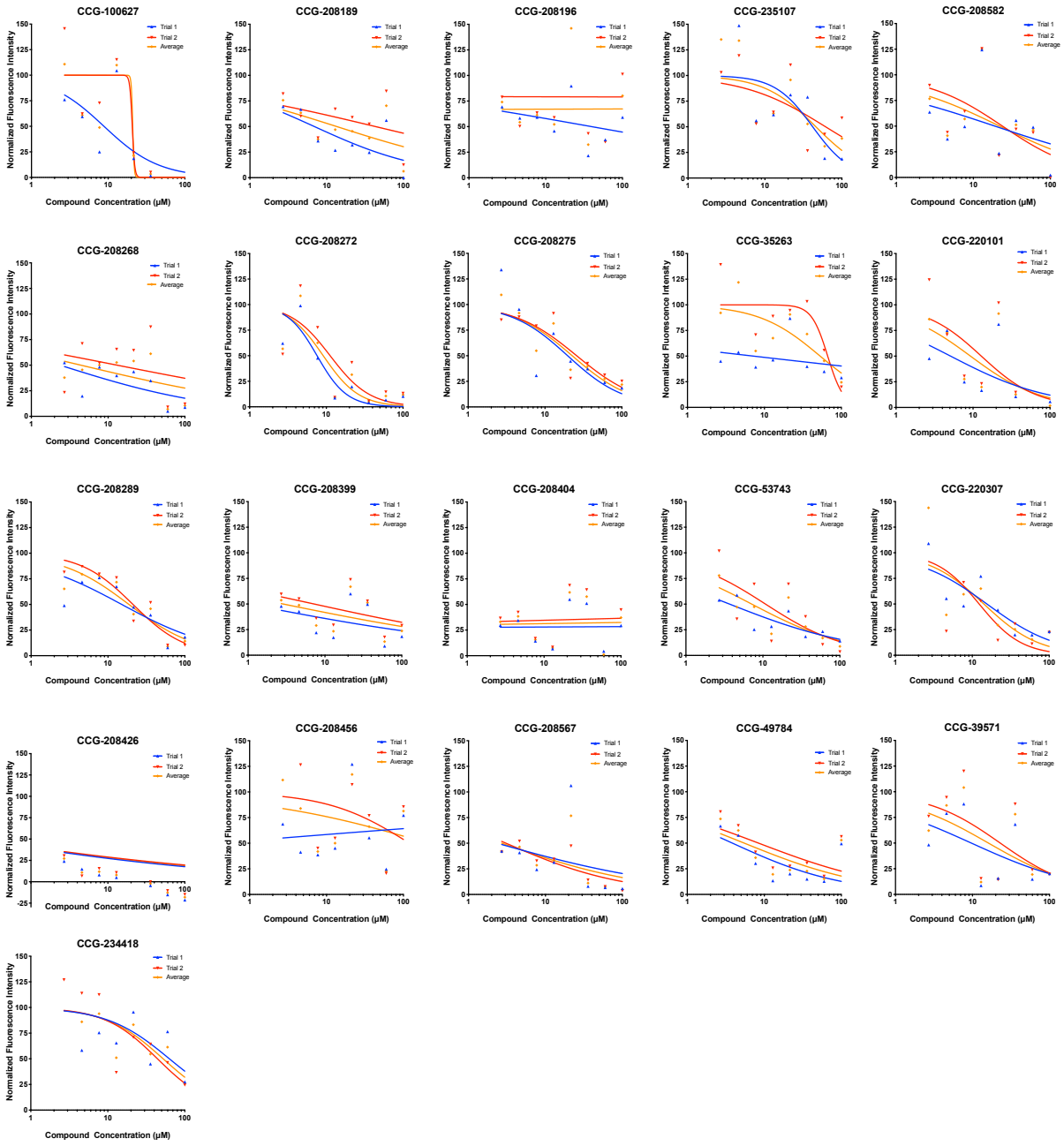

Figure B.2. Concentration response curves for the 21 compounds selected further investigation. The concentrations of compounds ranged from 2-100 μM.

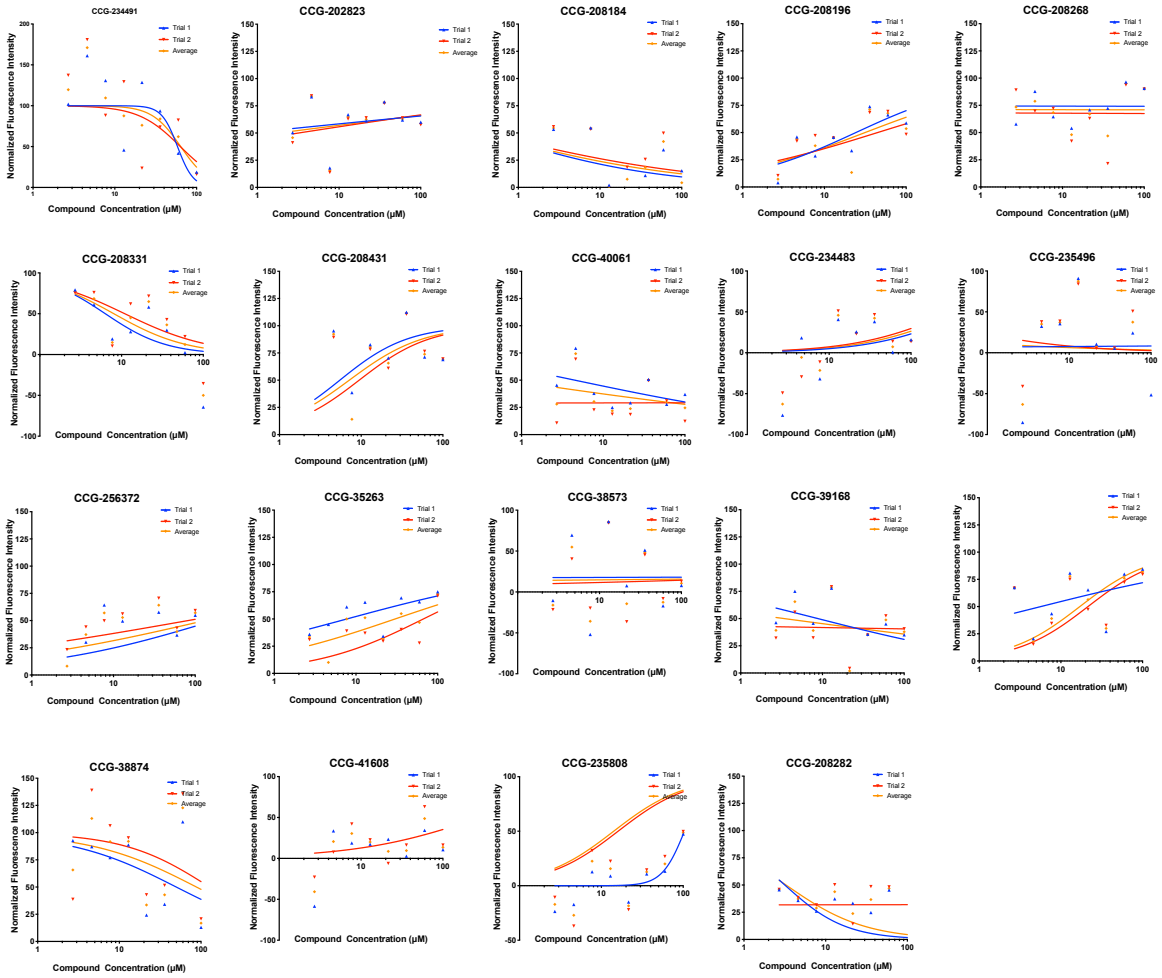

Figure B.3. Concentration response curves for compounds not selected for further testing. Compound concentrations ranged from 2-100 μM.

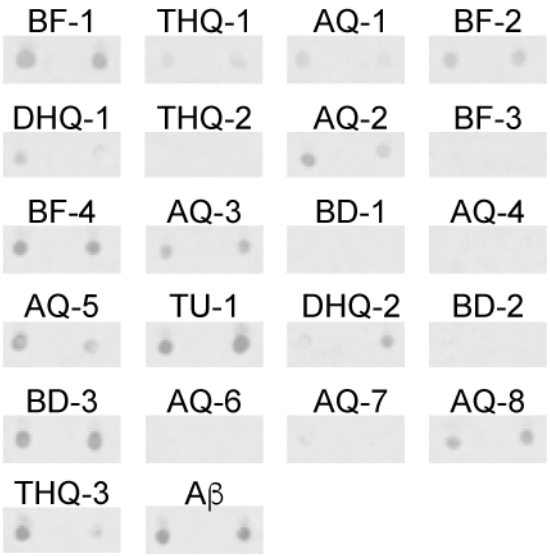

Figure B.4. Dot blot images of samples after the ThT experiments using the OC antibody. Wells containing 10 μM of $A\beta_{40}$ + LUVs with 5 equivalents of the small molecule used for blotting.

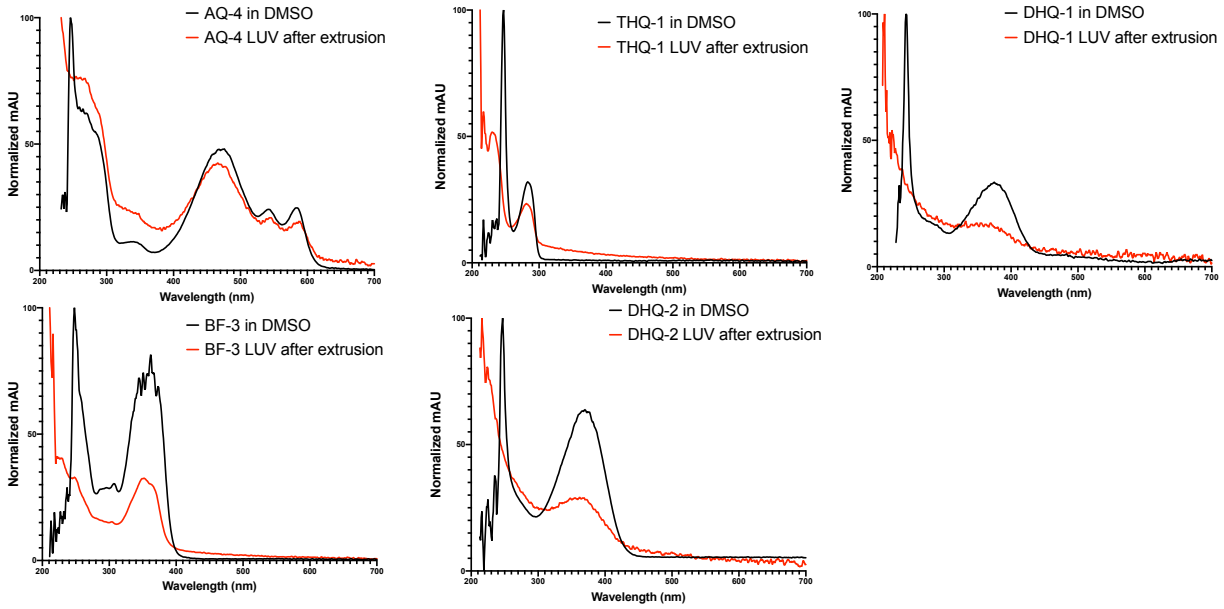

Figure B.5. UV-Vis spectra of AQ-4, THQ-1, BF3-, DHQ-1, and DHQ-2 in DMSO (black) and incorporated into LUVs after extrusion (red). Molar ratio of lipids to compound was 10:1.

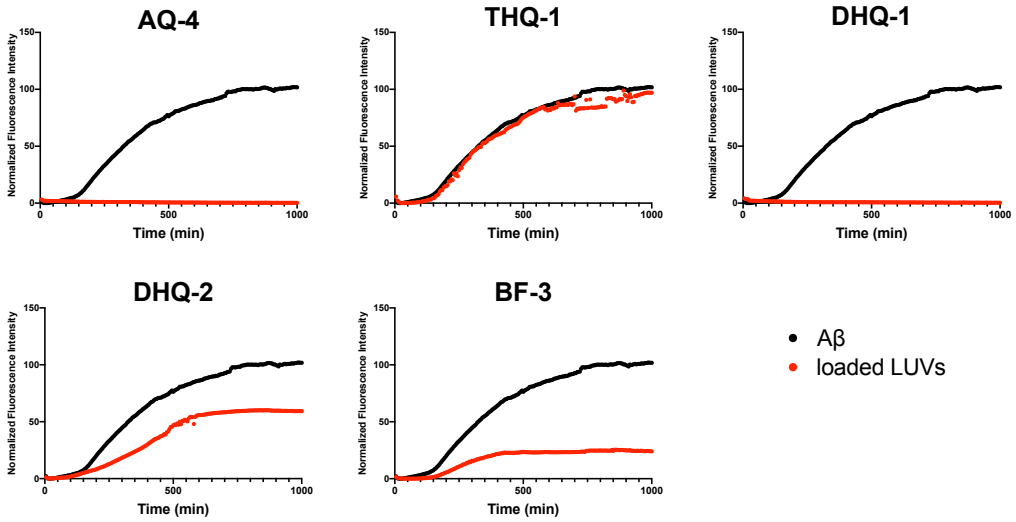

Figure B.6. ThT fluorescence kinetics of 10 μM $A\beta_{40}$ (black) and $A\beta_{40}$ + 500 μM of compound loaded LUVs (red) at a 10:1 lipid:compound molar ratio.

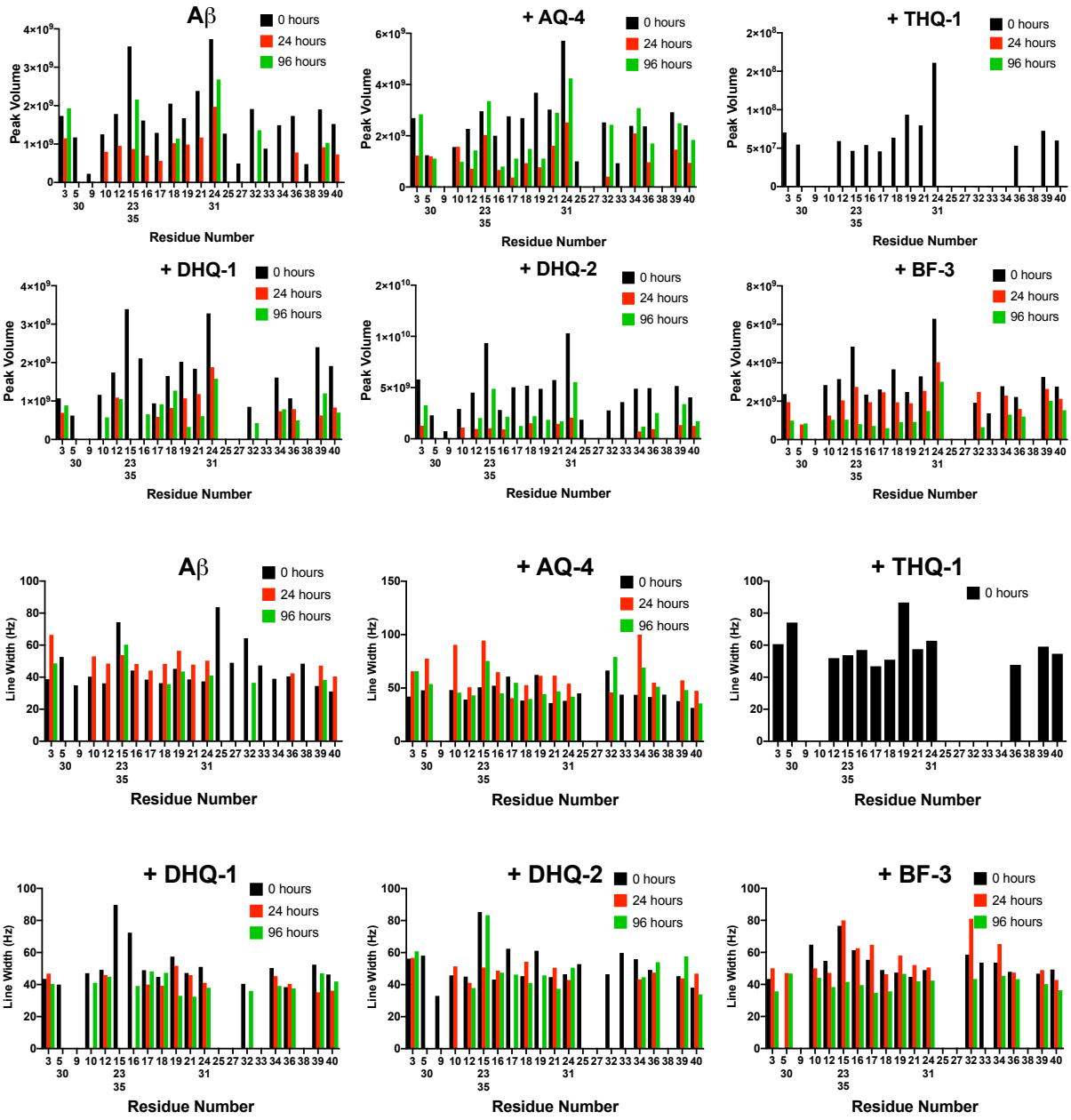

Figure B.7. (Top) Peak volumes taken from SOFAST-HMQC NMR spectra of 25 μM ^{15}N- Aβ_{40} in the presence of 500 μM of compound loaded LUVs at 0 (black), 24 (red) and 96 hours (green). **(**Bottom**)** Linewidths taken from spectra at 0, 24 and 96 hours.

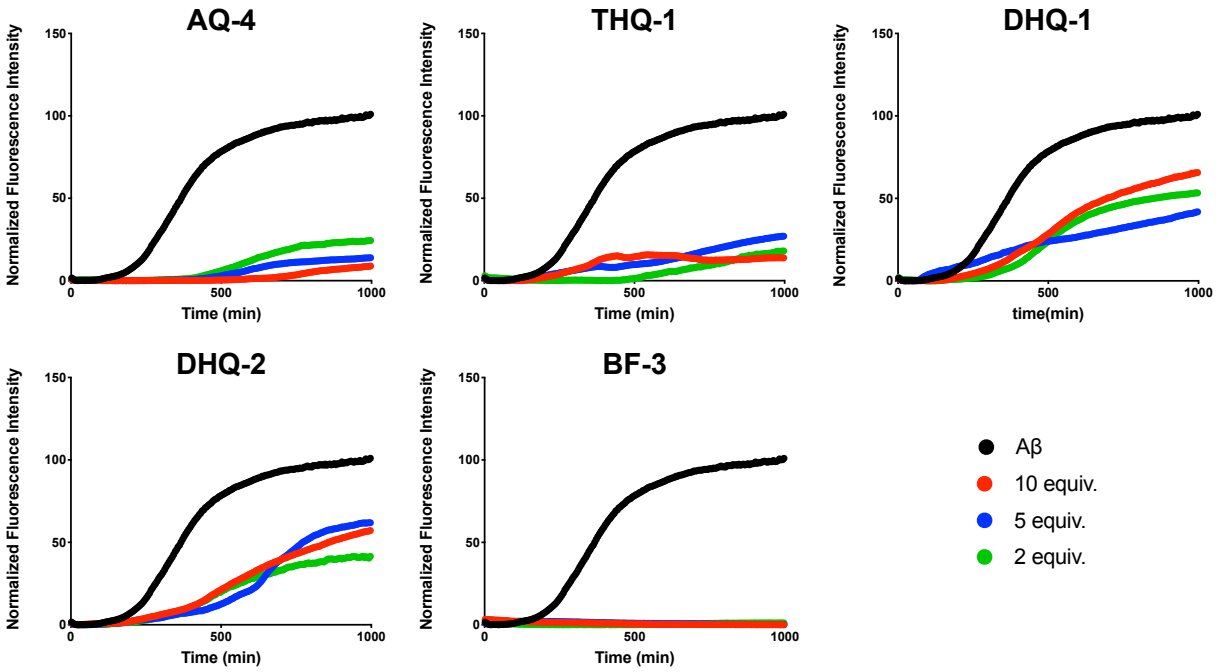

Figure B.8. ThT fluorescence kinetics for 10 μM $A\beta_{40}$ (black) and varying equivalents of compound in the absence of lipids.

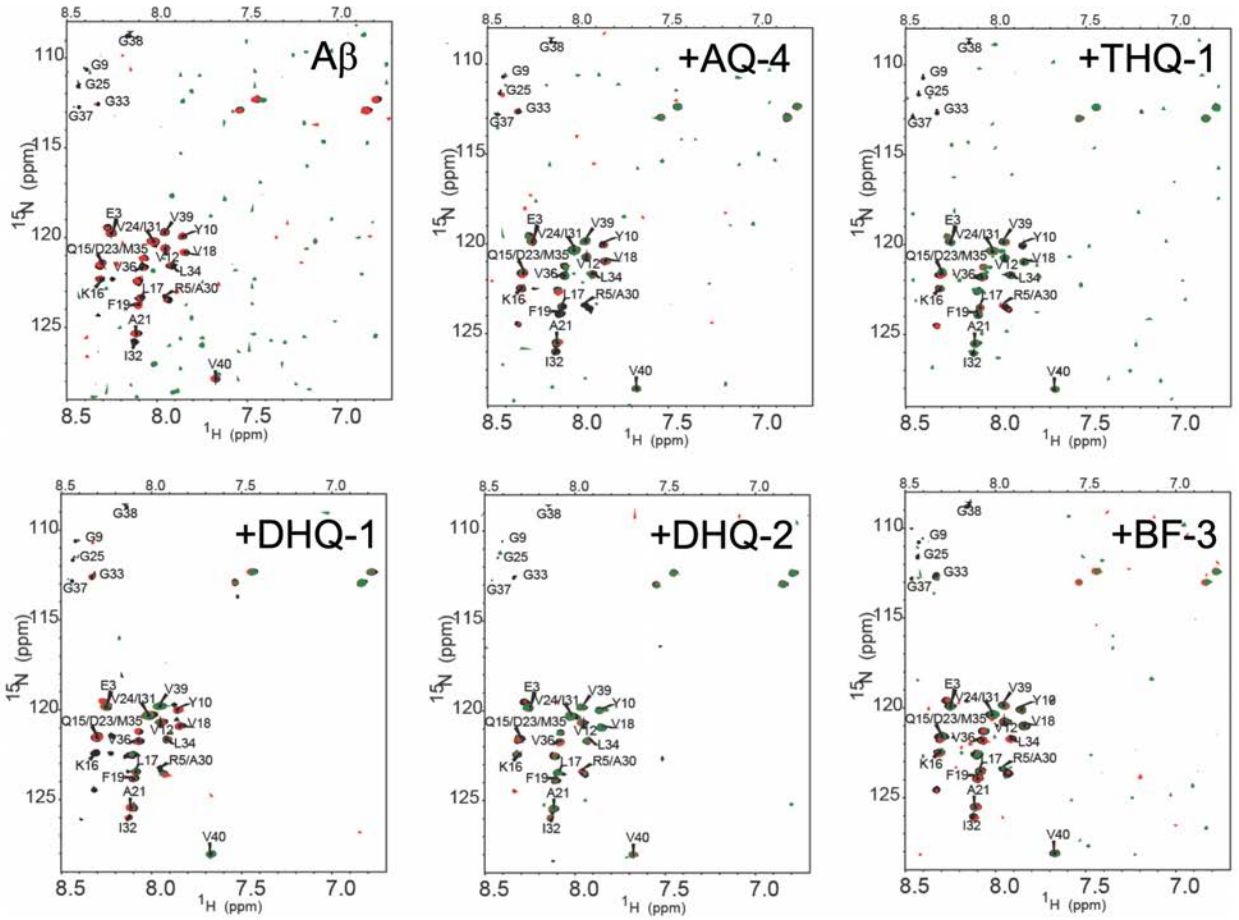

Figure B.9. SOFAST-HMQC NMR spectra of 25 μM ^{15}N- Aβ$_{40}$ in the presence of 50 μM compound at 0 (black), 24 (red) and 96 hours (green).

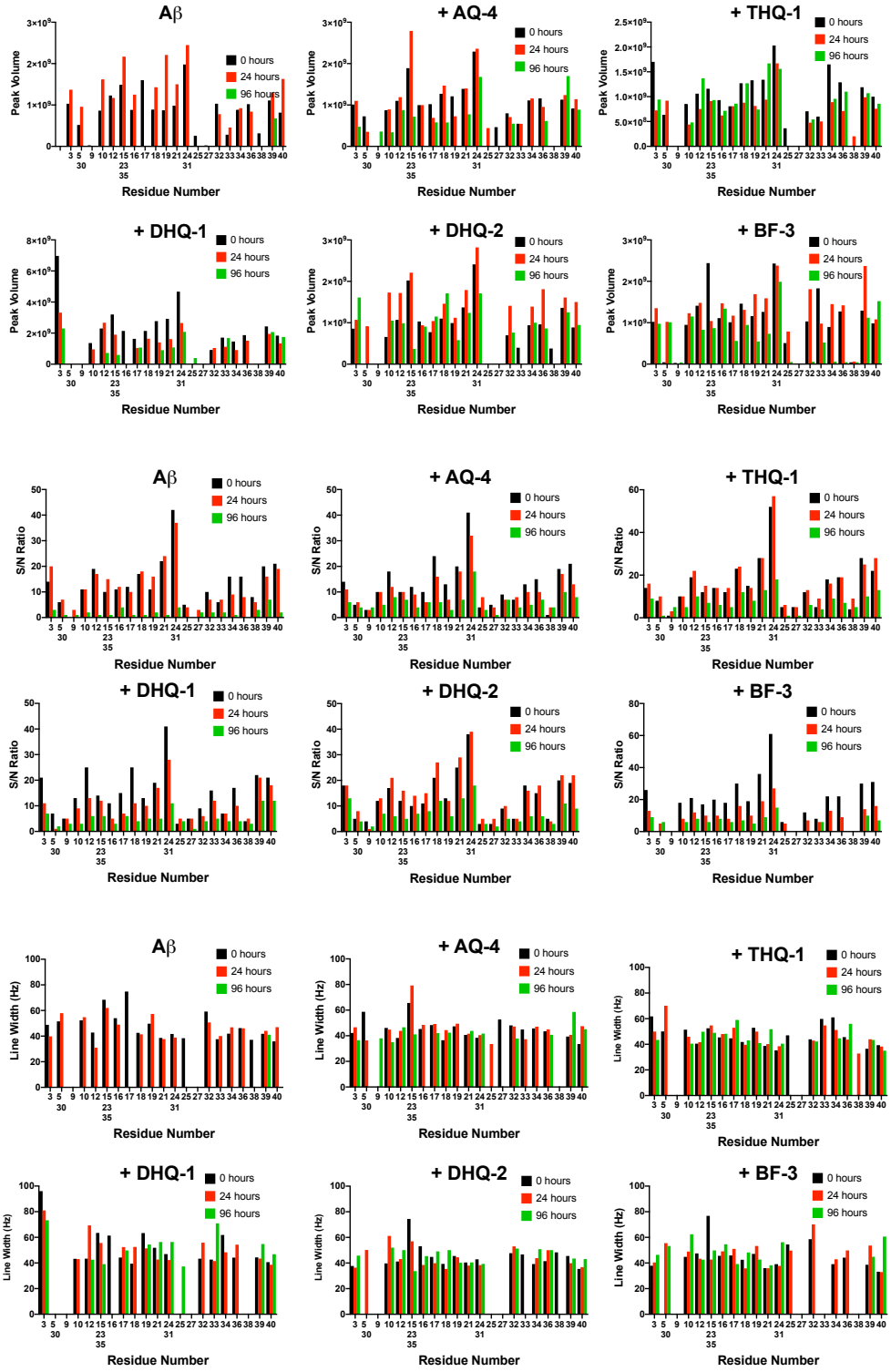

Figure B.10. (Top) Peak volumes taken from SOFAST-HMQC NMR spectra of 25 μM ^{15}N- Aβ_{40} in the presence of 50 μM compound at 0 (black), 24 (red) and 96 hours (green). (Middle) S/N ratios taken from spectra at 0, 24 and 96 hours. (Bottom) Linewidths taken from spectra at 0, 24 and 96 hours.

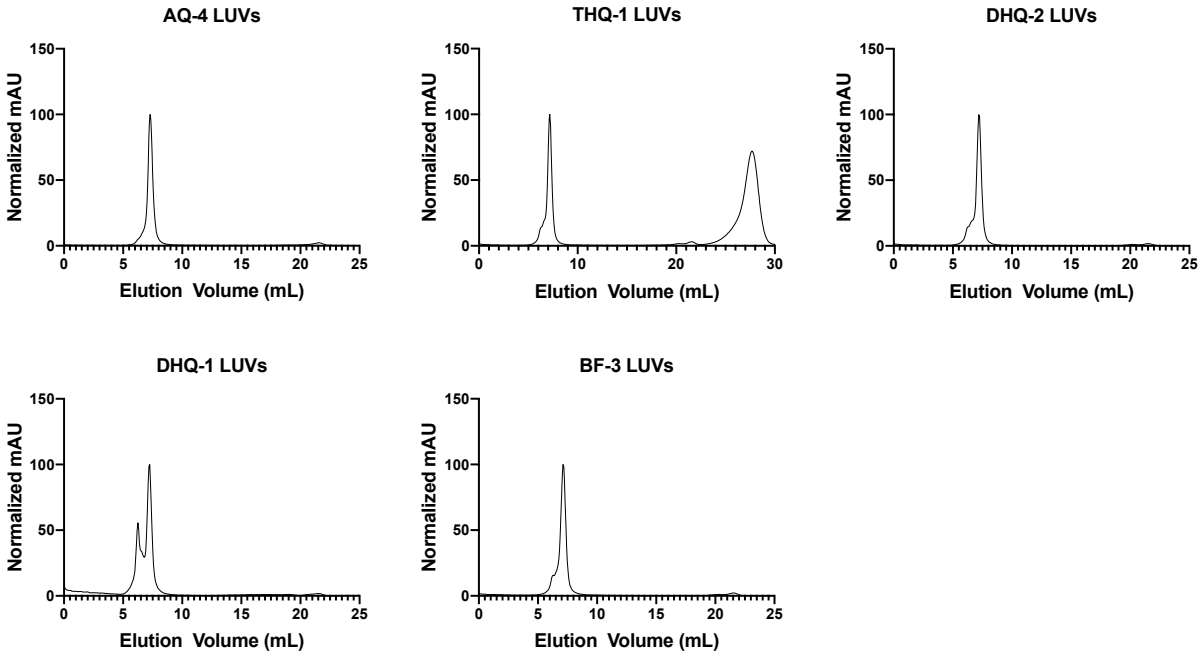

Figure B.11. SEC profiles of 100 nm LUVs loaded with small molecules at a 10:1 lipid:compound molar ratio.

B.1 Supplementary Tables

Table B.1. Information on the 21 primary hits selected form the screen.

CCG Code	Average IC50	Name (IUPAC or Common)	Supplier
CCG-208404	15	Maritimein	Carbosynth
CCG-49784	5.4	1-(3,4-dimethoxybenzyl)-6,7-dimethoxy-1,2,3,4-tetrahydroisoquinoline hydrochloride	Sigma Aldrich
CCG-208399	2.86	Shikonin beta	Sigma Aldrich
CCG-208567	2.7	Dihydrotanshinone	Molport
CCG-53743	7.2	2-(1,3-benzodioxol-5-yl)-6-nitro-1,2,3,4-tetrahydroquinazolin-4-one	Molport
CCG-220101	9.2	Apomorphine hydrochloride hemihydrate	Sigma Aldrich
CCG-208272	9.114	Shikonin	Sigma Aldrich
CCG-208289	18.7	Wedelolactone	Molport
CCG-208275	22.6	Tanshinone IIA	Sigma Aldrich
CCG-220307	14.15	Oxytetracycline dihydrate	Sigma Aldrich
CCG-100627	20	Piceatannol	Molport
CCG-208582	21	Hypocrellin A	Carbosynth
CCG-208456	207	Aloe-emodine	Molport
CCG-235107	50	1-(3,4-dimethoxyphenyl)-3-(3-methoxyphenyl)thiourea	Molport
CCG-234418	50	6-nitro-2-(3,4,5-trimethoxyphenyl)-2,3-dihydro-1H-quinazolin-4-one	Molport
CCG-39571	16	Levodopa	Sigma Aldrich
CCG-208268	4	Rosmarinic acid	Sigma Aldrich
CCG-208196	50	Doxorubicin	Molport
CCG-208189	13	Daunorubicin	Molport
CCG-35263	53	Emodin	Sigma Aldrich
CCG-208426	0.18	Laudanosoline	Molport

Table B.2. Common name, given abbreviation, and structure of the 21 primary hits.

Common or IUPAC Name	Abbreviation	Structure
Maritimein	BF-1	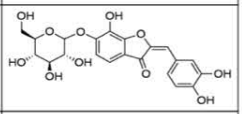
1-[(3,4-dimethoxyphenyl)methyl]-6,7-dimethoxy-1,2,3,4-tetrahydroisoquinoline hydrochloride	THQ-1	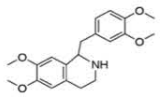
Shikonin beta	AQ-1	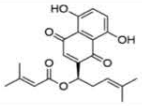
Dihydrotanshinone	BF-2	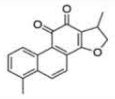
2-(1,3-benzodioxol-5-yl)-6-nitro-1,2,3,4-tetrahydroquinazolin-4-one	DHQ-1	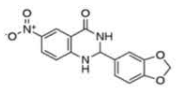
Apomorphine hydrochloride	THQ-2	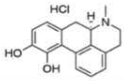
Shikonin	AQ-2	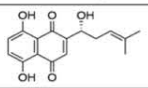
Wedelolactone	BF-3	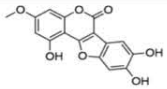
Tanshinone IIA	BF-4	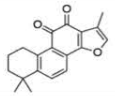
Oxytetracycline	AQ-3	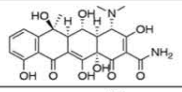
Piceatannol	BD-1	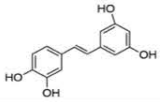
Hypocrellin A	AQ-4	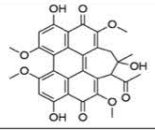

Common or IUPAC Name	Abbreviation	Structure
Aloe-emodine	AQ-5	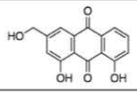
3-(3,4-dimethoxyphenyl)-1-(3-methoxyphenyl) thiourea	TU-1	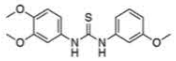
6-nitro-2-(3,4,5-trimethoxyphenyl)-2,3-dihydro-1H-quinazolin-4-one	DHQ-2	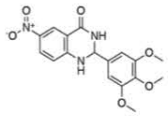
Levodopa	BD-2	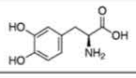
Rosmarinic acid	BD-3	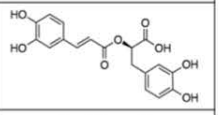
Doxorubicin	AQ-6	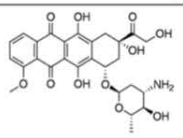
Daunorubicin	AQ-7	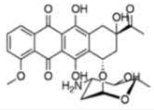
Emodin	AQ-8	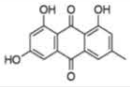
Laudanosoline	THQ-3